uOttawa

L'Université canadienne
Canada's university

FACULTÉ DES ÉTUDES SUPÉRIEURES ET POSTOCTORALES

uOttawa

L'Université canadienne
Canada's university

FACULTY OF GRADUATE AND POSDOCTORAL STUDIES

Mark Marschner
AUTEUR DE LA THÈSE / AUTHOR OF THESIS

Ph.D. (Earth Sciences)
GRADE / DEGREE

Department of Earth Sciences
FACULTÉ, ÉCOLE, DÉPARTEMENT / FACULTY, SCHOOL, DEPARTMENT

"Determining the Origins of ^{13}C-Enrichments in Biomineralized Fissure Calcrete Deposits from the Western Northwest Territories, Canada ; Comparing Acetogenic and Methanogenic Bacterial Processes"

TITRE DE LA THÈSE / TITLE OF THESIS

Ian Clark
DIRECTEUR (DIRECTRICE) DE LA THÈSE / THESIS SUPERVISOR

CO-DIRECTEUR (CO-DIRECTRICE) DE LA THÈSE / THESIS CO-SUPERVISOR

EXAMINATEURS (EXAMINATRICES) DE LA THÈSE / THESIS EXAMINERS

Ramon Aravena

Frances Pick

Danielle Fortin

Frederick Michel

Gary W. Slater
Le Doyen de la Faculté des études supérieures et postdoctorales / Dean of the Faculty of Graduate and Postdoctoral Studies

"Determining the Origins of ^{13}C-Enrichments in Biomineralized Fissure Calcrete Deposits from the Western Northwest Territories, Canada; Comparing Acetogenic and Methanogenic Bacterial Processes"

Mark Marschner

Thesis submitted to the
Faculty of Graduate & Postdoctoral Studies
University of Ottawa
In partial fulfillment of the requirements for the
Ph. D. degree in Earth Sciences

Ottawa Carleton Geoscience Centre
and
University of Ottawa
Ottawa, Canada

Your file Votre référence
ISBN: 978-0-494-25884-2
Our file Notre référence
ISBN: 978-0-494-25884-2

Table of Contents

General Abstract

The occurrence of secondary carbonate deposit within limestone fissures, called "endostromatolites", is evidence of biomineralization occurring in Canada's permafrost regions. Clustered growth columns propagating orthogonally to the fissure surface grew under saturated conditions during a period of climate amelioration after the end of the last major period of glaciation in North America (~ 13 000 years b.p.). The enriched $\delta^{13}C$ signal along endostromatolite growth columns (compared to the host rock) was previously interpreted as the result of methanogenesis. A conceptual model of the original growth environment links bacterial communities in soil horizons overlying the limestone outcrops with the microorganisms living within the rock mass. A field investigation of surface waters within the thawed active layer above permafrost in a periglacial limestone terrain did not show any ^{13}C-enrichment trends in DIC (dissolved inorganic carbon). Microsampling of individual growth columns from endostromatolite hand specimens yielded $\delta^{13}C$ values enriched compared to the host rock but no real trends along the growth column that could be used as clear evidence of a Rayleigh-type distillation process (i.e. the isotopic enrichment of a residual substrate). A series of laboratory closed-system incubation experiments using bacterial communities cultured from field materials was performed. Acetogenesis, rather than methanogenesis, was the predominant process at low temperatures and/or when DIC was provided as a substrate. The development of new methodologies, including compound-specific isotopic analyses of DOC components in complex matrices, provided enough results for a carbon mass balance to be calculated on the systems. A very distinct Rayleigh-type ^{13}C-enrichment trend was observed for methanol as a substrate, but enrichment of DIC was ubiquitously short-lived due to negative feedback signals from production of $^{12}CO2$. However, DIC enrichment occurred during production of acetate, thus pointing to the origin of enriched $\delta^{13}C$ signals in endostromatolites as being from acetogenic processes.

Keywords: endostromatolite; acetogenesis; methanogenesis; permafrost; ^{13}C; ^{18}O; DIC.

Les dépôts secondaires carbonatés à l'intérieur de fissures sont nommés endostromatolites et représentent une évidence de biominéralisation dans les régions périglaciaires au Canada. Les agrégats de calcite sous forment de colonnes se sont développés perpendiculairement à la fissure dans un milieu saturé en eau lors de la période climatique chaude survenue à la fin de la dernière glaciation majeure en Amérique du Nord (13 000 ans BP). L'enrichissement de la composition des isotopes stables du carbone ($\delta^{13}C$) des endostromatolites comparativement à celle de la roche mère a précédemment été attribué à la méthanogenèse. Un modèle conceptuel de l'environnent de croissance des endostromatolites lie les communautés bactériennes vivant dans les horizons des sols recouvrant les affleurements de calcaire aux microorganismes vivant à l'intérieur de la masse rocheuse. L'analyse de l'eau provenant de la couche active d'un sol calcareux en région périglaciaire n'a pas démontré d'enrichissement du ^{13}C du carbone inorganique dissous (CID). Des

microanalyses effectuées le long des colonnes d'endostromatolites présentent des valeurs $\delta^{13}C$ enrichies comparativement à celles de la roche locale. Cependant, les valeurs de ^{13}C n'indiquent aucune tendance d'enrichissement de la base vers le sommet des colonnes, phénomène qui aurait supporté l'hypothèse d'un fractionnement isotopique de type Rayleigh. Une série d'expériences d'incubation en système fermé utilisant des cultures bactériennes obtenues à partir d'échantillons de sols récoltés sur le terrain ont été réalisées en laboratoire. Les résultats ont démontré qu'à basse température et/ou lorsque le CID est introduit en tant que substrat, l'acétogenèse plutôt que la méthanogenèse, est à l'origine de l'enrichissement en $\delta^{13}C$. Le développement de nouvelles techniques permettant l'analyse isotopique des composés spécifiques du carbone organique dissous (COD) dans des matrices complexes, a permis la réalisation du bilan de masse du carbone dans les expériences d'incubation. Un patron de l'enrichissement en ^{13}C de type Rayleigh a été observé lorsque du méthanol a été utilisé en tant que substrat. Cet enrichissement fut de courte durée conséquemment à la rétroaction négative causée par la production de CO_2 léger (^{12}C). Cependant, l'augmentation en ^{13}C du CID, produit lors de la production de l'acétate, suggère que le processus d'acétogenèse a provoqué l'enrichissement de $\delta^{13}C$ dans les endostromatolites.

***Mot clés** : endostromatolites, acétogenèse, méthanogenèse, pergélisol, ^{13}C, ^{18}O, CID*

(Special thanks to D. Lacelle for the above translation.)

Chapter One

Introduction

New knowledge is waiting to be discovered around every corner and in every crevasse. Some of these corners are in far-away places that have barely been touched by the hand of mankind throughout the centuries. Canada's cold climate regions hold potential knowledge databases in some of its most mundane and overlooked features. How often have some of North America's earliest inhabitants arrived at a limestone outcrop and noticed the textured surfaces along some of the rock faces and within open cracks? And how often did they think nothing of these strange features and continued with their lives, never knowing that these textured surfaces preserve a paleoclimate signal from thousands of years in the past?

It was not until the late 20th century that researchers visiting a small area within Canada's vast arctic landscape witnessed limestone outcrops containing secondary carbonate deposits within exposed fissure surfaces and collected some samples for more observation and analyses. The newly-discovered (or re-discovered) material was called "endostromatolites". *Endo* means within. *Stromatolite* is a name given to a type of sedimentary structure created by photosynthetic filamentous and unicellular cyanobacteria in shallow marine waters (Tucker and Wright, 1990). Comparison between stromatolites and endostromatolites reveal a few key similarities. Both structures are laminated with a degree of relief (i.e. they tend to grow away from an attachment surface). However, the respective structures exhibit similar morphological growth forms on very different size scales. Stromatolites occur as individual growth columns that can be up to several metres in height, or they can form "ridge and rill" structures that are laterally extensive over entire subtidal to intertidal marine environments. Endostromatolites occur in limestone fissures with obvious spatial constraints, so individual columns occur on the scale of millimeters to centimeters. Both structures are microbial in origin, although little is known about what kinds of microorganisms were involved in the creation of endostromatolites. Stromatolites are ubiquitous features in current shallow marine environments and in the geological rock record. Regions of ongoing endostromatolite growth are unknown at present. The photic dependence of sediment trapping and binding organisms in stromatolite growth is well-established. Limestone fissures are sheltered environments receiving negligible to no

input of light, so the microbial community within them must be composed of respiring organisms. Hence a review of the available extensive literature about all aspects of stromatolites would be academically interesting but would not produce any conclusive information about the origins of endostromatolites.

A thorough description of endostromatolites is deemed appropriate. They occur as semi-continuous layers of clustered columns attached to the surfaces of limestone outcrops within open fissures. The columns propagate orthogonally to the fissure surfaces on which they are attached. Columns exhibit a great abundance of sizes and morphologies. They can be less than 100 microns to more than ~3 centimetres tall. The diameter of individual columns can likewise vary significantly with little or no correlation to column height. Thus groups of columns can have very different three-dimensional morphologies, from tall and delicate to low and robust and all forms in between. They can form tight clusters and/or individual columns can take on "dendritic" shapes (i.e. like branches on a tree), giving some specimens a typical *cauliflower* texture, or they can be much more sparsely distributed (like an open-crown forest). Some endostromatolite deposits contain two or more "stacks" of columns, meaning that the tops of the columns forming one distinct layer became the growth surface on which a subsequent layer of columns grew. Porosities of endostromatolites are also quite variable. Intra-columnar spaces can remain empty or be filled with secondary cements. Porosity typically decreases away from the fissure surface as growth columns widen and/or "branch outward" from the central "pillar".

Images of endostromatolites are shown in Figures 10, 11, 13, 14, and 15.

Endostromatolites have a widespread distribution across Canada's vast arctic landscapes. They have been observed in limestone terrains in the Yukon and western Northwest Territories. On the scale of individual limestone outcrops, endostromatolites exhibit preferential spatial distributions. Without exception, every fracture that contains endostromatolites has growth columns attached to one side of the fracture, never both sides. The side of the fracture opposite the growth surface often displays a dissolution

surface, and moreover, the dissolution surface often expresses the texture of the growth clusters but in reverse. Endostromatolite-filled fractures tend to be found on southward exposures. Fissures on northward-facing outcrop exposures are usually void of any secondary deposits. Moreover, the side of the fracture where growth occurred is invariably on the southward side or, for horizontal fractures, the upper side. Finally, endostromatolites have been observed only within the top few metres of outcrops, in effect confining themselves to the outermost "layer" of limestone outcrops. The distribution of similarly uniform climate conditions in many northern areas of Canada could play a role in allowing endostromatolite growths to develop the aforementioned small-scale growth preferences across larger regional scales.

When endostromatolites are examined in thin sections, their internal growth structures become evident. Well-preserved samples exhibit light and dark alternating growth bands stacked upward along individual growth columns (see Figure 13). These bands are evidence of biomineralization.

Since their discovery, *fissure calcretes* have become the focus of several published investigations (see Lauriol and Clark, 1999; Chauret, 2000; Clark *et al.*, 2004). Most notably, ^{18}O analyses of carbonate collected from microsampling of growth columns have been used as a paleotemperature signal of a warmer Holocene climate during endostromatolite emplacement (Clark *et al.*, 2004). Calcium carbonate ($CaCO_3$) precipitating in equilibrium with meteoric water will fractionate ^{18}O according to the temperature of the depositional setting, and the ^{18}O-isotopic composition of the meteoric water is related to the mean annual air temperature of the region. Radiocarbon analyses of these samples have calculated age dates for the climate events and have shown that the Holocene warming period is directly related to an insolation maximum.

Stable isotopic analyses of carbonate ^{13}C reveal enriched signals with values ranging from normal marine limestone (~ 0‰ VPDB) to about +14‰ VPDB. Fractionation of dissolved inorganic carbon (DIC) in the original depositional environment can only be mediated by anaerobic respiring bacteria. Interpretation of the

carbon isotopic signals by researchers has implicated methanogenesis as the likely process in fractionating the DIC pool (Lauriol and Clark, 1999). This evidence validates the assumptions that the original depositional environment had to be saturated and that little evaporation could take place. Any evidence to the contrary would invalidate the interpretations of the ^{18}O data.

The primary purpose of this thesis is to determine what bacterial processes are responsible for creating strong ^{13}C enrichments in endostromatolites. To achieve this objective, aqueous geochemical conditions from field sites within limestone terrains where endostromatolites occur were analyzed. As well, frozen bacterial communities from periglacial soil at the same field locations were cultured and used in incubation experiments in which the flow of carbon through various reactants and products was monitored quantitatively and isotopically. The rationale behind this rather ambitious project is simply that it is inconceivable to "grow" endostromatolites under controlled laboratory conditions. The assumption that present-day soil bacteria from permafrost in a periglacial limestone terrain can be directly linked to bacterial colonies in the same region thousands of years ago is justifiable. Methanogenic bacteria are ubiquitous and active in many permafrost regions, and cold-climate regions are known to evolve slowly over time. Thus it is highly conceivable that the bacteria present during endostromatolite growth in the recent geologic past are still present in the surrounding soil horizons where they are frozen for eight months or more each year.

A conceptual model of the original growth environment is shown in Figure 1. Endostromatolite-bearing limestone outcrops that are exposed today were covered by mineral soils (i.e. tills) deposited on them by continental glaciers from the last major period of glaciation in North America. These soil horizons may have become extensively vegetated over time given that Canada's cold climate regions experienced a period of climate amelioration since the end of glaciation approximately 10,000 years before present. Abundant vegetation can affect the local water table by keeping saturated conditions at shallower depth compared to barren landscapes. Distribution of permafrost likewise plays a significant role on local drainage as frozen soil is nearly impermeable if

it is continuous. Fissures in limestone outcrops may have helped to drain the overlying soils like small-scale taliks. The porosity of limestone outcrops is determined by the abundance, size and distribution of fissures. Fractures parallel to and orthogonal to bedding planes within limestone masses are common, and limestone deposits tend to form blocky talus deposits as they erode from physical weathering processes. Thus fracture networks within limestone outcrops occur in three dimensions and cannot be adequately depicted in Figure 1.

Respiration by bacteria in the overlying soil horizon generates biogenic CO_2 from the decomposition of organic matter. Since most plants in cold climate regions are C-3 plants, biogenic CO_2 released from organic decomposition will be isotopically similar to the $\delta^{13}C$ of C-3 plants (approximately -26‰ VPDB). Atmospheric CO_2 ($\delta^{13}C \approx$ -7‰ VPDB) can also diffuse into the soil, but its overall contribution to the DIC (dissolved inorganic carbon) pool is expected to be small. Biogenic CO_2 reacts stoichiometrically in a 1:1 ratio with inorganic carbonate phases and thus generate an aqueous DIC pool that is roughly 50% from each source. Marine limestones have $\delta^{13}C$ values around -3 to 0‰ VPDB, and hence soil zone DIC should have a $\delta^{13}C$ in between biogenic CO_2 and marine limestone (i.e. -15 to -10‰ VPDB). The residence time of DIC in the soil is unknown. Diffusion of CO_2 from the soil zone would be expected to impart an enrichment of ^{13}C on the residual DIC pool.

Once the soil water enters a limestone fissure, different processes appear to become significant in altering the aqueous geochemistry. DIC entering the fissures does not automatically precipitate ^{13}C-depleted $CaCO_3$ (relative to marine limestone). Observations that endostromatolites grow only on one side of the fissure point to different processes occurring on opposite surfaces. There is no known ^{13}C-enriched source material that can impart an enrichment on the DIC pool. Also, the sheltered environment of fissures renders any quick freeze-thaw or desiccation reactions that would incur a strong kinetic isotopic fractionation quite doubtful. The selective removal of ^{12}C from the DIC pool can be achieved by anaerobic respiring bacteria such as methanogens and acetogens that produce isotopically light products. These microorganisms likely

originated from the overlying soil horizon, though their roles within the diverse bacterial community may or may not have been significant. The number of active species of bacteria in a community may be quite small compared to the overall number of different species present at any given time. The same could be said of the community living within the fracture environment. In fact, the communities in both environments could be identical in terms of diversity but very different in terms of activities. For example, the availability of DIC in the limestone fissures may favour autotrophic processes over heterotrophic processes.

It is important to note here that this thesis is not concerned with the actual physical processes responsible for endostromatolite growth. Water in contact with limestone will be at or very close to saturation with respect to $CaCO_3$, and any small changes to pH or the partial pressure of CO_2 will cause either dissolution or precipitation. Bacterial processes can change aqueous geochemistry both on a microscale (i.e. on their cell walls) and on a larger scale. At near-freezing temperatures and circumneutral pH, fractionation of ^{13}C between $CaCO_3$ and aqueous DIC (dissolved inorganic carbon) is very small, even negligible compared to the large fractionation involved in some anaerobic bacterial reactions. The processes that enrich DIC in ^{13}C are of considerable interest, since these processes are very likely behind the ^{13}C-enrichments of endostromatolites. Methanogenesis can reduce DIC to CH_4 and enrich residual DIC in ^{13}C. Acetogenesis can transform DIC to acetate with a similar isotopic fractionation. One of the key objectives of this thesis is to evaluate the relative importance of each process and how they affect the system as a whole.

This thesis is presented as a series of research papers intended for submission to scholarly journals for publication.

Chapter 2 presents a new methodology for using an HPLC system to separate and collect short-chain fatty acid fractions for subsequent $\delta^{13}C$ measurement. The development of this new methodology was necessary in the development of a sampling protocol required for the incubation experiments presented in Chapter 4. This chapter

builds on the remarkable technological integration of a wet oxidation TOC analyzer as a peripheral device to a continuous flow mass spectrometer. In short, the HPLC-fraction collection system opens the door to compound-specific isotopic analyses of DOC (dissolved organic carbon). The new method was validated using fatty acid standards prepared in clean water and complex matrices, and it is shown that sample recovery and sample integrity can be achieved using carbon-free carrier solvents. Since acetic acid is a major product of the bacterial incubation experiments of Chapter 4, this methodology greatly reduces speculation that the results of fatty acid analyses in Chapter 4 are inaccurate. This chapter was accepted for publication (Marschner, 2005) on the first submission without any extensive revisions.

Chapter 3 presents new data obtained from endostromatolites and from the present-day hydrological environment of a periglacial limestone terrain where exposed outcrops contain abundant endostromatolite growth surfaces. In dealing with endostromatolite hand samples, well-preserved samples (containing unaltered microstructures) are chosen for microsampling to generate a new data set using a new methodology for both collecting the tiny powder samples and analyzing them isotopically with a continuous-flow mass spectrometer. Numerical modeling of Rayleigh-type distillation processes theorized to be occurring in the original depositional environment is used to interpret the analytical data. Field data collected from shallow groundwaters in a cold-climate region underlain by continuous permafrost likewise present insights into the interpretation of the original fracture setting. The main purpose of this paper is to attempt to relate the bacterial processes occurring (or not occurring) in modern transiently-thawed periglacial soils with processes that took place in limestone fissures. The results of this preliminary investigation lead into Chapter 4 that focusses on more hands-on data collection from bacterial microcosm experiments.

Chapter 4 presents results from successful closed-system bacterial incubation experiments. Frozen soil taken from the field sites described in Chapter 3 was cultured to

revive dormant bacteria, and the bacterial culture created served as the inoculant of several closed-system incubation systems. Flaws in the experimental design of the earlier investigation presented in Appendix 3 (below) were addressed and corrected prior to the onset of incubation. Methanol was chosen as the major substrate for bacterial growth for two reasons: it was responsible for some very interesting results during early investigations (Appendix 3) and it suited the purpose of demonstrating Rayleigh-type isotopic enrichments. The new methodology outlined in Chapter 2 was used to generate a carbon mass balance data set more complete than earlier experiments had achieved (Appendix 3). Mass balance calculations are used to demonstrate Rayleigh-type isotopic enrichments for methanol. The results show that acetogenic bacteria are better able to compete for DIC and are more productive at low reaction temperatures than are methanogenic bacteria.

Implications of this research are related to previous assumptions about the "openness" of endostromatolite systems and how the carbon data figure into age dating. The origin of carbon during endostromatolite growth and how that carbon is cycled are vitally important toward interpreting radiocarbon age dates. The main product of acetogenesis, acetic acid, could release significantly more limestone-derived DIC (i.e., "dead carbon") to aqueous solution than any methanogenic reactions. The ramifications of the research presented here could alter how paleotemperature signals from other carbonate materials are interpreted.

Appendix 1 contains a detailed explanation, including reactions and equations, used to build the numerical Rayleigh-type distillation model discussed in the first half of Chapter 3.

Appendix 2 contains charts of numerical field data measured from field samples discussed in the second half of Chapter 3.

Appendix 3 shows the intricate calculations used to derive the numerical results for Chapter 4.

Appendix 4 is a scholarly paper written to present some results of the earliest bacterial incubation experiments attempted during the course of this investigation. Some of the results were included in a published paper by Clark *et al.* (2004).

References (cited in Chapter 1 – Introduction)

Chauret Y (2000) Étude sur le développement des calcrètes de fissures du Yukon Septentrional, du Pléistocène à aujourd'hui. (Master's Thesis, Department of Geography, University of Ottawa, 85p)

Clark I, Fritz P (1997). *Environmental Isotopes in Hydrogeology*. Boca Raton, Lewis Publishers.

Clark I D, Lauriol B, Marschner M, Sabourin N, Chauret Y, Desrochers A (2004) Endostromatolites from permafrost karst, Yukon, Canada: paleoclimatic proxies for the Holocene hypsithermal. *Canadian Journal of Earth Sciences*. **41**: 387-399.

Lauriol B, Clark I (1999). Endostromatolites in the arctic: a paleohydrologic indicator. *Applied Geochemistry*. **14**: 775-785.

Marschner M, Middlestead P, Clark I (2005). Using a simple high-performance liquid chromatography separation and fraction collection methodology to achieve compound-specific isotopic analysis for dissolved organic compounds. *Rapid Communications in Mass Spectrometry*. **19**: 261-268.

Tucker M E, Wright V P (1990). *Carbonate Sedimentology*. Oxford, Blackwell Science, 482p.

Chapter Two

"Using a simple HPLC separation and fraction collection methodology to achieve compound-specific isotopic analysis (CSIA) for dissolved organic compounds"

Abstract

A new application for the quantitative and isotopic analyses of dissolved inorganic and dissolved organic carbon compounds is developed. Dissolved organic matter (DOM) in natural water samples can be separated on an HPLC column and collected as fractions. Each discrete fraction can then be analyzed using the technique of St-Jean (2003). Experimental data using short-chain fatty acid standards (formic, acetic, and propionic acids) show that fraction recoveries of 100% are possible and sample integrity is maintained. ^{13}C isotopic analyses of products prior to and subsequent to extraction and collection show no isotopic effects associated with the methodology, and errors are well within the accepted analytical uncertainty of the IRMS. Comparison of data from pure standards and organic-rich natural waters shows that quantitative analyses still need to be done with standards that more closely imitate the matrices of the samples to achieve an appropriate calibration curve. Injections of organic rich matrices on the HPLC column did not affect fraction recovery nor did they create high backgrounds of partially-retained organic compounds slowly released from the HPLC column, and hence ^{13}C isotopic results are relatively unaffected. The specific limitation on this methodology is the use of carbon-free carrier solvents due to potential memory effects associated with the TIC/TOC analyzer. Further developments of this application could make routine compound-specific isotopic analysis (CSIA) for a wider range of organic materials possible.

Introduction

Previously it has been shown that a total inorganic carbon / total organic carbon (TIC/TOC) analyzer interfaced with a continuous-flow isotope ratio mass spectrometer (CF-IRMS) can be used for precise quantitative and isotopic analyses of dissolved inorganic and organic carbon compounds in aqueous solutions (St-Jean, 2003). Reproducibility of results from the methodology is within the analytical error of the mass spectrometer and allows for dependable routine analyses with minimal overhead costs.

Organic matter present in soils and dissolved in natural waters contains extremely diverse compounds composed of mainly carbon, oxygen, hydrogen, nitrogen and sulfur. For general investigations, the isotopic characterization of dissolved organic matter (DOM) as a single group is sufficient. More detailed investigations focus on specific compounds or groups of compounds within organic fractions. For example, Molina *et al.* (1999) have examined phospholipid fatty acids in estuarine surface sediments to determine the contributions of C3 versus C4 plant degradation and the role of microbial communities in the cycling of organic compounds. Blair and Carter(1992) have focused on the carbon isotopic composition of acetate isolated from porewaters of coastal marine sediments.

Previous methods for compound specific isotopic analyses (CSIA) required manual separation and purification techniques to isolate specific compounds prior to introduction into analytical instrumentation (eg. Thiel *et al.*, 2001; Yavitt *et al.*, 1997). One of the benefits of the automated technique developed by St-Jean (2003) is that samples require a minimal amount of treatment prior to analysis. Inorganic and organic fractions are selectively reacted by chemical reagents and removed as CO_2 from the aqueous sample before being "scrubbed" (i.e. purified) and chromatographically separated to remove contaminants.

To enhance the range of applications created by the technique of St-Jean (2003), a simple chromatographic method for separating and collecting organic compound

fractions prior to introduction of samples into the TIC/TOC analyzer is developed. The role of carboxylic fatty acids (i.e., formic, acetic, and propionic acids) in natural degradational systems has been of particular interest to microbiological and earth science research (eg. Fey and Conrad, 2000; Conrad, 1999; Waldron *et al.*, 1998). Using a high performance liquid chromatography (HPLC) system interfaced with an automated fraction collector, a series of experiments were performed to determine if fraction recovery of fatty acids had any effects on sample integrity (quantitatively and isotopically).

Three separate experiments reported herein were created to determine the viability of this new methodology in applying it toward the compound specific isotopic analysis of natural water samples. The first experiment demonstrates that 100% fraction recovery of pure fatty acid standards prepared in deionized water is possible. The second experiment uses the TIC/TOC analyzer to demonstrate that products of HPLC sample separation and collection are not subject to isotopic effects Finally, the performance of the instrumentation is further tested by preparing organic-rich complex matrices, such as active bacterial media and natural waters, and comparing the results to the pure standards used in the first two experiments. The HPLC extraction method is proven to be a viable process as a simplified substitute for previous chemical-separation techniques, and we anticipate that these results will stimulate more research toward adapting the analytical technique toward many other applications.

Apparatus and Procedure

TIC/TOC analyzer and IRMS

The TIC/TOC analyzer described here is the same instrument used by St-Jean (2003). The analyzer is a modified OI Analytical model 1010 wet oxidation TOC analyzer with a 53 sample autosampler. The autosampler carousel is designed specifically to hold 40mL TraceClean^{TM} borosilicate vials. The vials used throughout

this study are 40mL pre-cleaned amber borosilicate vials with 0.125" silica gel septa liners inside open-top caps (VWR catalogue # 15900-024). The analyzer is connected to a Finnegan MAT Delta Plus IRMS with a ConFlo III continuous-flow interface. For the specifics relating to how the instruments are interfaced and how samples from the TIC/TOC analyzer are treated before being sent to the IRMS for isotopic analyses, the reader is referred to the paper by St-Jean (2003).

HPLC and fraction collector

The chromatographic system used is a Cecil Instruments ADEPT^{TM} series HPLC. The components of the HPLC system are shown in Figure 2. Two dual piston pumps (CE 4100) are situated in parallel to create a gradient pumping system so that different carrier solvents (or one solvent in different concentrations) can be combined with flow ramping. Not shown in Figure 2 are the electrical connections to the Chromatography System Manager (CE 4900) that acts as the interface between the HPLC components and Powerstream 2.0, the software used for data capturing. The Rheodyne injector with 1.0mL sample loop, the column, and the UV/Vis and RI detectors (CE 4200 and CE 4700, respectively) are assembled in series and are also controlled via the CSM. The column used in conjunction with the 1.0mL sample loop is a CSC-Tribute 120A/ODS C-18 reversed phase column, approximately 25 cm in length and with an internal diameter of 0.94 cm. An identical column with a much smaller internal diameter was also used in conjunction with a 20 μL sample loop for more precise analytical work. An in-line filter apparatus and a guard column are situated between the injection port and the column to remove particulate matter. An Isco Foxy 200 X-Y Fraction Collector at the end of the flow path recovers sample fractions into 10mL glass vials using preprogrammed internal software that is not integrated with any of the HPLC components. Hence fractions of chromatographically-separated components are collected by time, not by peak. The fraction collector is equipped with two sample trays that can each hold 144-10mL glass vials. The collection parameters were determined experimentally and are explained briefly in the following section.

Calibrating the fraction collector

Because the fraction collector is operated independently of the HPLC system, the time required for a peak component to move from the detectors to the end of the flowpath must be calculated and calibrated over a range of programmed flow rates. This was achieved by visual observation of distilled water samples containing blue food colouring moving through the system. The calibration curve (not shown) was used to calculate offsets in time events for fraction recovery compared to the response of the detectors.

Calibrating the pumps

The programmed flow rates of the dual-piston pumps were calibrated versus actual solvent volumes recovered. Using a 10mL graduated cylinder, the time required to collect 10mL of carrier solvent was measured for several programmed flow rates. The results comparing programmed and calculated flow rates are shown in Figure 3. Calculated flow rates are between 82 and 91% of the programmed flow rates, with the results moving away from 100% at higher flow rates. An exponential relationship was calculated for the calibration curve, with the formula given in Figure 3. There was no significant change in the calculated flow rates when the carrier solvent was collected directly from the pump instead of at the end of the flow path, so components in series with the flow path did not inhibit flow.

Standard preparation

Four reagent-grade short-chain fatty acid standards were chosen for experimental work with the HPLC: formic acid, acetic acid, propionic acid, and butyric acid. Details of these compounds appear in Table 2.1. Working standards of each acid were prepared to 4,000 ppmC (parts per million carbon) concentration. Deionized water for diluting the concentrated reagents was obtained from a Barnstead NANOpure 4-cartridge filtration unit that produces a product with a resistance in excess of 17 MegOhms/cm. A mixture of standards (referred to herein as "cocktail") was prepared by mixing equivalent volumes

of each of the working standards. Subsequently, it was determined that butyric acid requires much higher carrier flow rates and run times to be removed from the HPLC column, and this acid was replaced by deionized water when preparing the "cocktail" mixture (see Figure 4). Since each acid has a different overall composition of carbon, the analytical concentration of the total acid molecule for each compound in the "cocktail" is different and is shown in Table 2.1. The TIC/TOC analyzer detects and reports organic compounds in concentration units of carbon, and hence it is simpler to prepare standards and report results based on these units. We have assumed that the densities of our working standards are not significantly different from that of water, so units of ppm are roughly equivalent to μg/mL.

Table 2.1 also gives the carbon isotopic composition of each acid standard. The isotopic analyses were performed on pure acid aliquots using a CE Instruments model 1110 elemental analyzer. The values given are averages of four analyses per acid (n = 4), and errors expressed as two standard deviations (2σ).

The linear detection range of the TIC/TOC analyzer was determined experimentally to be between ~1 ppmC and 150 ppmC. The multiple aliquot injection design of the TIC/TOC analyzer allows for larger volumes of trace concentration (ppbC) samples to be analyzed; however, background levels of TOC from HPLC fractions are around 1-2 ppmC. Hence our decision to work with very concentrated standards effectively eliminates background contamination from calculations based on our results. A 1mL aliquot of a 1000 ppmC fatty acid standard diluted to 40 mL to fit the TIC/TOC autosampler vial required volume produces a sample with a concentration of 25 ppmC, in the middle of the instrument's linear calibration range. Extraction of a 1 mL aliquot of a 1,000 ppmC standard on the HPLC column and collected as a fraction dilutes the aliquot based on the flow rate and the size of the collection window, but this dilution is not important since the fraction is subsequently diluted to the autosampler vial volume. In theory, 100% recovery of an aliquot run through the HPLC should produce a sample for TIC/TOC analysis of the same concentration as an aliquot that is manually diluted to 40mL without extraction.

HPLC Methodology

Dilute phosphoric acid was chosen as the carrier solvent for separating fatty acid standards on the HPLC column. Preparation of organic fraction samples for TIC/TOC-IRMS analysis eliminated the possibility of using any organic solvents. Likewise, a bicarbonate-based solvent could not be used as high TIC concentrations have been shown to create a "memory effect" on TOC analysis. The best resolution of peaks was achieved using a 10^{-3} M solution of phosphoric acid as the carrier. A sample chromatogram for all four fatty acids is shown in Figure 5. A programmed flow rate of 3.0 mL/min was necessary to resolve the first three acids. Butyric acid is partially-retained on the column at this rate and was removed by increasing the flow rate to 8.0 mL/min.

All HPLC work was done with the UV/Vis detector set at 230 nm and a column temperature of 60°C. The RI detector signal was not recorded.

Reducing the TOC backgrounds on HPLC-extracted samples was of critical importance to our experimental work. Deionized water used for standard preparation above was also used for making carrier solvent and is routinely used as the zero standard for the TIC/TOC analyzer. After the HPLC column is cleaned with acetinitrile for several minutes to remove organic contaminants from previous runs, the column is flushed overnight with deionized water at 2.0 mL/min. The carrier is then changed to dilute phosphoric acid as described above and the flow is increased to 3.0 mL/min for at least ten minutes. A 15-minute fraction window is used to collect solvent coming from the HPLC, and this fraction is used to determine the average background level of organic contamination. Because backgrounds are ubiquitously low, the results of analysis of the blank are qualitative and hence used as a check on the performance of the HPLC components.

Experimental Procedure

Three sets of experiments were performed to determine the effects of simple chromatographic separation on sample recovery, both quantitatively and isotopically, and to compare results between standards prepared in pure solutions versus standards prepared in natural waters that are highly-charged with complex TOC species.

Experiment 1

The fraction collector was set to collect fractions at 1 minute intervals into 10mL glass collection vials. Three identical one milliliter aliquots of standard fatty acid "cocktail" were injected separately onto the column under normal conditions and fractions were collected during a twenty minute time interval after each injection. One milliliter aliquots of each collected fraction were subsequently reinjected under identical conditions to evaluate the fatty acid content versus the average of the three "cocktail" injections. All of the resulting chromatograms were integrated and the results were used to determine the recovery of each acid.

Experiment 2

Fatty acid standards were prepared for the TIC/TOC-IRMS by taking one milliliter of each 4,000 ppmC stock solution and diluting separately with deionized water to a final volume of 100mL, thus giving a final concentration of 40 ppmC and more than enough solution to fill two 40mL autosampler vials. A one milliliter aliquot of "cocktail" was diluted in the same manner, giving a solution with a final concentration of 30 ppmC. These standards were measured against three TIC/TOC reagent standards to calibrate both quantitative and isotopic data. Two one milliliter aliquots of "cocktail" were injected onto the HPLC column and extracted as fractions using predetermined peak windows for (hopefully) full recovery of each chromatographically-separated fatty acid. Each fraction was diluted to 40mL with deionized water in autosampler vials and run on the TIC/TOC-IRMS for quantitative and isotopic data with which to compare to the previous unextracted standards.

Experiment 3

Because acetic acid is a ubiquitous biodegradational product of organic matter in natural and anthropogenic decompositional environments, further experimentation focussed exclusively on this organic acid. A second 4000 ppmC stock solution of acetic acid was prepared using organic-rich *soil water* instead of deionized water as the matrix. Soil water "broth" was prepared from homogenized (i.e. dried and powdered) tundra soil. The soil was previously collected from the thawed surface layer of a limestone terrain near Inuvik, Northwest Territories, Canada, and was preserved by freezing in resealable plastic storage bags. Ten grams of homogenized soil powder were boiled in one liter of deionized water, then cooled and filtered with 0.45 μm cellulose acetate membrane paper. The organic carbon concentration of the soil water itself was not determined. Because the pH of the soil water was higher than 3.0, a few drops of concentrated phosphoric acid were added to lower the pH. Calibration curves of the two acetic acid stock solutions were created over a range of concentrations (200 to 1,500 ppmC). Diluted solutions of each standard were made using the appropriate matrix (i.e. deionized water for the pure stock solution; acidified soil water for the organic-rich stock solution).

Fractions of acetic "broth" were collected separately on one milliliter aliquots having acetic acid concentrations of 1000 ppmC and 700 ppmC respectively. A blank aliquot of soil "broth" was also injected onto the HPLC column to monitor the baseline response of the UV/Vis detector. No peaks were detected from the resulting chromatogram, but this does not indicate that no organic compounds were being released from the column during the acetic acid "window". Comparing quantitative and isotopic data from the "broth" fractions to the pure products of Experiment 2 will determine the levels of potential contamination and/or signal overlap from other organic compounds.

A natural water source containing acetic acid produced in-situ was obtained from mixed microbial cultures of methanogenic and acetogenic bacteria. These bacteria were cultured from the same frozen soil samples from which the powdered soil used to make "broth" was obtained. A small volume of culture water was filtered to 0.20 μm and

acidified with concentrated phosphoric acid. A 1 mL aliquot was injected into the HPLC for quantitative acetic acid measurement, and a fraction of the background acetic acid was also extracted for isotopic analysis on the TIC/TOC-IRMS. Also, a mixture of culture water and standard 4,000 ppmC acetic "broth" was prepared in a 7:1 ratio and analyzed quantitatively and isotopically for acetic acid.

‰ Notation

Isotopic results are reported in standard ‰ (per-mil) notation expressed against the universal Vienna Pee-Dee Belemnite (VPDB) standard that is reported to have a $^{13}C/^{12}C$ ratio of 0.0111796. All samples prepared for TIC/TOC analysis are calibrated against working standards of sucrose, potassium biphthalate (KHP), and citric acid. These working standards had their $\delta^{13}C$ compositions determined by measuring them against an isotopic calibration curve for universal standards NBS-35, NBS-36 and IAEA-CO9. The working and universal standards were reacted using an identical procedure on a CE Instruments model 1110 elemental analyzer. Twelve to fifteen replicates of each working standard produced an error range ($\pm 2\sigma$) of less than 0.1‰. The actual ‰ notation is defined as a comparison of the $^{13}C/^{12}C$ ratios of a sample to the universal VPDB reference (R_{sample} and R_{VPDB}, respectively):

$$\delta^{13}C_{sample} = \left[\frac{R_{sample} - R_{VPDB}}{R_{VPDB}}\right] \times 1000 \text{ ‰}$$

Results and Discussion

Experiment 1

The uncalibrated data from the HPLC extractions of fatty acid "cocktail" are shown in Table 2.2. Signal data of two peak parameters were chosen for comparison: peak area and peak height. Three measurements of each parameter for each fatty acid in the cocktail were used to derive an average.

The uncalibrated data from the secondary analyses of fractions derived from the "cocktail" are shown in Table 2.3. Only the fractions that produced a discernible peak are included. For practicality, we assume the relationship between signal and concentration to be linear (i.e. of the form $y = b + m \bullet x^n$ where b and m are parameters of offset and slope, and $n = 1$). Hence the signals of individual fractions can be added together. The dilution factor is derived from Figure 3 in recognition that the programmed flow rate is not equal to the actual flow rate. Using the calibration curve equation of Figure 3, we note that a programmed flow rate of 3.0 mL/min gives an actual flow rate of about 2.56mL/min. So the concentrations of fatty acids in our fractions are diluted by a factor of 2.56 compared to the original 1.0 mL aliquots. When the peak signals for formic and acetic acid fractions are multiplied by 2.56 and compared to the data in Table 2.2, a recovery of 100% of the acids is calculated. The recovery of propionic acid is not as certain. When using peak area, a recovery of only 81.7% is measured. When using peak height, the recovery is 98.2%. The data in Table 2.2 are not absolute and show some variation. The shape of the propionic acid peaks is quite irregular with significant tailing, and this can likely account for the poor results when using peak area for calibrating this species. Both parameters, area and height, are thus proven to be reliable when performing analytical calibrations, though it appears a higher relative error is inherent for peak area than for peak height at lower concentrations due to differences in peak shape.

Hence, 100% peak recovery is proven to be possible for pure fatty acid standard solutions using the given HPLC parameters. At least for formic and acetic acids, column retention and "smearing" of compounds into the background signal are insignificant or non-existent.

Experiment 2

Figure 6 compares the recovery of standard acids from diluted stock solutions (not prepared on the HPLC) and from extracted fractions. The three individual acids had very comparable recoveries of 93 to 95%, meaning that 40 ppmC solutions were returning measurements of about 38 ppmC. Previous results from an earlier trial of this experiment gave close to 100% recoveries, so the deviations in this trial may have been due to an uncalibrated micropipette used to prepare the dilutions. Curiously, the mixture of standards ("cocktail") gave a result of just over 100%, so the error on the individual standards may instead be related to the TIC/TOC analyzer's performance.

Very similar results were obtained for the extracted acid fractions. The time windows used to collect each fraction were different and correlated to retention time. Formic acid was resolved from the HPLC column the quickest and was collected in an 80 second window. Acetic acid required 120 seconds. Propionic acid required 180 seconds. Hence if there were any contamination problems with the HPLC, they would be expressed as higher than expected apparent recoveries and increasing recoveries with retention time for each acid. Fortunately, we do not see any contamination problems. Recoveries of formic and acetic acids were almost identical to the standard solutions. Propionic acid yielded a lower result, confirming that the apparent loss of this acid in Experiment 1 was real and not simply an artifact of poor measurement or integration of the peak parameters. The recovery of the "cocktail" is expressed in Figure 6 as an average of the three acid fractions, and is about 12% lower than the recovery of the unextracted mixture. Because the mixture was used to generate the fractions instead of the individual stock solutions, there is a higher inherent error in comparing the results of individual acids before and after fraction collection. The good agreement in the results for formic and acetic acids is then, perhaps more coincidental, and the results of the mixture more accurately predict closer to 92% fraction recovery.

Figure 7 shows the ^{13}C isotopic data for the standard acids from stock solutions and from HPLC fractions. The results prove beyond reasonable doubt that there are no

isotopic effects related to the HPLC extraction and fraction recovery method. The results of the two acetic acid samples deviate by 0.58‰, and this is still within the analytical uncertainty of the IRMS (± 0.3‰ per sample). The other two acids show deviations of less than 0.1‰. Furthermore, the calculated per-mil value of the mixture (based on the values of the three separate acids) and the actual $\delta^{13}C$ measurement of the "cocktail" differ by only 0.06‰. The average isotopic value of the three fractions appears in Figure 7 as the calculated value of the mixture. A physical measurement of this could only be accomplished by literally combining the extracted fractions, and this was not feasible.

Experiment 3

The acetic acid standards prepared in deionized water and in soil "broth" were analyzed on the HPLC using both column and sample loop combinations (i.e. large column with 1.0 mL sample loop; small column with 20 μL sample loop). The results are shown in Figure 8 along with best fit power correlation equations. For the large column and sample loop combination, the standard prepared in soil broth gave larger results with a lower coefficient of correlation (R^2) than the standard prepared in deionized water. A repeat of this experiment gave very similar results (not shown). When the experiment was repeated using the smaller column and sample loop, both standards gave very good and very similar correlations. The soil broth standard had been refrigerated for at least two weeks prior to injection in the latter trial, so it was not as "fresh" as when it was previously injected on the large column. The results for the large column cannot be easily explained. It should be noted that the larger sample loop used with the preparative column is 50 times larger than the smaller sample loop, while the flow rates used between the two configurations differ by a factor of 3. So a larger ratio of sample to carrier reaches the column for the larger sample loop, and this may induce a more complicated interaction between acetic acid and other organic compounds (if present) with the column's stationary phase. What is clear from the results is that organic-rich samples cannot be analyzed quantitatively with as much certainty using the larger column and sample loop, and comparing such samples with data from pure standards leads to significant errors.

The bacterial matrix solution "methbuff" was analyzed separately for acetic acid, and the concentration was calculated to be 6.8×10^2 ppmC (or 1.7×10^3 ppm). A 1 mL aliquot was also extracted on the HPLC and the acetic acid fraction was collected and analyzed on the TIC/TOC. The TOC concentration of the fraction (corrected for dilution) was measured at 7.5×10^2 ppmC. Previous investigation on this bacterial culture solution has shown that there is background organic carbon that elutes from the HPLC column just before the acetic acid time window used for fraction collection, so the slightly larger TOC result may be due to an overlap of organic phases eluting from the column. Background levels of TOC from the HPLC carrier acid showed concentrations no higher than 2 ppmC, and since the collected fractions are diluted with deionized water to 40 mL to fit the TIC/TOC autosampler vials, the contribution of HPLC background TOC is almost zero. The ^{13}C-isotopic composition of the "methbuff" acetic acid fraction was measured to be -49.2‰ ± 0.3‰ VPDB.

The isotopic data for organic-rich samples and standards gave very good results shown in Figure 9. For comparison purposes, the $\delta^{13}C$ datum for pure acetic acid is shown (and was measured to be -37.68 ± 0.3‰ VPDB). The average $\delta^{13}C$ of two fractions extracted from the acetic acid "broth" is -37.34 ‰ VPDB, giving a difference that is only just beyond the analytical error of the IRMS.

The 7:1 mixture of "methbuff" extract to 4,000 ppmC acetic "broth" has a calculated acetic acid concentration of 1.1×10^3 ppmC (or about 2.7×10^3 ppm). So 55% of the acetic acid in the mixture is from "methbuff" and 45% is from the standard "broth". Using the measured $\delta^{13}C$ values for these two end members in an isotopic mass balance calculation, an expected $\delta^{13}C$ value of -44.25‰ is calculated for the mixture. The expected and measured isotopic values are shown in Figure 9. The measured $\delta^{13}C$ of -43.96‰ is an average of two measurements with a mean deviation of 0.01‰. So the results are within the analytical error associated with the IRMS.

Conclusions

Clearly, the HPLC methodology developed herein is suitable for sustaining organic compound integrity when extracting short-chain fatty acids as fractions from both simple and complex aqueous matrices. It is feasible to recover 100% of a peak using a fraction collector provided that there is no partial-retention of the compound on the column. The difference in isotopic (^{13}C) composition between unextracted and HPLC-separated fractions of the same fatty acid compounds is within the accepted analytical error of a functional mass spectrometer meeting operational specifications. This is true of both pure standards and natural samples containing a large diverse component of DOM. However, for performing quantitative analyses, it is still best to use standards that are prepared specifically to match the compositional matrix of the samples for which a calibration curve is intended. Moreover, a smaller sample loop for injection has shown to produce a calibration curve with a better correlation.

The chromatographic separation method eliminates the need for complicated chemical methods that are time-consuming and laborious, and that also add other compounds to samples, thereby compromising sample integrity. The main limitation on this methodology is with the carrier solvent used for HPLC separation. The TIC/TOC analyzer performs bulk carbon analyses and hence does not discriminate between different components in a given fraction, so carbon-based solvents cannot be used in preparing fractions for this instrument. Moreover, an abnormally large TIC or TOC component in a sample may have a "memory effect" on the next sample as the instrument's procedure is made up entirely of time events, not peak events.

More research needs to be performed to develop additional HPLC methods specific to other organic compounds of interest and to further validate chromatographic separation and fraction collection as a viable process for routine sample preparation for compound specific isotopic analysis using established TIC/TOC-IRMS technology.

Acknowledgements

This research project was funded by NSERC Research Grant 42590 to I.D.Clark and by a research bursary (PGS-B) provided to M. Marschner. Analyses were performed at the G. G. Hatch Stable Isotope Laboratories, Ottawa, Carleton Geoscience Centre, University of Ottawa, and we are most grateful to G. St. Jean, W. Abdi, and P. Wickham for their help, expertise and many suggestions. Much appreciation is also given to Dr. D. Fortin for her guidance and the use of her facilities, and to Graham Hughes and his support team at Graden Instruments Inc for their help in setting up our liquid chromatography system.

References

Blair NE, Carter Jr WJ (1992) The carbon isotope biogeochemistry of acetate from a methanogenic marine sediment. *Geochim Cosmochim Acta*. **56**: 1247-1258.

Conrad R (1999) Contribution of hydrogen to methane production and control of hydrogen concentrations in methanogenic soils and sediments. *FEMS Microb. Ecol.* **28**: 193-202.

Fey A, Conrad R (2000) Effect of temperature on carbon and electron flow and on the Archaeal community in methanogenic rice field soil. *Appl. Environ. Microb.* **66**: 4790-4797.

Molina M, Cox J, Burke RA (1999) Examination of sedimentary microbial lipids using compound specific isotopic analysis to determine carbon transformation along an estuarine continuum. ASLO Aquatic Sciences Meeting, Santa Fe, SS32-II.

St-Jean G (2003) Automated quantitative and isotopic (13C) analysis of dissolved inorganic carbon and dissolved organic carbon in continuous-flow using a total organic carbon analyser. *Rapid Commun. Mass Spectrom.* **17**: 419-428.

Thiel V, Peckmann J, Seifert R, Wehrung P, Reitner J, Michaelis W (1999) Highly isotopically depleted isoprenoids: Molecular markers for ancient methane venting. *Geochim. Cosmochim. Acta*. **63**: 3959-3966.

Waldron S, Watson-Craik IA, Hall AJ, Fallick AE (1998) The carbon and hydrogen stable isotope composition of bacteriogenic methane: A laboratory study using landfill inoculum. *Geomicrob.* **15**: 157-169.

Yavitt JB, Williams CJ, Wieder RK (1997) Production of methane and carbon dioxide in peatland ecosystems across North America: Effects of temperature, aeration, and organic chemistry of peat. *Geomicrob. J.* **14**: 299-316.

Table 2.1 : Details of Standard Acids Used

reagent	formula	purity	MW* (g / mol)	% carbon	working standard concentration		$\delta^{13}C$ ‰ VPDB
					ppmC	ppm	
formic acid	HCOOH	0.98	46.03	26.09	4000	$1.53x10^4$	-18.90 ± 0.33
acetic acid	CH_3COOH	0.998	60.05	40.00	4000	$1.00x10^4$	-38.02 ± 0.27
propionic acid	CH_3CH_2COOH	0.99	74.08	48.64	4000	$8.22x10^3$	-29.22 ± 0.08
butyric acid	$CH_3CH_3CH_2COOH$	0.99	88.11	54.52	4000	$7.34x10^3$	-27.87 ± 0.04

* molecular weight

Table 2.2: Raw signal data of fatty acids separated on the HPLC column

Reagent	Signal (area)	Signal (pk height)
formic acid	26658.7	1037.1
1000ppmC	26290.5	1009.0
	26189.8	1009.6
average:	**26379.7**	**1018.6**
acetic acid	6848.6	216.4
1000ppmC	6665.2	209.4
	6653.6	209.0
average:	**6722.5**	**211.6**
propionic acid	6119.9	80.4
1000ppmC	6535.0	82.6
	6494.6	80.6
average:	**6383.2**	**81.2**

Table 2.3: Signal data from fractions re-extracted on the HPLC column

fraction (minutes)	SIGNAL (peak area)			SIGNAL (peak height)		
	formic	acetic	propionic	formic	acetic	propionic
6 to 7	10108.5			390.0		
7 to 8	255.1			9.0		
8 to 9	3.1	2035.6		0.6	63.7	
9 to 10		614.4			19.2	
17 to 18			1210.8			18.4
18 to 19			827.9			12.8
total	10366.7	2650.0	2038.7	399.6	82.9	31.2
dilution factor	**2.557**	**2.557**	**2.557**	**2.557**	**2.557**	**2.557**
corrected total	26507.4	6776.0	5212.9	1021.8	212.0	79.8
% recovery	100.5	100.8	81.7	100.3	100.2	98.2

Chapter Three

Biogenic Carbonate Deposits: A Field Investigation Presenting Isotopic and Hydrogeochemical Data From a Periglacial Limestone Terrain, Inuvik, Northwest Territories

by

Mark Marschner

Abstract

Unique biogenic carbonate deposits ("endostromatolites") are found ubiquitously in periglacial limestone terrains across Canada's cold climate regions. They preserve some interesting isotopic signals that have been used as paleoenvironmental indicators for past climate change. The enriched $\delta^{13}C$ signals could only have been produced by anaerobic bacteria. Two groups of microorganisms are capable of selectively using $^{12}CO_2$ and thereby enrich residual dissolved inorganic carbon (DIC) in ^{13}C: methanogenic and acetogenic bacteria. The feasibility of these bacteria and the actual processes they use are investigated using theoretical models and hydrogeochemical data from groundwaters within a limestone terrain where endostromatolites are found. The Rayleigh enrichment models predict ^{13}C-isotopic enrichments similar to actual $\delta^{13}C$ measurements from microsampling growth columns in well-preserved samples. Acetogenic bacteria are shown to be more capable at fractionating DIC per equivalent of DOC (dissolved organic carbon) consumed despite having a lower fractionation factor for reacting CO_2 and H_2. The model also predicts that contributions of dissolved ^{14}C-free limestone become more significant to the DIC pool proportional to the increased activity of acetogenesis. Actual measured $\delta^{13}C$ signals from endostromatolite growth columns show strong enrichments as predicted by the model, but transport of products from the system may play a significant role in limiting that enrichment during emplacement.

Field results show that organic decomposition and production of biogenic CO_2 in soils outweighs other bacterial processes such that the sites with the highest methane concentrations had the lowest $\delta^{13}C_{DIC}$ values. Fermentation may outweigh CO_2-reduction as the dominant methanogenic reaction pathway, thereby running contrary to the Rayleigh distillation model and contributing ^{13}C-depleted DIC to solution rather than preferentially consuming $^{12}CO_2$. Geochemical data show that methane is being generated at sites containing abundant SO_4^{2-} and low levels of dissolved oxygen such that Eh measurements do not accurately predict the processes that are occurring at the field sites. Since modern periglacial environments do not favour ^{13}C-enrichment of DIC over time, experimental work with natural cultures from frozen soil is required to assess the

importance of the Rayleigh distillation model in proving that enriched ^{13}C sisnals from endostromatolites are due to biogenic processes fractionating DIC.

Introduction

Periglacial limestone terrains are host to some unusual secondary carbonate deposits. Commonly referred to as "endostromatolites", these calcretes are found within limestone fissures and exhibit features that are indicative of unique growth conditions Clark *et al.*, 2004). They occur as semi-continuous layers of clustered columns (see Figure 10). The columns propagate orthogonally to the fissure surfaces on which they are attached (see Figure 11). Columns exhibit a great abundance of sizes and morphologies. They can be less than 100 microns to more than 3 centimetres tall with a range of diameters that make them thin and delicate or more robust. They can form tight clusters, giving some specimens a typical cauliflower texture, or be much more sparsely distributed. Some endostromatolite deposits contain two or more "stacks" of columns, meaning that the tops of the columns forming one distinct layer became the growth surface on which a subsequent layer of columns grew. Porosities of endostromatolites also show large variations. Intra-columnar spaces can remain empty or be filled with secondary cements. Porosity typically decreases away from the fissure surface as growth columns take on more dendritic growth forms (i.e., smaller growth columns branch out from the original "stem", like branches on a tree).

Exposed endostromatolite outcrops are prone to alteration from being in contact with Earth surface processes. Tall, delicate columns with little occluding cement are particularly vulnerable compared to densely-clustered columns and/or well-cemented deposits. Well-preserved specimens exhibit distinct microstructures when examined in thin sections cut along growth columns. Dark and light bands are organic-rich and organic-poor zones and are evidence of a biogenic origin. These bands are stacked upward, probably indicative of optimal growth conditions farther away from the contact surface on which the columns are attached (i.e., growth did not occur concentrically over the entire column surface like tree rings).

Endostromatolites are found exclusively within limestone fissures. They have never been witnessed on exterior outcrop surfaces; only where weathering and

anthropogenic activity have opened up a fracture can they be seen on an open surface. Even then, the distribution of endostromatolites throughout an outcrop and even within a fissure is far from uniform. Without exception, growth columns are found on one side of the fracture only. Many fractures containing growth columns exhibit a dissolution surface on the side opposite of growth, and moreover, the dissolution surface often expresses the "cauliflower" texture of the growth clusters but in reverse. These compelling observations are good evidence for very different geochemical processes occurring simultaneously across limestone fractures.

Endostromatolite-filled fractures tend to be found on southward exposures. Fissures on northward-facing exposures are usually void of any secondary deposits. Moreover, the side of the fracture where growth occurred is invariably the southward side or, for horizontal fractures, the upper side. Using the terminology of structural fault systems, growth is seen invariably on the "hanging wall" side of the rupture as opposed to the "footwall" side. Finally, endostromatolites have been observed only within the top few metres of outcrops. No deposits were seen at greater depth at several limestone quarries examined. Hence it appears that endostromatolites confine themselves to the outermost "layer" of limestone outcrops, settling in small spaces sheltered from the surroundings and yet seemingly in favour of certain conditions originating from these surroundings.

All of these observations lend support to a strong biogenic origin for endostromatolites. Solar radiation in northern regions reaches the surface at a low angle on southern exposures. Northern exposures receive almost no sunlight throughout the year except in the extreme north where the sun hovers over the horizon during the summer. However, it is not known what conditions on the "hanging wall" side of fractures along southward-facing exposures are directly or indirectly responsible for preferential endostromatolite growth.

Previous research has determined that growth within limestone fissures occurred under saturated anaerobic conditions (Clark *et al.*, 2004). This means that fractures were

filled with water and lacked direct contact with the atmosphere. Drainage and exposure of the fractures since endostromatolite emplacement prevent continued growth, and as such, no actively-forming deposits have been witnessed *in situ*. Well-preserved endostromatolites have been used as paleoenvironmental indicators since they grew in equilibrium with meteoric waters, and hence the ^{18}O-signal of carbonate preserves a signal of past climate temperature. Interpretation of the ^{13}C-signal from endostromatolites is not straightforward. Many well-preserved fissure deposits show increasing ^{13}C enrichment along growth columns away from the host rock surface. Methanogenic activity has been invoked as a probable cause for the enriched carbon signal (Lauriol and Clark, 1999; Clark *et al.*, 2004).

^{14}C-age dating requires knowledge of carbon inputs for accuracy. It is assumed that 50% of carbon in dissolved inorganic carbon (DIC) is from the host rock and 50% is derived from dissolved organic carbon (DOC) transported into the fracture environment. While methanogenic bacteria are known to strongly fractionate carbon substrates favouring ^{12}C in their products, the significance of their activities and those of other microorganisms during the decomposition of organic matter in cold climate environments are largely unknown.

Currently, northern periglacial regions are a major source of methane to the global methane flux despite sub-freezing temperature conditions through most of the year (Martens *et al.*, 1992; Hines *et al.*, 2001). Methanogenic bacteria may not be favoured by the difficult growth conditions of periglacial regions as much as other bacterial groups are inhibited by restricted access to nutrients and electron donor compounds. Despite brutally cold conditions during long winters in many northern regions, the microorganisms that inhabit these areas return to productivity every year. Not surprisingly, then, periglacial soils brought back to the lab and preserved by freezing produce active methanogenic cultures once they are "revived".

Climate signals from endostromatolites show that northern regions were significantly warmer thousands of years ago compared to today (Clark *et al.*, 2004). This

implies that talik (i.e., thawed areas within permafrost) was much more widespread and allowed greater groundwater circulation. The microorganisms in tundra soils at present were likely present when endostromatolites were being formed. Hence it is useful to study and compare historical carbonate deposits and modern natural materials to determine which processes were significant in creating endostromatolites.

The following investigation presents some preliminary results obtained from natural materials collected from northern landscapes where endostromatolites occur. An initial examination of the ^{13}C-signals directly from endostromatolites will provide new data to compliment previous research and will serve as the basis for a discussion of the theoretical origin of these signals. The second half of this investigation focuses on aqueous geochemical data of surface and ground-waters from present-day periglacial limestone terrains. Though the present climate in Canadian northern regions is different than it was in the past, analysis of aqueous environments in modern limestone terrains where endostromatolites grew in the past provide a preliminary basis to begin assessing how these secondary deposits came to be. The knowledge gained from these field studies will serve as the basis for more in-depth investigations using bacterial cultures and the development of new analytical methodologies.

Endostromatolites

Field locations

Hand specimens of endostromatolite carbonate deposits were collected from several periglacial field locations. Samples designated "O-1" and various similar acronyms starting with the letter O were taken from the Ogilvie Mountains in central Yukon Territory, Canada (see Clark *et al.*, 2004). Other samples designated as "IC-4" came from a limestone quarry near the Inuvik airport. No groundwater and surface water sampling was performed in this particular region.

A more extensive sampling protocol for soil, water and rock samples was undertaken in a small limestone-dolostone suite to the south and east of Inuvik, Northwest Territories, Canada. The Campbell Uplift (approximately 68° 15' N, 133° 20' W) is a peculiar carbonate formation previously described by Dyke (1975) and Ritchie (1976). The largest portion of this formation outcropping at the surface lies to the north and west of Campbell Lake. The Dempster Highway runs through the northernmost tip of the Campbell Uplift, and then follows the eastern shoreline of Campbell Lake as it turns southward. Small outlier carbonate deposits from the same formation are found along the highway to the east of Campbell Lake and the highway. Sampling locations were set up at sites close to the highway (see Figure 12). Two periods of groundwater and surface water sampling were performed and are described in detail in the second half of this investigation dealing with aqueous geochemical data.

Hand Specimen Descriptions

An extensive array of hand specimens from the field locations described above was collected. Several specimens that demonstrate the best potential preservation were selected to be cut and made into thin sections. As the thin sections revealed, outward appearances can be deceiving in assessing alteration when you're not a carbonate specialist. Many thin sections showed growth columns with little or no discernable internal features and a micritic fabric indicative of dissolution and re-precipitation. These particular samples were not used for microsampling. Those samples that showed excellent microstructures such as internal layering were chosen for more extensive study.

Sample "O-1" contains a thick endostromatolite deposit more than 20mm tall and shows what appears to be several "layers" of columns (see Figure 13). There is much internal porosity throughout this sample section, and very little secondary carbonate is visible inside the pores. The contact with the host rock occurs at a very sharp boundary that resembles a stylolitic suture. No basal layer is apparent. It appears that dissolution occurred between the host rock and the overlying endostromatolite deposit, likely the result of weathering after emplacement. While the host rock well below the contact

surface is very dark with organic matter, the closest 1-2mm are much lighter by comparison.

Sample "O1-east" is a thinner endostromatolite deposit, ranging from 5-10mm tall, with simpler and more uniform growth column morphologies throughout (see Figure 14). In contrast to the previous sample, "O1-east" has a very significant basal layer that is continuous throughout the section and shows incredible light and dark banding. Below this basal layer, a thin, clear, micritic band sits between it and the host rock. Intracolumnar porosity is high with only minor sparry cement deposits within pores. The purple discoloration seen in Figure 14 is not authentic to the sample, and probably originated during impregnation of the sample with epoxy prior to cutting of slabs.

Sample "IC-4" is the most unique sample of the three. Individual columns are not discernible and the endostromatolite deposit, varying in thickness from a few millimetres to over 1cm, appears uniformly ambiguous throughout (see Figure 15). The basal layer is thin (generally less than 1mm) but more or less continuous. Light and dark banding is quite subdued. Internal porosity is low due to widespread cementation. No alteration rims are evident anywhere and the endostromatolite appears to have a high organic matter content based on its colour index, reducing the likelihood that leaching and recrystallization occurred.

Microsampling

A Merchantek MicroMill solid sampling system (New Wave Research) was used for the drilling of the thin sections. This instrument is equipped with a video microscope, motorized stages, and a drill with video camera. Operation of the instrument is achieved using the Merchantek EO MicroMill System software installed on a computer interfaced with the instrument. The software can automate the drilling process, but all calibrations and drilling functions were performed manually.

The purpose of sampling the endostromatolite thin sections using the microdrill apparatus is to measure the ^{13}C-isotopic composition of endostromatolite deposits along the length of growth columns. Each thin section was inspected closely and a single column from each sample was chosen for drilling. As discussed above, sample "IC-4" contains ambiguous microstructures, and individual columns could not be discerned. Drilling of this sample was done at a more-or-less arbitrarily chosen location.

After mounting a thin section in place on the stage, the drill was carefully lowered until it contacted the surface. Vertical and lateral displacement of the drill bit occurred in steps of 15μm. Only one hole was drilled at a time. The powder was collected using a flat-edged metal spatula to amass it together at the edge of the thin section before tapping the powder into a 10mL glass Exetainer vial. The procedure was repeated at regularly-spaced intervals. For samples "O1-east" and "IC-4", holes were made about 1mm apart. For the much larger "O-1" sample, holes were drilled at 2mm intervals. The thin section surface and the drill bit were wiped with Kimwipe tissues to remove any residual powder between holes.

Static electricity on the drill bit and on the Exetainer vials made sample recovery far from perfect and the total quantity of powder recovered from individual holes varied considerably. In the end, very few vials contained enough powder to derive an isotopic result, and the ones that did were just above the detection level but below the instrument calibration range. So it was decided to sample thick sections instead of thin sections. Thick sections are not mounted on glass slides; they are just slabs of rock about a centimetre thick and they are not polished. However, before slicing the slabs, epoxy was applied to the top surfaces to prevent the delicate columns from disintegrating.

Powders from thick sections were collected using the same procedure as the thin sections, i.e., a metal spatula was pushed across the surface to make transfer of the powder into an Exetainer vial simple. Greater amounts of powder were generated than with the thin sections. Average drilling depth was 60μm. Thin sections, by comparison, are usually only 30μm thick. Contamination from drilling too deep was not a great

concern. Columns in two of the three samples are spaced far apart, and pores contained far more epoxy from sample impregnation than intraporous carbonate cements. Epoxy contamination of samples, if they occurred, is not expected to change the isotopic results of analyses given the slow reaction of phosphoric acid with organic compounds at 25°C. For sample "IC-4", the material was assumed to be more-or-less laterally homogeneous given the lack of regular internal structures. A possible minor contamination of samples may have occurred when the metal spatula pushed across the surface of the thick section to collect the powders could have "shaved off" more powder in the process. This represents a possible source of random error of unknown magnitude

Isotopic Analyses

Carbon and oxygen isotopic composition of calcrete sample powders were measured with a Thermo Finnigan DeltaPlus XP continuous-flow gas-isotope mass spectrometer interfaced with a Thermo Finnigan GasBench II. With the Exetainer vials containing the samples sitting horizontally, 0.1mL of 100% phosphoric acid was added at the open end away from the powder at the bottom, and then the vials were sealed and flushed with pure helium gas. At the time of analysis, the vials were tipped vertically and put into the sample block where the powder would mix with the acid at 25°C and equilibrate for 24 hours. The headspace of each vial is sampled with a two-way needle. The CO_2 in the headspace is separated from N_2 and other gases on a Poraplot Q packed capillary column. Each sample analysis generates 8 measurements measured against 4 reference pulses. Three calcite standards were likewise prepared and run in the same batch such that the samples are calibrated against these standards for greater accuracy. Isotopic data are reported in standard per-mil (‰) notation versus universal standards VPDB and VSMOW:

$$\delta^{13}C_{sample} = \left[\frac{R_{sample} - R_{VPDB}}{R_{VPDB}}\right] \times 1000 \text{ ‰}$$

$$\delta^{18}O_{sample} = \left[\frac{R_{sample} - R_{VSMOW}}{R_{VSMOW}}\right] \times 1000 \text{ ‰}$$

where R is the isotopic ratio ($^{13}C/^{12}C$ or $^{18}O/^{16}O$). The instrument gives results with an accuracy of ± 0.3 ‰. Precision of the 8 measurements per sample is often less than ± 0.1 ‰.

Results

Figures 16, 17 and 18 show the results of isotopic analyses performed on the endostromatolite thick sections O-1, O1-east and IC-4, respectively. Images of the actual sections after they were sampled are shown beside the graphs. Drilling was done twice per section, but no results were obtained from the first set because of an instrument malfunction. The vertical scales in Figures 16 to 18 are quite different and hence the data from each section are presented separately.

The boundary between the endostromatolite growths and the host rock was defined as 0 and the height of each drill hole is measured versus this reference. One hole in each section was drilled below the boundary in the host rock. Measured values for ^{13}C of the host rock in all three sections were between -3 and 0‰ VPDB, within the accepted limits of marine limestone. ^{18}O data for the host rock ranged between 20 and 25‰ VSMOW. The ^{13}C and ^{18}O data for the endostromatolites are similar to results obtained by Lauriol and Clark (1999). In all three sections, ^{13}C is enriched and ^{18}O is depleted in the growth columns compared to the host rock.

Each section has a unique trend in isotopic data. In sample O-1, the carbon data show some scatter, with $\delta^{13}C$ values ranging from +4 to +13‰ VPDB. The two most enriched carbon data were generated from small powder samples that produced peaks below the calibration range of the mass spectrometer but above the detection limit. The ^{18}O data show much less scatter with values around +15‰ VSMOW throughout the profile. No anomalous ^{18}O results are apparent relative to the peak sizes, so the strongly

enriched $\delta^{13}C$ values cannot be discounted. In particular, the sample hole drilled third from the top is located within a lightly-coloured laterally-continuous band (~2-3mm thick) that is obvious in Figure 16. The strongly-enriched $\delta^{13}C$ signal measured within the light band may be due to a decreased importance of organic matter in the original growth environment at the time of emplacement.

In sample O1-east, the $\delta^{13}C$ and $\delta^{18}O$ signals are very consistent from bottom to top, varying by no more than 2‰. Only at the very top of the profile does carbon become slightly less enriched and oxygen becomes slightly more enriched; otherwise the two sets of isotopic data show a good correlation. No holes were drilled in the thick basal layer showing considerable banding.

In sample IC-4, there is a well-defined enrichment trend for ^{13}C and ^{18}O. In fact, the enrichment of ^{18}O from the contact surface to 6mm above it is twice as strong as for ^{13}C. More precisely, $\delta^{18}O$ values climb from +15.4‰ to +19.5‰ VSMOW, while $\delta^{13}C$ values rise from +0.3‰ to +1.8‰ VPDB. At more than 6mm from the contact surface, $\delta^{13}C$ values start to climb by much greater steps while $\delta^{18}O$ values drop. There are no visual clues from the thin or thick sections of sample IC-4 to suggest any compositional variations.

Discussion

The origin of endostromatolites has previously been explored in-depth by Clark *et al.* (2004). Carbon age-dating techniques used with organic and inorganic fractions of endostromatolite samples have determined that deposits within limestone outcrop fissures located in Arctic periglacial terrains are relatively young, though emplacement may have occurred over thousands of years since the end of the last major North American glaciation event (~13,000 years b.p.). Given these long reaction times, $\delta^{18}O$ data from endostromatolites provide a potentially very good paleotemperature signal since oxygen from CO_2 equilibrated with oxygen from meteoric H_2O. However, there is a danger of creating a circular argument if the $\delta^{18}O$ signals are, in turn, used to interpret carbon

cycling processes. The $\delta^{13}C$ signals from endostromatolites offer some insights into carbon cycling that may help to improve interpretation of paleotemperature data.

Limestone dissolution and precipitation in natural depositional settings is commonly expressed as a *disproportionation* reaction or acid-base reaction as follows:

$$CaCO_3 + CO_2 + H_2O \leftrightarrow Ca^{2+} + 2HCO_3^- \quad (3\text{-}1)$$

Where CO_2 is a weak acid that dissolves in and reacts with water, i.e.:

$$CO_{2(g)} \leftrightarrow CO_{2(aq)} \quad (3\text{-}2)$$

$$CO_{2(aq)} + H_2O \leftrightarrow HCO_3^- + H^+ \quad (3\text{-}3)$$

Thus the composition of DIC (dissolved inorganic carbon) in equilibrium with limestone in a closed system is 50% derived from limestone, 50% derived from CO_2 (i.e., atmospheric CO_2, biogenic CO_2, etc). The above reactions overwhelm the low solubility of limestone in pure water:

$$CaCO_3 + H_2O \leftrightarrow Ca^{2+} + HCO_3^- + OH^- \quad (3\text{-}4)$$

While CO_2 is a ubiquitously weak acid in natural environments, organic acids produced from the decomposition of organic matter may be significant in the carbon cycle.

The decomposition of organic matter produces acetic acid, CO_2 and H_2 in a ratio of 1:4:8 (Clark *et al.*, 2004; based on Klass, 1984; see Appendix 1). Acetic acid is a stronger acid than CO_2, and we can assume that the reaction of acetic acid with limestone is spontaneous in liberating more DIC to solution, i.e.,

$$CaCO_3 + CH_3COOH \leftrightarrow Ca^{2+} + HCO_3^- + CH_3COO^- \quad (3\text{-}5)$$

Based on the given ratio of products from organic matter decomposition, the resultant DIC in solution would be about 55% from limestone. The presence of homoacetogenic bacteria will alter the ratio of products greatly:

$$2CO_2 + 4H_2 \rightarrow CH_3COOH + 2H_2O \qquad (3\text{-}6)$$

Acetogenic activity makes it possible for 100% of organic matter to be converted to acetic acid, thus reducing organically-derived inputs of CO_2 to the DIC pool to theoretically negligible levels.

Solid organic matter extracted from endostromatolites and analysed by NMR and radiocarbon techniques was shown to be about 50% derived from modern materials (Clark *et al.*, 2004). These results support the initial hypothesis that endostromatolite deposits are at least partially derived from the host rock (versus the null theory that the deposits merely fill void space within the rocks and that they originated exclusively from outside of the fractures). Still unclear, though, is the relative abundance of limestone-derived DIC in the total DIC pool, called the "dilution factor". When an equivalent of CO_2 reacts with an equivalent of limestone to create 2 equivalents of DIC as shown by reaction (3-1) above, the dilution factor is 0.5 . Clark *et al.* (2004) suggest a dilution factor of 0.6 for their numerical modelling of carbon age data, citing a small but significant input from "open system conditions". Such an assumption conflicts with their previous assumption of closed-system anaerobic conditions in the depositional setting. Microorganisms capable of fractionating substrates and enriching residual DIC in ^{13}C, namely methanogenic and acetogenic bacteria, are obligately anaerobic microorganisms, meaning they should not be capable of growth in the presence of oxygen. In summary, methanogenic bacteria are capable of two distinct reaction pathways. The hydrogenotrophic pathway utilizes molecular hydrogen and is most commonly expressed as CO_2-reduction:

$$CO_2 + 4H_2 \rightarrow CH_4 + 2H_2O \qquad (3\text{-}7)$$

The fermentation pathway lacks hydrogen and must utilize partially reduced substrates (i.e., organics) to derive energy from disproportionation, such as in the fermentation of acetic acid:

$$CH_3COOH \rightarrow CH_4 + CO_2 \qquad (3\text{-}8)$$

The main acetogenic pathway is shown above in reaction (3-6).

There are many variables in the depositional setting of endostromatolites that complicate the determination of an appropriate dilution factor. The presence of "young" carbon in the solid organic fraction preserved in endostromatolite carbonate materials suggests that the aqueous fissure environment was organic-rich. Soily material within horizontal fissures where endostromatolites grew was observed at one particular field location (SQ- see Figure 12). No age dating of the soily material at site SQ was attempted to determine if it was emplaced during endostromatolite growth or at a later time. An in-situ source of organic matter decomposition would generate CO_2 and acetic acid that would react directly with the host rock. The resulting dilution factor would depend on the rates of reaction and of transport of dissolved compounds both in and out of the system. These parameters are largely unknown and would be difficult to estimate. Limestone fissures are dynamic three-dimensional networks covering large surface areas. Some endostromatolites grew within fissures close to the outcrop surfaces while others grew deeper (i.e., up to several metres) within the rock mass. Hence flow-through conditions varied from one location to another. For example, groundwater entering a fissure may have been initially undersaturated with respect to calcite, and reactions with the limestone increased [DIC] and the saturation index and altered the aqueous geochemistry along the fracture flowpath. The ^{13}C-isotopic composition of DIC also changes during equilibration. Hence the dilution factor of 0.6 suggested by Clark *et al.* (2004) should be interpreted as an overall average. If a groundwater is recharged by meltwaters through carbonate-free soils, more than 60% of the DIC in solution could be organically derived and thus radiogenically active. The presence of old carbonate phases

will contribute proportionally more "old" carbon to the DIC pool before it reaches the limestone fractures.

The carbon isotopic profiles along growth columns of three different endostromatolite deposits (see Figures 16 to 18) show very different trends of ^{13}C-enrichment. These results suggest that many variables in the growth environment were simultaneously at play and that endostromatolites are capable of growth in a variety of conditions. Conversely, if a narrow range of conditions were necessary for continued growth, a similar pattern of results would have been expected from all three profiles examined. Section O-1, the tallest endostromatolite sample of the three, shows considerable variation in $\delta^{13}C$ values but no distinct trend toward higher or lower ^{13}C-enrichment along the profile. These results may indicate very episodic carbonate precipitation under changing conditions throughout growth history. Section O1-east also lacks an enrichment trend, but there is less variability in $\delta^{13}C$ values, inferring episodic or constant growth under more stable conditions. Section IC-4 shows two phases of ^{13}C-enrichment. $\delta^{13}C$ values increase slowly through the earliest growth stages, then accelerated during later growth. This section most clearly resembles a Rayleigh-type distillation of DIC occurring with sustained growth at different rates under evolving conditions in the growth environment. The lack of very distinct growth banding in this sample could be evidence of a less sporadic, more continuous growth history and not merely the destruction of the original layering by secondary alteration processes.

When a chemical reaction produces an isotopic fractionation between reactants and products, the isotopic composition of the reactant is said to be undergoing a Rayleigh distillation. The Rayleigh distillation model is summarized by the following equation:

$$R = R_o \bullet f^{(\alpha-1)} \qquad (3\text{-}10)$$

where R is the isotopic ratio ($^{13}C/^{12}C$) of the reacting compound, R_o is the initial ratio (before reaction), f is the dimensionless residual amount of the reacting compound (where $0 \leq f \leq 1$), and α is the isotopic fractionation factor. When $\alpha=1$, $R = R_o$ and no isotopic

fractionation results. When the product of reaction favours ^{12}C, the reactant becomes enriched in ^{13}C. In this case, $\alpha < 1$ and R increases inversely with respect to *f*. Such is the case with methanogenesis and acetogenesis. These microorganisms have a strong predilection for $^{12}CO_2$, and hence they produce isotopically light products. The isotopic fractionation factor for CO_2-reduction by methanogens (reaction 3-7, above) is 0.934 at 25°C, meaning that methane generated by this reaction is depleted by about 70‰ versus CO_2 (Clark and Fritz, 1997). Autotrophic acetogenesis produces a similar fractionation (calculated as 0.941 at 30°C based on the results of Gelwicks *et al.*, 1989).

Terrestrial methanogenesis is assumed to be largely aceticlastic (i.e., fermentative; see reaction (3-8) above) (Whiticar *et al.*, 1986). However, acetate fermentation is a reaction that produces CO_2, and any contribution to the DIC pool from organic matter will impart an isotopic depletion since tundra vegetation is largely composed of C-3 plants ($\delta^{13}C$ = -28 to -26‰ VPDB). Organic decomposition of cellulose from C-3 plants is not expected to impart a large fractionation on any products, including acetate. So if methanogenesis is a viable bacterial process in the formation of endostromatolites, the hydrogenotrophic pathway would be the only process that could impart a significant ^{13}C-enrichment on DIC. Recent research indicates that acetate is accumulating in modern periglacial terrains, with transient losses resulting from aerobic decomposition during dry conditions (Hines *et al.*, 2001).

Previous research focusing on the intracellular cycling of acetate by methanogens raises some possible concerns of negative feedback signals on the DIC pool even when production is via the hydrogenotrophic pathway. Radiolabelled acetate was used in experimental incubation systems performed by Krzycki *et al.* (1982) and Baresi (1984) to show that $^{14}CO_2$ was produced as a result of methyl group oxidation of acetate during growth of *Methanosarcina barkeri* on various substrates. Acetate is an important intermediary compound in the process of methane production, and the results demonstrate potential isotopic mixing of CO_2 and acetate. So it is conceivable that isotopic enrichments of DIC incurred during CO_2-reduction could be marginalized or even reversed by acetate decarboxylation within methanogenic bacteria. Coincidently,

DNA sequencing was used to determine that bacteria cultured from periglacial soil samples, collected from a limestone terrain where endostromatolite occur commonly, are closely-related to several strains of *Methanosarcina*, including the extensively-studied organism *M. barkeri* (Marschner, unpublished data). *M. barkeri* is a versatile organism capable of growth on a wide variety of substrates. Studies have shown that *M. barkeri* prefers most substrates over acetate (for example, see Hutten *et al.*, 1980; Baresi, 1984), and that its adaptability to grow on acetate is constrained by its ability to synthesize large amounts of carbon monoxide dehydrogenase (CODH) (Krzycki *et al.*, 1982). Other research shows that acetogenic bacteria have a competitive advantage over methanogens for competitive substrates at low temperature (Conrad *et al.*, 1989; Fey and Conrad, 2000). Moreover, *M. barkeri* appears to have a lower affinity for acetate at low temperatures (Fey and Conrad, 2000). Although methanogenic bacteria are found to exist in certain environments, they may not be active under certain conditions, and results of experimental incubations tend to corroborate the published findings (see Chapter 4).

Rayleigh-type distillation numerical models can help to constrain the unknown variability of methanogenic versus acetogenic processes on ^{13}C-enrichment of DIC. Suppose we have a closed system where water is in contact with limestone and no gas phases are present. The temperature is 4°C. The initial concentration of DIC is 1.2ppmC (parts per million carbon), the $\delta^{13}C$ of DIC is 0‰ VPDB, and the water is at saturation with respect to $CaCO_3$. The initial dilution factor is 0.5 (i.e., half of the DIC present is derived from the limestone itself). The carbon isotopic composition ($\delta^{13}C$) of DOC in the water is -26‰ VPDB, and that of limestone is 0‰ VPDB. Organic matter (CH_2O) decomposition generates H_2, CO_2 and acetic acid in a ratio of 8:4:1. CO_2 equilibrates isotopically with DIC. Acetic acid reacts with limestone to release more radiogenically "old" DIC (according to reaction 3-5 above).

Acetogenic and methanogenic bacteria start to consume and isotopically fractionate CO_2. The methanogenic isotopic fractionation factor is calculated to be 0.9268 at 4°C, based on the calculations of Clark and Fritz (1997). The fractionation factors of bacterial processes and the equations used to calculate the resulting isotopic

enrichment of DIC are given in Appendix 1. The model assumes that the bacteria consume no more DIC than was produced by DOC decomposition. In fact, the consumption of DIC hinges on the availability of molecular hydrogen which is a limiting reagent in most bacterial processes, so it does not matter if the bacteria in this model can use deprotonated DIC species as there will not be enough H_2 in the system to react additional quantities of DIC. The model's main independent variable is the relative activity of both bacterial processes. Because the relative growth rates of methanogenic and acetogenic bacteria are unknown, results from the model are calculated separately for different relative bacterial activities. The model calculates incrementally the $\delta^{13}C$ of DIC and the dilution factor as successive 0.03ppmC DOC "packets" are reacted and the products of organic decomposition are consumed by methanogenic and acetogenic bacteria. The model assumes that no aceticlastic methanogenesis takes place. Any conversion of acetate according to Reaction (3-8) above or any other bacterial processes (i.e., sulphate reduction) will add ^{13}C-depleted DIC to the DIC pool and thus curtail the Rayleigh-type enrichment.

Figure 19 shows the modeled ^{13}C-enrichment of DIC relative to DOC decomposition for three different bacterial systems. In one system, 95% of the CO_2 is used by acetogenic bacteria, leaving 5% for the methanogenic bacteria. Because methanogens need twice as much hydrogen to react CO_2 to CH_4, they consume only half of the remaining CO_2 not used by acetogens. Thus methanogens use only (1 - 0.95)/2 = 2.5%, and together, both groups of bacteria consume (1 + 0.95)/2 = 97.5% of the CO_2. In another system, 50% of the total DIC pool is available to each organism. In the third system, acetogenesis is completely shut down, and all of the available H_2 is used by methanogens. The results in Figure 19 show that ^{13}C-fractionation of DIC is much greater per equivalent of DOC reacted when acetogenic activity is greater. This result runs contrary to the implicit assumption that methanogens will more strongly fractionate DIC because they are more efficient at selectively reacting $^{12}CO_2$. The enrichment caused by acetogenic activity is of a similar magnitude as the $\delta^{13}C$ values measured in actual endostromatolite hand specimens (Figures 16-18).

Figure 20 shows how DIC becomes "older" over time under the same three system conditions given above. Because DOC decomposition produces acetic acid, "old" limestone DIC is generated even in a system where homoacetogenesis is not occurring. Leftover CO_2 from methanogenesis reacts 1:1 with limestone to dilute the DIC pool with "50% old" DIC, but this does not reverse the trend toward older DIC in solution. Acetogenesis, by contrast, removes DIC from solution and replaces it with a stronger acid that liberates more limestone DIC. If we examine Figures 19 and 20, a 7-8‰ ^{13}C-enrichment of DIC is concurrent with a shift in the dilution factor from 0.50 to about 0.36! This result is completely different from the assumed dilution factor of 0.5-0.6 by Clark *et al.* (2004).

The theoretical model presented above is just one possible interpretation of the original environment in which endostromatolites formed. The model represents a closed system in which no products escape. If transport of products out of the system is allowed, more DOC can be reacted to generate the same Rayleigh-type enrichments presented in Figure 19. In fact, the growth column profiles shown in Figures 16-18 could represent systems with strong components of transport of products out of the system such that the Rayleigh distillation is always being "reset". The limitation posed by hydrogen availability is also a constraint on the model. If the model is re-tooled to allow complete DIC consumption and incorporates an iteration calculation for DIC released by acetogenic production, methanogenesis would still not surpass acetogenesis for ^{13}C-enrichment of DIC (data not shown). Thus it is not reasonable to assume that methanogenic bacteria are the only microorganisms capable of generating the ^{13}C-enrichment profiles measured in endostromatolite columns.

The second half of this chapter contains actual aqueous geochemical data from a periglacial limestone terrain where endostromatolites grew in the past. Some of the waters collected from the field site show much more elevated levels of DIC (10-15ppmC) and DOC (~10 ppmC) than was used in the above theoretical model. If these elevated concentrations of DIC and DOC are substituted into the model, similar distillation curves would result with the main difference being that proportionally more DOC would have to

react to enrich the DIC pool (data not shown). The field collection program will be discussed in the following section. Clearly, a source of ^{13}C-depleted DIC is needed to reverse the enrichment trends observed from endostromatolites and the theoretical model, and the field component of this research will elucidate other potential processes and their significance toward endostromatolite formation.

Field Investigations

Site Descriptions

Two independent field investigations were conducted in and around a limestone protrusion called the Campbell Uplift near Inuvik in the Northwest Territories (see Figure 12). Inuvik is located on the eastern edge of the Mackenzie River delta (68°30'N, 133°45'W). The geology and geomorphology of the Campbell Uplift and surrounding region have been described previously (Dyke, 1975; Ritchie, 1976). The limestone-dolostone outcrops are Ordovician to Devonian in age and form local topographic highs in the area. The largest exposed area of the limestone outcrops to the west of Campbell Lake. A smaller "outlier" outcrop is found to the east of the lake. The area was chosen for investigation because of the ubiquitous occurrence of "endostromatolites" in the uppermost exposures of limestone. According to the conceptual model shown in Figure 1, the overlying soils are host to microbial communities that likely played a role in the creation of endostromatolites in the recent geological past. Periglacial wetlands are currently a significant source of methane to the global atmospheric methane flux (e.g. Martens *et al.*, 1992). It was previously believed that methanogenic bacteria were responsible for the enriched carbon isotopic signatures measured in endostromatolite samples (Lauriol and Clark, 1999). By collecting and analyzing surface waters and groundwaters proximal to regions of endostromatolite formation, inferences to the geochemical and paleohydrological conditions of limestone fissures can be proposed and evaluated.

The first field investigation took place from June 19th to July 7th, 2000. The second investigation occurred June 17th to 24th, 2003. Figure 12 shows the distribution of various monitoring stations set up proximal to the Dempster Highway. Table 3.1 (Appendix 2) gives descriptions of each site including soil horizons in the active layer and the depth of piezometers installed at each location. Despite the region's undulating topography, ideal sampling conditions (i.e., where water is seeping through the active layer, the seasonally thawed surface horizon, with minimal contact from the atmosphere) could be found at only a few locations. The study area is normally an arid region. Winters are long, cold, but relatively dry. The winter of 1999-2000 produced abnormally high amounts of precipitation, as told by residents of Inuvik, and localized flooding during the spring snowmelt washed out several roads. Surface runoff was relatively good by the time the first investigation began. The weather was hot (i.e., daytime temperatures exceeding 20°C) and dry for almost the entire month of June. July 2000 was cooler, and several significant episodes of precipitation occurred, allowing for an extended monitoring period. The second field investigation in 2003 was not as fruitful due to dryer conditions during the previous winter. Levels of surface runoff were low during the monitoring period. The spring snowmelt period was much more ephemeral and was essentially over by the time monitoring had begun.

The most productive monitoring site was established at the "North Quarry" (NQ) location. It is situated at the northeastern corner of the large topographical highland that makes up most of the Campbell Uplift. The limestone is fossiliferous at this location, containing abundant brachiopods and crinoids, and little if any iron staining is visible on weathered surfaces. The site was being quarried by employees of Bob's Garage, a major business in Inuvik. The eastern boundary of the quarry where the vegetated slopes of the limestone ridge meet the quarry floor was chosen for monitoring. This area represented a transitional zone between the quarry and natural vegetation. Puddles visible at the surface may have been replenished by groundwaters percolating through the outcrop slope (and perhaps through the limestone itself). Pieces of PVC tubing with holes cut into the side at one end were put into the ground with the use of steel poles driven into the soil with mechanical force. These PVC tubes thus became makeshift piezometers. A linear

series of four piezometers were installed extending away from the outcrop along the hypothetical groundwater flow path, and these piezometers became stations NQ-1 through NQ-4. A fifth piezometer was inserted into the active layer a short distance off to the side from the linear transitional zone where no quarry residue was ostensible, and this station was called NQ-P. The active layer depth was much greater in the transitional zone covered by talus debris than on the vegetated slope (see Table 3.1 – Appendix 2).

The "South Quarry" is located in the outlier limestone outcrop to the east of Campbell Lake. The location had been quarried in the past, but all anthropogenic activities had apparently ceased before the field study began. The exposed walls of the quarry exhibit much iron oxide staining, and hand specimens reveal iron sulphide minerals. Evidence of fossils is lacking. The outcrop facing the road forms a natural escarpment that is too steep for soil to develop. The quarry is behind this topographic high and is not visible from the highway. A small stream flows along the gravel road leading into the quarry. Waters from the vegetated ridge behind the quarry drain into this stream. No monitoring stations were established at this site as no subsurface flow could be reached. The area immediately surrounding the limestone escarpment was parched.

An interesting manmade site (herein referred to as "MZ") is located off the highway between the NQ and SQ sites. To the north of the small limestone "outlier" where SQ is situated, limestone gravel sits atop two abandoned construction sites. These sites are accessed from the highway by a path that splits into two leading into each site. A stream follows the edge of the main path, and a culvert was installed at the split. While the stream receives water draining the upland vegetated areas to the east, it also drains the exposed gravel floors of the construction sites. In particular, a small tributary channel coming from one of the sites flows over limestone mud before it reaches the stream. In 2000, the culvert was washed out, a telling sign of how much meltwater was produced from the wet winter previous. In 2003, the culvert was intact, having been rebuilt at some point in the intervening 3 year hiatus. One piezometer (MZ-1) was installed along the talus-covered shore of the stream near the culvert. Another piezometer (MZ-2) was put into the lime-rich mud of the tributary "delta".

The "Airport Quarry" site is located to the west of the Inuvik Airport. Like NQ, this site is an active quarry. A limestone ridge containing endostromatolite deposits flanks the northern shore of Dolomite Lake. Some of the most beautiful scenery in the region can be found at this location. Unfortunately, the ridge was dry like the SQ site, so no monitoring stations associated with it were generated. However, the shallow vegetated slope to the east of the quarry and ridge yielded some visible flows. A stream flowing alongside the road toward Dolomite Lake drains the area, receiving inputs from the slope and the quarry. Two monitoring stations were created on the slope itself. The flow drained the thin active layer and proved to be ephemeral.

A location outside of the limestone terrain was needed for comparison data. The "Shale Site" (SH) was established well to the south (not shown in Figure 12). Located on a topographic high in some very undulating terrain, weathered shale outcrops form a wall resembling a crater around the site with a shallow pond occupying the floor of the local depression. White salty deposits are seen on the shore of the pond. The soil is full of platy shale debris. The origin of the soil is not clear, whether it be natural or put there by anthropogenic activities. Two piezometers were put into the soil at different locations, though chosen rather arbitrarily. The pond water was also monitored.

One site was accessed in 2003 that had not been previously monitored. Along the highway between the Airport and the NQ site, patterned ground containing ice wedges is used by other researchers (notably J. Ross Mackay) to measure yearly permafrost thawing. There are no limestone lithologies outcropping at the surface, and the land is locally quite flat. The site is herein referred to as "Kokelj's Peat" (KP). A small unnamed lake sits beside the patterned ground. Water samples from an ice wedge were extracted from both the surface and the thawed soil immediately beneath. It should be noted that this location is proximal to the highway and receives inputs of airborne dust frequently from speeding cargo traffic.

Analyses

Measurements made directly in the field from water samples pumped to the surface include temperature, pH, Eh (electromotive potential), E.C. (electrical conductivity), salinity, T.D.S. (total dissolved solids), D.O. (dissolved oxygen), and alkalinity. Temperature data were collected with three different instruments, but only the data from the pH meter were included in Tables 3.2 and 3.4 (Appendix 2), the summary of results. The pH meter used was a Hanna Instruments field portable unit with separate pH and ATP probes, and buffer solutions ranging from pH 4.00 to 10.01 were used for calibration. For the 2000 field season, a KCl-refillable glass microvolume pH probe was used with the Hanna meter. In 2003, non-refillable VWR-brand epoxy probes were used. A silver-silver chloride (Ag-AgCl) probe was used with the Hanna meter to measure Eh. The probe could not be calibrated, but verification that it was working properly was regularly performed using two standard solutions prepared from potassium ferricyanide and potassium ferrouscyanide. Corrections to Eh to compensate for the probe were made using calculations shown in Clark and Fritz (1997).

Measurements of E.C., salinity, and T.D.S. were all done with one portable E.C. meter (details unknown). The probe was checked to make sure it was functioning with a standard solution (Thermo Orion 1413 mS; VWR catalogue # 52458-146).

Measurements of D.O. were made using a YSI Model 85 dissolved oxygen meter.

Alkalinity was measured by titrating a given volume of water with sulphuric acid. Depending on the concentration of dissolved inorganic carbonate species in solution, the acid used was either 1.6N or 0.16N concentration. The titration was monitored using the pH meter and probes described above. The amount of acid added determines the alkalinity and the endpoint pH. Since alkalinity and endpoint pH are both unknown, iteration calculations were used to derive solutions.

Measurements that could not be performed in the field required samples to be collected and taken back to analytical facilities. These measurements include [DIC],

$\delta^{13}C_{DIC}$, [DOC], $\delta^{13}C_{DOC}$, [CH_4], $\delta^{13}C_{CH_4}$, cations, anions, $\delta^{18}O$ and δD. Not all types of samples were collected for every sample site or in both field seasons. The DIC and DOC samples, as well as anion samples, were filtered using 0.45um cellulose acetate filter papers.

DIC samples were collected in amber borosilicate glass bottles with screw-top lids containing plastic liners that create a gas-tight seal. In 2000, the samples were not given any chemical preservatives. In 2003, the samples were poisoned with a few drops of a concentrated HgCl solution. In 2000, [DIC] was measured during cryogenic extraction and purification on a glass vacuum line using the phosphoric acid reaction technique. Extracted DIC was then transferred to glass breakseals for analysis on a SIRA-12 multiport dual inlet mass spectrometer. [DIC] was also calculated from alkalinity using temperature and pH data for comparison. New laboratory methodologies were in place in 2003, allowing [DIC], $\delta^{13}C_{DIC}$, [DOC], and $\delta^{13}C_{DOC}$ to be analyzed in one procedure using an OI Instruments model 1010 wet oxidation TOC analyzer configured to a Finnegan MAT Delta Plus IRMS with a ConFlo III continuous-flow interface (see Marschner *et al.*, 2005).

In 2000, DOC samples were collected in clear glass 20mL vials with cardboard-lined aluminum inserts under screw-top caps. No reliable methodology for analyzing DOC was available at the time, and long-term storage of these samples resulted in degradation of the liners and thus possible contamination. No results for DOC are included in the results for 2000. In 2003, DOC samples were collected in almost identical vials as DIC, and samples were preserved by adding a few drops of 10% hydrochloric acid in the field. The DOC samples were analyzed with the same instrumentation and methodology as DIC samples (described above). Furthermore, DOC samples were also injected into an HPLC instrument configured with a fraction collector for fatty acid detection and fraction collection (see Marschner *et al.*, 2005). The concentrations of fatty acids were too low for the fractions to be analyzed by the TOC analyzer.

Methane (CH_4) samples were collected in air-tight gas sampling bottles sealed with grey butyl rubber septa and crimped shut with aluminum seals. The bottles were not completely filled, allowing for a small headspace into which dissolved methane could volatilize. An SRI Instruments field-portable GC was set up in the laboratory in Inuvik so that methane samples could be analyzed within 24 hours. Sample injection was achieved using a gas-tight Hamilton SampleLock syringe with a 26S-gauge needle used to remove gas from the headspaces. The GC is configured with a flame ionization detector (FID) for detection down to <5ppmV. The GC signal was calibrated with pre-made methane standards in septa jars identical to the sample bottles. Initially, no preservatives were added to the methane samples. Gas bubbles generated in these samples indicated uninhibited biological activity, so subsequent samples were poisoned with HgCl. In 2003, the GC was not brought to the field, so methane samples were analyzed 1-2 weeks after collection. The ^{13}C-isotopic composition of methane was obtained from a Finnigan MAT Delta Plus IRMS configured with a cryogenic Pre-Con interface.

Samples for oxygen and deuterium isotopes of water were collected in 40mL PVC bottles and were not filtered or preserved. $\delta^{18}O$ results were obtained using a SIRA-12 multiport dual inlet mass spectrometer. δD results were obtained by reducing water to H_2 with zinc in glass breakseals and then by analyzing the gas on a VG 602E dual inlet mass spectrometer. Only samples from the 2000 field season were analyzed. The data (not shown) confirm that the waters were meteoric in origin without any discernible enrichments from evaporation.

Cation and anion samples were collected in 40mL PVC bottles. Samples from the 2000 field season were not properly preserved and thus generated very limited data. Cations were analyzed by ICP-AES (inductively coupled plasma atomic emission spectroscopy) using a Thermo Jarrell-Ash Atomscan 25. Two different peaks were measured for calcium and results of both peaks show good precision, so the calcium data is presented in Table 3.3 (Appendix 2) for use in calculations of calcite saturation index. Anion samples were preserved with nitric acid. In 2003, cation and anion samples were collected and nitric acid was added to the cation samples to keep iron from precipitating.

Cations were analyzed with a Varian VISTA-PRO simultaneous ICP-OES. Standards were prepared from concentrated stock solutions combined to approximately imitate the sample matrices. This instrument detects total sulphur and does not differentiate between SO_4^{2-} and S^{2-}. Anion analyses were not performed as it was deemed unnecessary since the samples are not expected to contain much chloride or nitrate. The cation data balanced well versus SO_4^{2-} and DIC except for the most dilute samples where many species were close to the lower detection level of the instrument.

Results

The data for samples analyzed in the field and in the laboratory during the 2000 field season are shown in Table 3.2A (see Appendix 2). Explanations of the measured parameters are provided in Table 3.2B (Appendix 2). Values shown in bold are assumed to be in error.

All of the sites located within the limestone terrain yielded waters with pH values that were circumneutral or higher. The shale site, by contrast, was much more acidic. The source of the acidity at the shale site is not known. Despite their low buffering capacity, the shale waters contained elevated levels of DIC. Concentrations of DIC at all of the monitoring stations increased over time throughout June 2000. As soon as the wetter weather started in July 2000, DIC levels stabilized and even decreased slightly. Dry sites such as AQ did not start to flow again after precipitation events. The piezometer at station AQ-1 was inserted at the juncture between high porosity overlying organic soil and much denser clay beneath. Dissolved oxygen levels in both AQ monitoring stations were elevated, indicative of open system aeration of the overlying soil.

The limestone waters maintained low salinities and electrical conductivities throughout the monitoring period. Not surprisingly, then, DIC is by far the largest contributor to alkalinity in these waters. The shale waters have much more elevated salinities and electrical conductivities.

The NQ and MZ sites produced water samples with significant levels of dissolved methane. Methane is reasonably soluble in water considering that it is a non-polar volatile organic compound. Data from Yamamoto *et al.* (1976) suggest that solubility of methane in non-saline water at 5°C should be about 2.2mmol/L, while at 24°C it should be about 1.4mmol/L. The data from the field sites indicate that methane concentrations are a couple of orders of magnitude below saturation for NQ and MZ, although some later values for station NQ-1 achieve about 10% saturation. Gas bubbles were observed being released from the sediments beneath surface water at the NQ site. Thus it is reasonable to say that at least some of the methane measured from samples of the NQ site is generated in-situ. All four of the NQ stations located on the edge of the quarry produced high levels of measured methane. Station NQ-P, located off to the side in the vegetation, generated only trace levels of methane. Levels of dissolved oxygen at NQ-P were higher than at the other NQ stations but still well below saturation levels. In general, there is a good inverse correlation between methane concentration and dissolved oxygen, and this includes the shale site where low but detectable levels of methane were measured.

Carbon isotopic data for DIC reveal a wide range of values across the field area. The lowest $\delta^{13}C_{DIC}$ values were measured from samples collected at the NQ stations and at MZ-1. Typical values between -14 and -16‰ VPDB were measured consistently at these locations. Coincidently, these are the same stations that have the highest methane levels. The most ^{13}C-enriched DIC samples were collected from surface runoff upstream of MZ-2 where two different samples gave nearly identical measured values of around -2‰ VPDB. The latter values are typical of open-system waters in contact with marine limestone under atmospheric CO_2. The shale site provided some enriched $\delta^{13}C$ values as well, typically between -4 and -8‰ VPDB. The AQ site gave results around -11‰ VPDB.

Geochemical data for the 2000 field samples are not shown as there are large imbalances between cations and anions (>10% for most samples). Questionable results were derived from the anion samples as they were improperly preserved by adding nitric

acid. The analyses by liquid chromatography show very high levels of sulfate. The low pH conditions of the sample waters were incompatible with the LC column. Sulfate data were corrected manually using cation and other anion data to achieve a proper balance, and the corrected data were used to estimate ionic strength according to calculations by Drever (1997). With the ionic strength, activities of Ca^{2+} and CO_3^{2-} and the saturation index (SI) of $CaCO_3$ could be calculated. The results are shown in Table 3.3. The sites within the limestone terrain are close to or exceed saturation with respect to calcium carbonate. The shale site is far below saturation despite having calcium levels that are very similar to the limestone sites. Station NQ-P is below saturation due to lower levels of carbonate in the organic soil. Stations AQ-1 and AQ-2 are right around saturation, possibly indicating some mixing with waters from the unfrozen clay horizon.

The field data from the 2003 sample collection season are shown in Table 3.4 (Appendix 2). The letter "R" was added to the identities of the monitoring stations to indicate that new PVC piezometer tubes were installed, except at station MZ-1 where the original piezometer remained intact.

The data in Table 3.4 (Appendix 2) are similar to data from the 2000 season. A couple of different sites were included, SQ and KP. The data from SQ resemble previously-collected data for AQ. The waters percolating down the vegetated slope are full of dissolved oxygen and are thus unsuitable for growth of anaerobic bacteria. Unlike AQ, though, the water from SQ-1 has very low alkalinity and low DIC concentration. The stagnant water sitting atop the ice wedge at station KP-1 has low levels of dissolved oxygen, but it is also very cold and acidic.

For the first time, DOC was measured, as well as $\delta^{13}C$ of methane. DOC levels at the NQ and MZ sites were quite low, around 10-12 ppmC (parts per million carbon) with the exception of NQ-P that produced a measurement 4 times greater. DOC levels were also higher in the waters from SQ-1 and the stream at the same location. The good inverse correlation between DOC and DIC may not be coincidental; this will be examined in the discussion to follow.

Methane concentrations were lower in 2003 at many of the field sites. The dryer conditions could be responsible for higher diffusion rates and/or lower biogenic activity. $\delta^{13}C$ values for methane are strongly depleted for many of the sites. The lowest values were found at MZ-1 where three measurements produced values between -72 and -71‰ VPDB. More enriched values were seen at MZ-2R located in the silty mud delta farther away from the stream. One measurement produced a result of -51‰ VPDB, and two subsequent samples gave results closer to -58‰ VPDB. The enrichment could be due to diffusion since the concentration at MZ-2R was consistently an order of magnitude lower. Values around -66‰ VPDB were obtained from NQ-1R, but a measurement of -38.4‰ VPDB resulted from NQ-2R. Again, diffusion is suspected for the enriched signal. The lower $\delta^{13}C_{CH_4}$ values suggest that CO_2-reduction is the dominant methanogenic process (according to Whiticar *et al.*, 1986).

The results for $\delta^{13}C_{DIC}$ in 2003 are generally lower than 2000. Average values at NQ-1R were around -18‰ compared to -15‰ at NQ-1 and NQ-2 in 2000. Similarly, values at MZ-1 dropped to -20‰ in 2003 from -16‰ and higher in 2000. Values at MZ-2R were around -17‰, down about 5‰ from three years previous. The consistency of the lower $\delta^{13}C$ values could be related to the change in analytical methods, though no previous investigations comparing offline DIC extractions to the continuous flow method yielded any notable differences. One measurement for sample KP-1 yielded a result of -27.2‰ VPDB, analogous to the $\delta^{13}C$ of organic matter from C-3 plants. Less surface runoff in 2003 could mean unsaturated conditions prevailed, thus allowing for more aerobic DOC degradation, thus shifting the $\delta^{13}C_{DIC}$ values closer to $\delta^{13}C_{DOC}$.

Results of geochemical analyses of cations and anions are shown in Table 3.5 (Appendix 2). The results are expressed as activities, and only data from samples for which temperature, pH and TIC data are known are shown in Table 3.5. Calculations of ionic strength require knowing all of these parameters. The geochemical data show that water from the NQ monitoring sites do not contain any iron while the waters from the MZ site contain some dissolved iron. These results seem to suggest that the limestone at

the MZ site came from the same formation as the outcrops at the SQ site where much iron staining on the quarry faces and debris was observed. The saturation index for $CaCO_3$ is also given in Table 3.5, and all of the samples are very close to saturation except for the dilute MZ-creek and KP-lake samples.

Discussion

Northern landscapes present some unique conditions for bacterial activities. In more temperate environments not underlain by permafrost, the development of "trophic horizons" occurs in soil and sediments. The bacteria that will thrive in a given environment either tend to derive the most energy from the available substrates or are the least inhibited by prevailing conditions. The field area investigated close to Inuvik in the western Northwest Territories is within continuous permafrost. The thawed "active layer" above permafrost is a thin horizon that constrains the spatial distribution of bacterial activities. When the active layer is wet and the flow of water is low, oxygen from the atmosphere will be consumed by aerobic oxidizing bacteria in the topmost few centimetres. The absence of oxygen and the presence/absence of other electron-accepting compounds provide environments in which anaerobic respiring bacteria can grow and form distinct communities. The field area investigated herein has an arid climate with a short spring snowmelt period. The drainage of the surface layer depends largely on topography.

Figure 21 shows a plot of dissolved oxygen data relative to Eh for samples collected from the 2000 field season. The data from stations in the limestone terrain (MZ, NQ, AQ) tend to plot well together. The data from the shale site (SH) tend to plot at higher Eh values. Unfortunately, no geochemical data from the shale site waters are available to determine what redox species are controlling the electromotive potential. Clearly, though, the shale site is quite different from any of the limestone terrain sites, with weathering of shale releasing relatively large amounts of various cations and anions to the surrounding environment.

Figure 22 shows a plot of Eh data versus pH for the 2000 field samples against calculated stability fields (at 25°C). The equations defining the limits of the stability fields were derived from calculations given by Drever (1997). The data plot well above the stability fields for methanogenesis (via CO_2-reduction), acetogenesis, and sulphate reduction, and yet several monitoring stations produced waters with significant amounts of dissolved methane. The geochemical data in Table 5 (Appendix 2) show that many of the monitoring sites have large amounts of sulphate. None of the waters smelled strongly of H_2S, and the Eh data corroborate the presence of SO_4 over H_2S. The stability fields predict Eh based on redox reactions at standard state conditions, and the field waters certainly do not contain enough of any compounds to be at standard conditions.

One explanation for the given results is that methane is merely diffusing into the waters sampled from the piezometers. However, the presence of live methanogenic bacteria in the samples was confirmed when some samples collected for methane showed increasing levels of methane over time (i.e., the samples were not sterilized). Methane diffusion into the headspace is rapid and cannot be invoked to explain the increasing methane concentration over several days. Gas bubbles were also seen rising from sediments at the bottom of unfiltered sample bottles. Furthermore, the chances that the bacteria were dormant in the soil and "revived" in the laboratory are highly unlikely given that the sample bottles were not flushed with anaerobic gas to remove oxygen from the headspaces (i.e., they were sealed with atmospheric gas). Methanogenic bacteria are theoretically incapable of growth in the presence of oxygen. Oxygen concentration in the headspaces could not be measured in the field. Sulphate is not an inhibitor of methanogenesis, but its presence indirectly inhibits methane formation due to competition for shared substrates with sulphate-reducing bacteria. The field results suggest that methanogenic bacteria at several of the monitoring sites are capable of growth in the presence of sulphate, and this is likely due to inhibition of sulphate reduction, the cause of which is unknown. The higher concentration of sulphate versus any other electron-acceptors would thus be responsible for high Eh values, and thus the Eh data do not appear to be useful in predicting bacterial processes from the field area.

Another possible explanation for the observed data is the presence of "microenvironments" in the active layer. Colonies of bacteria can change geochemical conditions in their immediate vicinity to make growth conditions more favourable on a local scale over time. Waters sampled from a soil containing microenvironments would thus produce data that are not representative of conditions suitable for bacterial growth. The problem with this explanation is that the presence/absence of microenvironments would be very difficult to prove, so no further discussion on this line of reasoning will be attempted.

Methanogenic growth media was taken to the field and was used to create closed incubation systems inoculated with water samples from the field. The purpose of this experiment was to detect the presence of methanogenic bacteria independently of any and all other observations. The media contained nutrients to stimulate growth as well as non-competitive substrates. A negative result does not confirm that methanogenic bacteria are absent, but a positive result confirms the presence of bacteria in places where they might not be producing methane at the time of sampling. All of the monitoring stations within the limestone terrain gave positive results. The shale site (SH) did not produce an active methanogenic culture. In a separate experiment, some of the methanogenic culture from one site was used to inoculate an iron-rich growth medium for sulphate reducing bacteria. The formation of copious amounts of FeS_x proved that sulphate reducing bacteria were present in the culture. The reasons for inactivity by sulphate reducers in the field and in experimental cultures remain unknown. Hence the diversity of microorganisms in periglacial soils is high, although many bacteria may not be active at any given time.

To corroborate the Rayleigh-type distillation signal for ^{13}C in endostromatolites with any bacterial processes occurring in present-day periglacial soils, a good correlation between observed $[CH_4]$ and $\delta^{13}C_{DIC}$ was necessary since methane production via CO_2-reduction would enrich residual DIC in ^{13}C. Unfortunately, no isotopic enrichments in DIC were found for the sites that yielded the highest methane concentrations. Instead, some sites (like NQ and MZ) produced negative correlations. The most ^{13}C-enriched

DIC values came from the shale site where methanogenesis was doubtful. Decomposition of DOC by bacteria to produce ^{13}C-depleted DIC is likely responsible for the lower $\delta^{13}C_{DIC}$ values seen within the limestone terrain. Methanogenesis likely proceeded via a fermentative pathway that produced ^{13}C-depleted DIC rather than consumed it. The identity of the preferred substrate(s) used by methanogenic bacteria in the field is/are unknown. Analyses of DOC produced results that were very low (10-13 ppmC), and selective analysis of fatty acids from field samples did not reveal any significant abundance (>2ppmC) of acetate. The low DOC concentrations may not accurately indicate the true availability of organic substrates to the bacteria, though.

Some interesting observations are noted with respect to the filtration of DIC-rich and DIC-poor waters both collected in the field and made in the lab. Standard 0.45μm cellulose-acetate filter papers (both 25mm and 47mm diameters) were used to filter field water samples after collection, and much smaller volumes could be pushed through a filter from the DIC-rich waters compared to the waters from the shale site. Recall that the shale site waters are less alkaline and more acidic, meaning that almost all DIC would be in the form of dissolved CO_2, whereas most DIC in water at circumneutral pH is partially deprotonated (i.e. the dominant species is HCO_3^-). The same observations were made in the lab during the preparation of culturing solutions. Culturing media used in incubation experiments (see Chapter 4) were prepared by mixing homogenized organic soil powder with deionized water and subsequent filtration. When DIC (in the form of sodium bicarbonate) was added to the soil "broth" prior to filtration, the time required to filter the solution increased exponentially, and filter papers had to be replaced once they became "choked". These observations suggest that complexation between ionic species and organics may be occurring, and the result is that less DOC in the DIC-rich waters will fit through the 0.45μm pores of the filter paper. For detached "floating" bacterial cells, this could represent decreased access to potential substrates, but for cells that grow on solid surfaces, this could effectively enhance the availability of substrates. More investigation needs to be accomplished to evaluate organic complexation, if it is a real phenomenon, and how it affects bacterial growth.

Clearly, present-day bacterial processes in periglacial soils bear little resemblance to processes that occurred thousands of years ago within limestone fissures. Emplacement of endostromatolites occurred under different climatic conditions than at present. Zones of talik (thawed soil within permafrost) must have been more extensive, thus permitting greater subsurface flow. It is reasonable to hypothesize that, under the warmer conditions of the past, vegetation grew more extensively, and decomposition of organic matter likely led to higher levels of DOC. Transport of DOC into limestone fissures may have played a significant role in stimulating bacterial growth of microbes living there, or it may have been largely insignificant due to complexation between DOC and DIC. None of the observations from the field suggest that methanogenesis by CO_2-reduction is a significant process at present in thawed periglacial soil within limestone terrains. Enriched ^{13}C signals from endostromatolites (discussed earlier) are very real, and the role of CO_2-reduction in the local environment of limestone fissures may have been quite significant simply due to much greater access to solid carbonate surfaces and inorganic substrates. The failure to identify processes leading to ^{13}C-enrichment in DIC in the field opens the door to controlled experimentation using field cultures in the lab. The following chapter will focus on bacterial incubation experiments used to attempt the recreation of Rayleigh distillation processes.

Conclusions

Endostromatolites are unique biogenic carbonate deposits that grew in cold-climate periglacial regions under conditions that are different from those at present. They exhibit some unique features related to their appearance and their distribution. They occur within fissures in limestone outcrops with strong tendencies to grow on southward-facing exposures and on one side of the fissure only, that side usually being on the "hanging wall" side of the fracture. Another key feature that has herein been investigated is the enriched ^{13}C signal measured along growth columns. Marine limestone typically has $\delta^{13}C$ values between -3 and 0‰ VPDB. A group of well-preserved endostromatolite hand specimens generated $\delta^{13}C$ values up to +13‰ VPDB. Previous research complements our findings that these deposits could not have formed abiogenically simply

by equilibrating with similarly enriched materials. Bacteria played a role as evidenced by internal microstructures and growth banding within individual columns. Two microorganisms capable of fractionating DIC and creating ^{13}C-depleted products are methanogens and acetogens. Conditions for their growth had to be saturated and anaerobic. Groundwater circulation must have been much more extensive in the past than at present. ^{18}O isotopic data from well-preserved endostromatolites have been used as climate signals since the waters flowing into limestone fissures were meteoric in origin and since past climate amelioration allowed for greater groundwater flow.

A new microsampling analytical technique was employed to generate $\delta^{13}C$ and $\delta^{18}O$ profiles along individual growth columns chosen from hand specimens of endostromatolites showing the best internal preservation. The results confirm previous findings that $\delta^{13}C$ increases away from the contact surface of the host rock, though the trend and degree of enrichment varies from specimen to specimen. Some ^{13}C-isotopic profiles appear very linear upward while others mimic a theoretical Rayleigh-type distillation curve. A theoretical model was used to show that both acetogenic and methanogenic bacteria can consume the products of organic matter decomposition and enrich residual DIC in ^{13}C, although acetogens appear to be the more effective organism at enriching DIC per equivalent of DOC reacted despite being less efficient. Moreover, acetogenic activity releases proportionally more radiogenically old limestone DIC into solution, thus contradicting previous assumptions used in ^{14}C age dating that limestone contributes 40-50% to endostromatolites under "partially-open" conditions. A higher dilution factor would generate an older ^{14}C age for endostromatolites.

The relative importance of methanogenic versus acetogenic processes was investigated. Theoretical considerations favour acetogens in competing for CO_2 and H_2 at low temperatures. Unlike acetogens, methanogenic bacteria may resort to fermentive reactions involving DOC and thus contribute ^{13}C-depleted DIC to solution rather than remove it. The geochemical field data show that this may, in fact, be occurring in carbonate-rich sediments at several sites where the DIC was actually quite depleted in ^{13}C relative to high dissolved methane concentrations. In fairness, the field sites do not

compare well to the fissure environments. DIC concentrations increased over time as biogenic CO_2 was released more quickly than it was consumed. The lack of acetate in the field waters could have been due to aceticlastic methanogenesis or other acetate oxidizing activities, but it should not be used as evidence that acetogens were not present or active.

Eh and dissolved oxygen provide useful measurements for predicting where bacteria might occur, but in modern periglacial environments, other variables are likely responsible for the distributions of bacterial processes. Geochemical data from field samples show that methane is abundant in waters containing high amounts of sulphate and even low levels of oxygen. According to thermodynamic models, other bacterial processes should be occurring at the measured Eh levels, but they are not. Periglacial environments may not suitably fit into thermodynamic models for predicting the processes that are occurring at a given site. In a very real sense, the harsh cold-climate environment favours organisms that are the least inhibited, not the most efficient.

The field investigation provided some interesting food for thought concerning what processes might be happening in original endostromatolite growth environments, but did not validate any particular processes. More investigation needs to be done with the actual microorganisms from the field site under controlled experimental conditions. Chapter 4 will present several experiments that test the viability of acetogenic versus methanogenic bacteria and the Rayleigh distillation model for ^{13}C-enrichment.

Acknowledgements

This investigation was made possible by NSERC Research Grant 42590 to I.D.Clark and by research bursaries (NSERC PGS-B and OGS) provided to M. Marschner. Additional funding was provided by the Graduate Students Association of the University of Ottawa. Analyses were performed at the G. G. Hatch Stable Isotope Laboratories, Ottawa-Carleton Geoscience Centre, University of Ottawa, and we are most grateful to P. Middlestead, G. St. Jean, W. Abdi, and P. Wickham for their expertise and many suggestions. Field assistance was provided by the Aurora Research Institute, and we wish to thank Les Kutny, Andrew Applejohn, Jason King and Norman Amikina for their assistance. Additional help in various aspects of this project were provided by Danielle Fortin and Accu-Test Laboratories.

References

Baresi L (1984) Methanogenic cleavage of acetate by lysates of *Methanosarcina barkeri*. *Journal of Bacteriology*. **160**: 365-370.

Clark I, Fritz P (1997). *Environmental Isotopes in Hydrogeology*. Boca Raton, Lewis Publishers.

Clark ID, Lauriol B, Marschner M, Sabourin N, Chauret Y, Desrochers A (2004) Endostromatolites from permafrost karst, Yukon, Canada: paleoclimatic proxies for the Holocene hypsithermal. *Canadian Journal of Earth Sciences*. **41**: 387-399.

Conrad R, Mayer H-P, Würst M (1989) Temporal change of gas metabolism by hydrogen-syntrophic methanogenic bacterial associations in anoxic paddy soil. *FEMS Microbiology Ecology*. **62**: 265-274.

Drever J I (1997) The Geochemistry of Natural Waters; Surface and Groundwater Environments (Third Edition). New Jersey, Prentice Hall, 436p.

Dyke L D (1975). Structural investigations in Campbell Uplift, District of MacKenzie. *Geological Survey of Canada, Paper 75-1 (A)*, 525-532.

Fey A, Conrad R (2000) Effect of temperature on carbon and electron flow and on the Archaeal community in methanogenic rice field soil. *Applied and Environmental Microbiology*. **66**: 4790-4797.

Gelwicks JT, Risatti B, Hayes JM (1989) Carbon isotope effects associated with autotrophic acetogenesis. *Organic Geochemistry*. **14**: 441-446.

Hines ME, Duddleston KN, Kiene RP (2001) Carbon flow to acetate and C_1 compounds in northern wetlands. *Geophysical Research Letters*. **28**: 4251-4254.

Hutten TJ, Bongaerts HCM, van der Drift C, Vogels GD (1980) Acetate, methanol, and carbon dioxide as substrates for growth of *Methanosarcina barkeri*". *Antonie van Leeuwenhoek*. **46**: 601-610

Klass DL (1984) Methane from anaerobic fermentation. *Science,* **223**: 1021-1028.

Krzycki J A, Wolkin R H, Zeikus J G (1982) Comparison of unitrophic and mixotrophic substrate metabolism by an acetate-adapted strain of *Methanosarcina barkeri*. *Journal of Bacteriology*. **149**: 247-254.

Lauriol B, Clark I (1999) Endostromatolites in the arctic: a paleohydrologic indicator. *Applied Geochemistry*. **14**: 775-785.

Marschner M, Middlestead P, Clark I (2005) Using a simple high-performance liquid chromatography separation and fraction collection methodology to achieve compound-specific isotopic analysis for dissolved organic compounds. *Rapid Communications in Mass Spectrometry*. **19**: 261-268. (Chapter 4, this volume)

Martens C S, Kelley C A, Chanton J P, Showers W J (1992) Carbon and hydrogen isotopic characterization of methane from wetlands and lakes of the Yukon-Kuskokwim delta, Western Alaska. *Journal of Geophysical Research*. **97**: 16,689-16,701.

Ritchie J C (1976) The Campbell Dolomite Upland near Inuvik, N.W.T. – A Unique Scientific Resource. *Musk-Ox*. **18**: 70-75.

Whiticar M J Faber E, Schoell M (1986) Biogenic methane formation in marine and freshwater environments: CO_2 reduction vs acetate fermentation- Isotope evidence. *Geochimica et Cosmochimica Acta*. **50**: 693-709.

Yamamoto S, Alcauskas J B, Crozier T E (1976) Solubility of methane in distilled water and seawater. *Journal of Chemical and Engineering Data*. **21**: 78-80.

Chapter Four

"Competitive acetogenic and methanogenic processes may be responsible for ^{13}C-isotopic enrichments in periglacial biogenic carbonate deposits: Experimental evidence"

Abstract

The ability of a natural consortium of bacteria from a periglacial limestone terrain to fractionate carbon from different carbon-bearing substrates was investigated. Bacteria from frozen soil were cultured and inoculated into closed systems containing methanol, acetic acid, trimethylamine, and various phases of inorganic carbon. Methanol proved to be a very good substrate for methanogenic bacteria, but when DIC (dissolved inorganic carbon) was available, acetogenic activity flourished and stifled methane production. A distinct Rayleigh-type enrichment trend was modeled on methanol that became enriched in ^{13}C over time. At low temperatures, acetogenesis was slowed but still very productive, but methanogenesis was almost completely inhibited. Rayleigh-type enrichments for DIC were very brief and not characterized because of interfering signals from other bacterial processes. ^{13}C enrichments in DIC were seen before the onset of aceticlastic methanogenesis. Under substrate-poor conditions, acetate was again the dominant product, and it is theorized that similar conditions prevailed during the growth of endostromatolites (i.e., unique bacterially-induced secondary carbonate deposits) in limestone fissures in periglacial environments.

Introduction

Periglacial environments contribute significantly toward the global atmospheric methane flux (for example, Chanton *et al.*, 1995; Lansdown *et al.*, 1992; Martens *et al.*, 1992). Biogenic methane production in terrestrial environments is traditionally assumed to be largely due to acetotrophic processes (i.e., acetic acid is the substrate of choice for methanogenic bacteria in these settings) (Whiticar *et al.*, 1986). Recent investigation has shown that acetic acid appears to be transiently accumulating in periglacial terrains (Hines *et al.*, 2001), thereby contradicting the previous assumptions and hence demonstrating that cold climate regions are unique terrestrial environments for methanogenic processes.

Biogenic carbonate deposits within limestone fissures, referred to as "endostromatolites", are paleoclimatic indicators because $\delta^{18}O$ data represent a signal of carbonate deposited in equilibrium with meteoric waters in the recent geologic past (Clark *et al.*, 2004). Endostromatolites occur as semi-continuous layers of clustered growth columns propagating orthogonally to the surfaces on which they grow within limestone fissures. Deposits are found only within limestone, not on outcrop surfaces, indicating an origin within a closed system environment with saturated and anoxic conditions (Lauriol and Clark, 1999). The height of individual columns can range from 1mm to several centimeters. *Mature* deposits can have several "stacks" of columns. These ubiquitous fissure deposits preserve evidence of a biogenic origin. Evidence includes microlayering of alternating organic-rich (dark) and organic-poor (light) bands within individual growth columns. Microsampling for carbon isotopic composition has shown that ^{13}C becomes increasingly enriched along growth columns away from the contact surface with the host rock. These ^{13}C enrichments have been interpreted as evidence of methanogenic activity (Lauriol and Clark, 1999). Reduction of CO_2 in a limestone environment would appear to be a logical process that preferentially removes $^{12}CO_2$ during biogenic production of CH_4, thus enriching residual dissolved inorganic carbon (DIC) in ^{13}C. Research into bacterial processes in periglacial environments largely ignores the potential of other microorganisms to fractionate CO_2. The role of

organic compounds is largely unknown despite the high concentrations of organic matter preserved in endostromatolite growth columns (up to 11 wt % according to Clark *et al.*, 2004).

The present study demonstrates the considerable importance of acetic acid as an organic product and precursor compound to processes occurring in bacterial systems endemic to periglacial terrains. Laboratory incubation experiments using natural bacterial consortiums harvested from periglacial soils proximal to endostromatolite outcrops show that bacterial communities are capable of isotopically fractionating various substrates that become enriched over time according to Rayleigh enrichment model. Acetic acid production and accumulation is especially enhanced in the presence of DIC. A simple isotopic mass balance model generated from the experimental data shows that carbon flow through acetogenic processes (or a combination of acetogenic and methanogenic processes) can create ^{13}C-enrichments like those measured in endostromatolites. These findings offer new insights into carbon cycling in periglacial bacterial systems. Acetogenic processes may be significant terminal steps in the reaction of ^{13}C-depleted organic carbon while enhancing the dissolution of radiogenically "old" and ^{13}C-enriched carbonate.

Bacterial processes – An Overview

The decomposition of organic matter in natural systems is performed by mixed populations of microorganisms. Fermentative bacteria break larger organic molecules (such as plant-derived polysaccharides, sugars and lipids) into smaller "fragments". Acetogenic bacteria further degrade the fermentation products into CO_2, acetate and hydrogen (Klass, 1984; also see Appendix 1). The pathways and the products generated by these reactions are quite diverse and depend largely on the organism present and what kind of substrate it is decomposing. Conrad (1999) suggests the product ratio of H_2/acetate is 2:1 unless homoacetogenic bacteria capable of reacting intermediate hydrogen and CO_2 to acetate are present, in which case the expected ratio would be lower. The numerical model in Chapter 3 uses a ratio of 8:1 (see Appendix 1).

Autotrophic methanogenesis proceeds via this reaction (Brock *et al.*, 1994):

$$CO_2 + 4H_2 \rightarrow CH_4 + 2H_2O \qquad (4\text{-}1)$$

Autotrophic acetogenesis proceeds via this reaction (Gelwicks *et al.*, 1989):

$$2HCO_3^- + H^+ + 4H_2 \rightarrow CH_3COO^- + 4H_2O \qquad (4\text{-}2)$$

It is clear from reactions (4-1) and (4-2) that methanogenic and acetogenic bacteria may compete for the same compounds.

Previous investigations have shown that methanogenic bacteria can use a limited variety of substrates, including methanol, formic acid, acetic acid, and trimethylamine. The reactions of these compounds with H_2 are similar to Equation (4-1), and these reactions are collectively known as *hydrogenotrophic methanogenesis*. For example, methanol can behave as a partially-reduced form of CO_2 as follows:

$$CH_3OH + H_2 \rightarrow CH_4 + H_2O \qquad (4\text{-}3)$$

(Ehrlich, 1996). Where H_2 is a limited substrate, methanogenic bacteria can react certain compounds without hydrogen in a process called fermentation. The cleavage of acetate is a proportionation fermentative reaction as follows:

$$CH_3COOH \rightarrow CH_4 + CO_2 \qquad (4\text{-}4)$$

Acetate is the only compound with a carbon-carbon bond utilized by methanogens. The reduction of the methyl group of acetate to methane effectively changes the valence state of methyl carbon from –III to –IV. The oxidation of the formyl group to CO_2 changes the valence state of formyl carbon from +III to +IV. Thus there is no net gain or loss of

electrons. Methanol is a methanogenic substrate with carbon in the –II valence state. Fermentation of methanol produces CH_4 and CO_2 in different proportions:

$$4CH_3OH \rightarrow 3CH_4 + CO_2 + 2H_2O \qquad (4\text{-}5)$$

One equivalent of methanol being oxidized from -II to +IV is offset by three equivalents of methanol being reduced from –II to –IV. Again, the net balance of electrons involved in reacting carbon is zero, because there are no electron donor compounds (like H_2) involved in the fermentative reactions.

It should be noted that all of the above reactions are "net" reactions that describe the overall bacterial processes.

Enriched cultures versus natural systems

The bacterial incubation systems created in three separate experiments described in this investigation were designed to investigate processes potentially occurring during endostromatolite growth in limestone fissures. However, the natural depositional setting of endostromatolites likely evolved over centuries or longer. While an experiment that recreates in-situ conditions would be suitable for the professed purpose, the timescale required is simply not feasible. Hence it is necessary to explain some of the conditions chosen for the experimental incubation systems.

Methanogenic bacteria are dependent on other microorganisms to produce viable substrates for methane production. Likewise, autotrophic methanogens require H_2, a product of organic matter decomposition. Providing carbonate to the experimental bacterial systems is not enough to ensure methanogenic growth since other respiring microorganisms, if present, are efficient scavengers of H_2. Providing a substrate to the enriched cultures reduces methanogenic inhibition and effectively "speeds up" carbon turnover. Choosing a substrate was the basis of earlier experimental work (Appendix 4). Methanol generated a positive response by methanogens as well as acetate-producing

microorganisms. Methanogenic growth from methanol is likewise not limited by presence/absence of H_2 (reaction 4-5 above).

Hydrogen is an electron-rich compound produced in degradation systems by fermentative bacteria and fatty-acid oxidizing syntrophs (Brock *et al.*, 1994). Free hydrogen is usually scavenged by anaerobic respiring microorganisms and maintained at extremely low levels (Lovely and Goodwin, 1988). Interspecies hydrogen transfer (ISHT) is a process by which syntrophic microorganisms produce and consume hydrogen under low ambient hydrogen levels, effectively making hydrogen cycling undetectable. Methanol is a reduced organic compound that requires less hydrogen to be reacted by methanogens (Reaction 4-3). By supplying methanol to the experimental incubation systems, the cycling of carbon by bacterial processes could be monitored more clearly as turnover of compounds was not limited by factors such as hydrogen availability and dependence on syntrophic organisms.

The argument that methanol is not a ubiquitous product of organic degradation in most systems has merit, though Conrad (1999) notes: "...methanol may be released from the methoxy groups (of lignin, a recalcitrant fraction of organic matter) and thus may support methanogenesis to a limited extent." The same argument could be used to conclude that molecular hydrogen is not involved in bacterial processes because it is maintained at levels that are barely detectable. The discovery of interspecies hydrogen transfer (ISHT) has shown that most hydrogen produced in a system is cycled between syntrophic organisms and does not form free hydrogen molecules, H_2 (Conrad *et al.*, 1989). While methanol may not behave in exactly the same way, it may be effectively scavenged much like free H_2. In an organic-poor natural system like limestone fissures, any methanol produced would be significant versus the pool of dissolved organic matter (DOM).

Another benefit of providing methanol as a substitute for CO_2/H_2 relates to Rayleigh distillation processes touched upon in Chapter 3 to explain the enriched ^{13}C signals found in endostromatolites. In active bacterial systems, DIC can be both a

product and reactant in different processes. Many processes have their own unique fractionation factors that produce interfering isotopic signals, making it difficult to impossible to apply a Rayleigh distillation model to the results of DIC. Using methanol has the potential to provide a much clearer isotope signal, even if it cannot be measured directly (see Methodology section to follow).

Methodology

Field work

Endostromatolite specimens and other materials were collected from a limestone-dolostone terrain to the south and east of Inuvik, Northwest Territories, Canada (Figure 12). Several exposed outcrops along the Dempster Highway were chosen for study, including sites where active limestone quarrying was occurring. The carbonate suite forms topographic highs on both sides of Campbell Lake, with the larger complex to the west called the Campbell Uplift, and a smaller area to the east being an "outlier" formation (Ritchie, 1976; Dyke, 1975). Images of limestone outcrops containing endostromatolite deposits are shown in Figure 23. Endostromatolite deposits were discovered in the exposed quarry walls, but they were limited to the topmost sections, never to be found below the first few metres. Though the limestone sites chosen for study have been classified as being of the same formation, compositional differences are suspected from visual evidence. Outcrop exposures at an abandoned quarry (SQ) display much iron oxide staining on exposed limestone faces, as well as pyrite in hand samples. Water samples from a manmade talus deposit (MZ) containing lime muds precipitate iron oxyhydroxides when exposed to air. An active quarry farther to the north (NQ) and another active quarry to the west (AQ) display no evidence of iron contamination, and hand specimens are much more fossiliferous.

Soil samples were collected from the active layer above permafrost in the study area. Soil samples were obtained by digging into the active layer, removing an intact section with a shovel, and placing the section in a plastic freezer bag. The bags were

sealed and kept cool until they could be frozen upon returning from the field. Our sampling implements were cleaned but not sterilized before use, and efforts were made to handle the samples with as little direct contact as possible to reduce potential contamination. Soil samples were preserved by freezing at -15°C until required for the inoculation of live cultures.

Lab work

Culturing media

Dehydrated and powdered organic-rich arctic soil, collected from the field area above, was prepared in advance for use in culture media. The media was created by boiling 10 grams of soil powder in distilled water over a hot plate until 1 litre of media remained (due to evaporational losses). After cooling to room temperature, 100 mL of media was measured into autoclaved 160 mL septa bottles along with 0.1 grams of hygroscopic trimethylamine hydrochloride (98%; Sigma Chemical Co.) and the bottles were sealed with nitrogen headspaces. Trimethylamine (TMA) is a non-competitive methanogenic substrate, and this compound was provided as an accessible growth compound since the rate of organic decomposition of larger DOC compounds in the media may not be sufficient to sustain a stable community of anaerobic respirers at room temperature.

A slurried media (i.e., containing solids) was used instead of a filtered media because previous experimental evidence determined that growth on the filtered media was partially inhibited. Media that was boiled prior to filtering (using 0.45 μm cellulose acetate filter paper) had much higher concentrations of DOM (dissolved organic matter). Lower growth rates on filtered media were measured regardless of whether filtration was done before or after boiling, so the presence of solid residue had a positive effect on bacterial activity.

Bacterial cultures

The first bacteria cultures were inoculated with thawed soil samples collected from the field (as described above), and the soil was added to culturing media prior to sealing the 140mL bottles. Subsequent reinoculations were made by transferring live culture to freshly-prepared media. The media was prepared as described above with a final concentration of 10 grams of soil powder per litre. Incubation vessels and all of the accessories necessary for culture preparation and inoculation were heated in an oven to 150°C. Once the vessels and media cooled to room temperature, 0.1g of TMA and 90mL of media were added to the vessels. Nitrogen was bubbled through the media using sterile disposable glass pipettes for several minutes prior to sealing. The gray butyl rubber septa liners used to seal the vessels were dipped in 95% ethanol to sterilize them. Aluminum seals were crimped over the septa liners to create permanent air-tight seals. Inoculation was carried out by injecting 6.0mL of live culture into the sterile media of the closed vessels using sterile disposable plastic syringes and needles (22 gauge, point style #2). Incubation was carried out at ambient room temperature. Bacterial activity was monitored by removing a small volume of headspace gases from each serum bottle with a gas-tight syringe and injecting the aliquot into a GC-FID to detect methane (instrumentation and methodology described below). Reinoculation occurred at intervals of two to three weeks.

Experimental cultures

Three sets of experimental incubation systems were created. Table 4.1 summarizes the details of these experimental systems. All experimental systems were carried out in 500 mL serum bottles. The purpose of these experiments was to monitor the major carbon-bearing compounds, both quantitatively (i.e. amounts) and isotopically, toward determining the processes responsible for carbon cycling in the systems. The compounds (and compound groups) that were analyzed quantitatively are: DIC, DOC, acetic acid, methanol, and methane. All of these species could be analyzed isotopically for $\delta^{13}C$ except methanol. Trimethylamine was not detectable with our HPLC apparatus

and a suitable method for analysis was not determined. pH was monitored and used in theoretical calculations to determine IC:

$$n_{IC} = n_{DIC} + n_{CO_{2(g)}} \quad (4\text{-}6)$$

where n is a quantity, not a concentration. The isotopic composition of IC was likewise determined by theoretical calculations using isotopic fractionation data from previous research and summarized in Clark and Fritz (1997). Recall that DIC is expressed as the sum of all protonated and deprotonated dissolved carbonate species:

$$n_{DIC} = n_{CO_{2(aq)}} + n_{HCO_3^-} + n_{CO_3^{2-}} \quad (4\text{-}7)$$

Experiment 1

All three incubation systems in this experiment were given methanol as a carbon-bearing substrate. The only variables between the vessels were the accessibility to and presence/absence of IC. One vessel was not given any IC and was identified as "meth". Crushed limestone was added to another vessel that was called "meth-lim". A third vessel was given a discrete quantity of sodium bicarbonate ($NaHCO_3$) and was called "meth-buff". All three vessels were allowed to incubate at ambient room temperature (~21°C ± 2°C). It should be noted that not all of the methanol was added to the systems at the onset of incubation. Incipient concentrations were low, and when bacterial consumption threatened to deplete methanol completely, additional quantities were added. For vessels "meth" and "meth-lim", the following quantities of methanol were added: On Day 0, the systems started with 12.3 mmol; after 8 days, 24.7 mmol were added; and after 54 days, another 74.1 mmol were added. System "meth-buff" was created two weeks after the onset of the other two vessels. On Day 0, "meth-buff" was given 49.4 mmol of methanol. After 40 days, another 74.1 mmol were added.

The limestone added to vessel "meth-lim" was obtained from crushed quarry debris at the surface of the NQ field site (see Figure 12; Chapter 3). The mineralogy of the limestone and its organic matter content were not determined, but it is known to be of

marine origin. Sorting of the granules was done to remove pieces with any dimension greater than 1cm. The limestone was washed in a weak acid solution to remove surface contamination and dust, and then dried at 150°C in a conventional oven. All equipment used to handle materials for this experiment was likewise sterilized at high temperature.

Experiment 2

Different organic substrates were tested in this series of bacterial incubations. The three substrates were methanol, trimethylamine, and acetic acid. All three vessels were given the same IC source, crushed limestone, and were incubated at low temperature in a refrigerator (~4°C). See Table 4.1 for a summary of the contents of each vessel. The system called "meth-cold" is identical to "meth-lim" from Experiment 1. System "trim-cold" had 0.5mL TMA and crushed limestone added to it. System "acet-cold" had 1.0mL acetic acid and crushed limestone added to it. At 62 days into incubation, system "acet-cold" was re-inoculated after the system was opened, purged with N_2 gas, and adjusted for pH using a concentrated NaOH solution. Five mL of CO_2 gas was added to the headspace as well.

Preparation of the limestone and handling of all materials was performed in the same manner as Experiment 1 (see above).

Experiment 3

Incubation systems containing lower concentrations of potential substrates were prepared for this experiment. A summary of the contents of the four systems prepared is shown in Table 4.1. The preparation of the culturing medias used in this experiment are slightly different from the details given above and are explained as follows.

Soil "broth" was prepared by boiling 3-4 grams of homogenized soil powder in 900mL of water, then filtering the residual (~700mL). Two grams of sodium bicarbonate were added, and then the volume was increased to 900mL with deionized water. The

solution was boiled again to sterilize, and the final volume was 750mL. The pH was adjusted to about 7 with a few drops of phosphoric acid. This solution was divided into 3 equal parts in three of the four septa jars. Crushed limestone was added to two of the three DOC-rich media solutions. The one system lacking limestone was inoculated with crushed endostromatolite powder from hand specimen IC-2 (see Chapter 3). The system was flushed with nitrogen before sealing it shut. This system was called "0713-calcrete".

Of the two remaining DOC-rich systems, one was given 0.3 grams of 2-bromoethanesulfonic acid, a selective methanogenic inhibitor (Alperin and Reeburgh, 1985). Both were inoculated with 20mL of live methanogenic culture (described previously). Both systems were flushed with nitrogen for a few minutes after inoculation and before closing the jars. The uninhibited system was called "0713-hetero"; the inhibited system containing BES was called "0713-control".

The last system had its own media prepared separately. To 350mL deionized water was added 0.7g of sodium bicarbonate. The solution was boiled down to 250mL and a few drops of phosphoric acid were added to bring the pH down to about 7. The solution was poured into the fourth septa jar and some crushed limestone was added. Then the media was inoculated with 20mL of the same live culture as the aforementioned systems, and nitrogen was bubbled through the solution before the jar was sealed. This system was called "0713-auto".

Preparation of the limestone and handling of all materials was performed in the same manner as Experiment 1 (see above).

All four systems had 10mL of hydrogen (H_2) gas added to their headspaces. Initially, the systems were placed in a fridge (at ~2 to 4°C). After one week, they were taken out and allowed to incubate at room temperature (~21°C).

Serum bottles

At no time during the experiments were the cultures prepared or stored in an anaerobic chamber. The 160mL and 500mL serum bottles used for culturing and incubating were tested for resistance to gaseous leaks. The 500mL bottles used for experimental incubations were obtained from Wheaton Scientific (product # 223952). The septa used to seal these bottles are made of red rubber. The 160mL bottles are in the same style as Wheaton product # 223748 and were used for incubating live cultures, preparing methane standards for GC analysis, and preserving headspace samples. The septa used with these bottles are made of grey butyl rubber.

High purity methane gas (99.94%) was used as a reference for preparing working GC standards. Two standards prepared in serum bottles were tested for their long-term ability to hold methane against freshly-prepared standards. The incipient concentrations of methane in the low- and high concentration standards were 3.4×10^3 and 8.5×10^3 ppmV Gaseous aliquots were removed with a 250 µL Hamilton SampleLock™ syringe (model #1725; Hamilton #H81156) and fitted with a 26S-gauge removable needle (point style #5) for injection into a GC-FID instrument (details below). Figure 24 shows normalized data from the bottles and demonstrates their effective long-term leak-free storage abilities. Despite repeated puncturing, methane diffusion from the bottles was imperceptible to non-existent over more than a year.

In another test, the bottles were sealed with an oxygen indicator solution and a nitrogen headspace. The methylene blue indicator solution (recipe obtained from D. Fortin) was boiled to strip it of dissolved oxygen (that, when present, gives the solution its deep blue colour) prior to sealing it inside the bottles. The media remained colourless for several weeks. The test was ended after a few weeks when a control sample that was not heated nor sealed from the ambient atmosphere became pale and started to stain the interior surfaces of the bottle. Hence the bottles were proven to be impermeable to oxygen and could be used safely outside of an anaerobic chamber.

Analytical techniques

Methane and methanol: amounts

Quantitative methane and methanol data were obtained by injecting gaseous headspace aliquots from incubation vessels into a stand-alone gas chromatograph equipped with a flame-ionization detector (GC-FID). Analytical precision for methane is less than ± 0.5%. The instrument response to methanol is non-linear and shows considerably higher variability in results for repeat analyses. Statistical analysis of variance from results of the experiments reported below show that error (expressed as +/- 2 standard deviations) is random and is about ± 20mmol/L. Results for the experiments are reported herein as calculated quantities (mmol), not as concentrations. Methanol standards were prepared in the same air-tight vessels as methane standards, and separate standards were prepared and maintained at the same temperature as the warm and cold systems of Experiment 1 and 2 (respectively).

Inorganic carbon: amounts

Quantitative DIC data was obtained by reacting liquid samples with phosphoric acid under vacuum. Aqueous samples were filtered with 0.20μm porosity filter paper and injected into a glass vacuum line are reacted with phosphoric acid to protonate DIC species and release them as gaseous CO_2. Trapping of CO_2 and cryogenic separation from water vapour is achieved by using cooled methanol (-80°C) and liquid nitrogen (-196°C). Extracted amounts are calculated from the measured pressure of CO_2 in one of the traps. Isolated and purified CO_2 is transferred into Pyrex breakseals that are used for isotopic analyses explained below. Measurements of DIC are converted to IC using the calculations in Appendix 1 below. Recall from Equation (1) above that IC is the combined sum of aqueous DIC and CO_2 from the headspaces in the incubation vessels.

Acetic acid: amounts

Data for acetic acid was obtained by using a Cecil Instruments ADEPT^{TM} series HPLC equipped with a CSC-Tribute 120A/ODS C-18 reversed phase analytical column.

A weak phosphoric acid carrier separated sample components at a constant flow rate of 1.0 mL per minute. Prior to injection, samples were filtered with 0.45μm pore size filter paper and were acidified to adjust the pH to below 3.5 to ensure that >99% of acetic acid present in the samples was protonated for detection. Detection of acetic acid was achieved with a UV/Vis detector at a wavelength of 230nm.

Methane: $\delta^{13}C$

The ^{13}C-isotopic composition of methane was obtained from a Finnigan MAT Delta Plus IRMS configured with a cryogenic Pre-Con interface for collecting small amounts of methane from gas sample volumes up to 100mL. The Pre-Con interface is preferable over direct-injection into a GC column for component separation interfaced to the IRMS because the former apparatus cryogenically removes CO_2 and methanol vapour prior to CH_4 combustion and cryogenic trapping. The purified sample is thus cryofocussed for release to the IRMS without a GC column, and thus peaks are sharper and produce better analytical results. Samples were prepared in advance by transferring headspace aliquots from the bacterial incubation systems into gas-tight septa bottles purged with air. Blank air samples were run separately to detect for background methane concentrations that were too small to quantify, hence the contributions of methane from air are assumed to be negligible and isotopic corrections are not necessary. Long-term storage of methane in air was proven to be safe and gave reproducible results (see section on "serum bottles" above). The same instrumentation was adapted for isotopic analysis of headspace CO_2; however, headspace samples could not be preserved for analyses of gaseous CO_2 since background levels of CO_2 on flushed bottles were high and posed contamination problems. The reproducibility of CH_4 results from multiple injections of the same sample is about ± 1 ‰, somewhat greater than the instrumental error of ± 0.3‰ for the IRMS.

Inorganic carbon: $\delta^{13}C$

CO_2 obtained from the vacuum-line cryogenic extraction of DIC (discussed above) and trapped in Pyrex breakseals was transferred to glass exetainers in a helium stream. A special transfer line connected to a four-way valve was prepared for this purpose. The exetainers, with open-top septa-lined gas tight caps, could then be loaded onto a GasBench configured to a Finnigan MAT Delta Plus IRMS with a ConFlo III continuous-flow interface for isotopic analysis. The analytical precision is 0.3 ‰. Combining the quantitative and isotopic results for DIC with measured pH values allows for corrected values of [IC] and $\delta^{13}C_{IC}$ to be calculated. See Appendix for the equations used to derive results for IC.

Acetic acid: $\delta^{13}C$

Isolation and collection of acetic acid for isotopic analysis was made possible using the same HPLC instrumentation for quantitative analysis discussed above. A larger sample loop and larger column are installed to handle greater sample volumes. While quantitative data can be obtained from this procedure, precision is not as good, so the technique is purely preparative. An Isco Foxy 200 X-Y Fraction Collector at the end of the flow path recovers sample fractions using manually-selected time windows. The recovered fractions are diluted with deionized water into 40 mL glass vials and are then run on the modified OI Analytical model 1010 wet oxidation TOC analyzer configured to a Finnigan MAT Delta Plus IRMS using the technique of St Jean (2003). The TOC analyzer does not discriminate between TOC components, but in this case, the chromatographic separation of fractions isolates components in advance, and the TOC results reported by the TOC analyzer are for discrete components. This new analytical technique for compound specific isotopic analysis (CSIA) has been extensively tested with results showing that isotopic values for chromatographically-separated fractions are often within the analytical error of the IRMS (i.e., ± 0.3‰), even for samples with complex matrices (Marschner *et al.*, 2005; see Chapter 2).

Results

Experiment 1

The purpose of this experiment was to monitor carbon cycling in selected bacterial incubation systems where methanol was the major substrate and different quantities and species of inorganic carbon were present. Refer to the Methodology section and to Table 4.1 for the names and contents of the incubation systems. System "meth" was not provided with any IC, while "meth-lim" and "meth-buff" were provided with crushed limestone and sodium bicarbonate, respectively. The starting $\delta^{13}C$ of methanol is -42‰ VPDB, highly depleted compared to soil DOC from C3 vegetation (apx. -27‰ VPDB). The important physical properties of the substrates and other incubation media components are shown in Table 4.2.

Quantitative and isotopic data for methane are shown in Figure 25. Accumulation of methane was initially rapid for vessels "meth" and "meth-lim", indicating that the presence / absence of IC was not by itself limiting on production. Very little methane production occurred in "meth-buff" by contrast. This result is consistent with a previous investigation (see Appendix 4). $\delta^{13}C$ values show similar trends for "meth" and "meth-lim". The replenishment of methanol after 54 days is responsible for distinct maxima in $\delta^{13}C_{CH_4}$ values for "meth" and "meth-lim" (Figure 25). The most depleted $\delta^{13}C$ values were obtained from "meth" and are consistently lower than values obtained from "meth-lim". Enriched $\delta^{13}C$ methane values are obtained from "meth-buff", but there is no distinct trend over time. The very low output of methane from this system dismisses the importance of the erratic isotopic trend of this system. Methane production slows to almost imperceptible rates after about 150 days for all three systems.

Levels of inorganic carbon (IC) remained low in all three systems throughout the incubation period. This trend toward depletion is ubiquitous for experimental systems containing methanol. As a result, routine cryogenic extraction of DIC using the phosphoric acid vacuum line method (described above) was not feasible since the method requires volumes of sample inversely proportional to DIC concentration. No other method for quantitative determination of IC was available. Isotopic results for headspace

CO_2 indicate that low DIC levels are maintained at isotopically very depleted values similar to soil DIC (~ -27‰ VPDB) but not as depleted as initial methanol (-42‰ VPDB).

Quantitative and isotopic data for acetic acid are shown in Figure 26. Initially, "meth-buff" had the highest production rate, but after methanol replenishment occurred on Day 40, accumulation ceased almost completely. By contrast, "meth" and "meth-lim" sustained more consistent production, albeit at much different rates. Higher overall production in "meth-lim" is attributable to the presence of a solid carbonate phase, so the production in this system cannot be attributed entirely to homoacetogenic reaction of DOC. The abrupt halt in acetic acid accumulation in "meth-buff" appears to be due to a drop in production, not to increased acetotrophic consumption by other microorganisms.

Isotopic data for HPLC-extracted acetic acid is also shown in Figure 26. System "meth" produced the most enriched acetate, with values close to or slightly enriched versus soil DOC (i.e., -26 to -20‰ VPDB). System "meth-buff" generated the most depleted acetate, with values consistently around -50 to -45‰ VPDB. This result, combined with the rapid uptake of IC, shows a strong predilection by bacteria for ^{12}C. System "meth-lim" produced abundant acetate with intermediary values (-40 to -35‰ VPDB), likely indicating acetate production from several sources including DOC, DIC, and possibly even methanol.

Figure 27 shows pH data collected during the experiment. Both systems lacking a solid carbonate phase, "meth" and "meth-buff", became more acidic over time. System "meth-lim" maintained circumneutral pH values (6.4-6.5) throughout the incubation period. The presence of limestone buffered pH in response to production of organic acids.

Figure 28 shows quantitative methanol data for the three systems. Consumption rates were initially high, so methanol had to be replenished to avoid starving the systems (see "Experiment 1" in methodology section for a more detailed explanation). Consumption of methanol was greatest in system "meth-lim" where the combined

production of methane and acetic acid was highest. Lower bacterial production in system "meth" resulted in lower overall consumption of methanol. In system "meth-buff", the least methanol was consumed likely due to inhibited methanogenic consumption. Carbon isotopic composition of methanol could not be measured, but instead was calculated using a simplified mass balance model discussed below (see Discussion section to follow).

Experiment 2

The purpose of this experiment is to determine how field temperature conditions impact bacterial processes during growth on various substrates. Refer to the Methodology section and to Table 4.1 for more information concerning the preparations for this experiment. The identities of the three systems, "meth-cold", "acetic-cold" and "trim-cold" refer to the major substrates added to them, i.e. methanol, acetic acid, and trimethylamine, respectively. The substrates are isotopically depleted: methanol $\delta^{13}C$ = -42‰; acetic acid $\delta^{13}C$ = -38‰; and trimethylamine $\delta^{13}C$ = -38.2‰ (see Table 4.2). All three systems contained crushed limestone as an IC source.

Methane data for the cold systems are shown in Figure 29. "Trim-cold" was the only system to produce a significant quantity of methane, but overall production was still lower compared to the room-temperature systems of Experiment 1 (Figure 24). The $\delta^{13}C$ values of methane from "trim-cold" are strongly depleted, similar to the methanol-bearing systems of Experiment 1. From a measured low of -97.5‰ VPDB, the $\delta^{13}C$ signal gradually increased during incubation. Systems "acetic-cold" and "meth-cold" generated ^{13}C-enriched methane by comparison. Values of -68‰ increasing to -52‰ observed for "meth-cold" are similar to data obtained from system "meth-buff" of Experiment 1. Few data from "acetic-cold" are availability due to insignificant methane production.

Quantitative and isotopic data for acetic acid are shown in Figure 30. Production in system "meth-cold" remained positive throughout the incubation period. A small net

consumption in "acetic-cold" is evident. System "trim-cold" initially accumulated acetate, but after reaching a peak concentration after 147 days, rapid consumption began. Increased methane production (Figure 29) coincided with the onset of acetotrophic activity. Acetate consumption slowed considerably toward the end of the experiment when about half of the peak quantity remained. ^{13}C-isotopic data show distinct trends for each system. "Meth-cold" acetate became more depleted in ^{13}C over time and reached a quasi-equilibrium composition around -58 to -59‰ VPDB. Acetate in "trim-cold" started at -45‰ and became progressively enriched until a measured high of -18.5‰ was reached at the end of the incubation period. No significant changes in "acetic-cold" are evident.

Inorganic carbon data are shown in Figure 31. All data are expressed as "IC" that is defined herein as the calculated sum of aqueous DIC and gaseous CO_2 (Equation 4-6 above). Results for system "meth-cold" were obtained intermittently since DIC levels were ubiquitously low, requiring much greater amounts of solution to be removed for an extraction. In the first 60 days of incubation, system "trim-cold" underwent a rapid isotopic adjustment. After starting at -18‰ VPDB, $\delta^{13}C_{IC}$ values peaked at -1.1‰ before retreating to -49‰ in a matter of days. Despite no obvious bacterial activity in system "acetic-cold", $\delta^{13}C_{IC}$ values increased from -0.7 to +2.9‰ VPDB in the first 60 days. After 60 days, the vessels were opened to change the septa liners as a precautionary measure to prevent leaks. The headspaces in each vessel were flushed with N_2. After resealing the vessels, 5.0mL of pure CO_2 gas (-36‰ VPDB) was added to each. In addition, the pH of system "acetic-cold" was adjusted to circumneutral values with a few drops of concentrated NaOH, and then reinoculated with a live bacterial inoculum. A vertical line in Figure 30 indicates the approximate time at which the systems were "reset".

After 60 days, system "acetic-cold" still showed no appreciable change in IC levels, and $\delta^{13}C_{IC}$ values gradually decreased to a low of -13.5‰ by the end of the experiment (not counting one anomalous result). In system "trim-cold", IC levels remained low until acetotrophic consumption was initiated after day 147. $\delta^{13}C_{IC}$ values

increased from -18‰ to just below 0‰ VPDB before acetate consumption, at which point values decreased to about -9‰ VPDB.

pH data (not shown) indicate that crushed limestone effectively buffered the production of organic acids, maintaining circumneutral pH conditions throughout incubation. When acetate consumption started in system "trim-cold" after 147 days, pH increased from 6.4 to about 7.1 .

Experiment 3

The purpose of this experiment is to monitor carbon cycling and aqueous chemistry of bacterial systems similar to Experiments 1 and 2 but lacking any concentrated substrates for rapid bacterial growth.

Figure 32 shows the ^{13}C-isotopic composition of IC (that is equal to DIC corrected for headspace CO_2) for the four unenriched systems. There is some noticeable variance within the first 10 days, and this is due to adjustments being made to the pH by adding a few extra drops of phosphoric acid. The inorganic "auto" system was the first system to undergo an enrichment trend after about 40 days. The two organic systems, "hetero" and "control", followed somewhere between 70 and 100 days. The enrichments were short-lived in all three systems. Data for "calcrete" are shown as a smoothed line because this system was essentially sterile and thus serve as a baseline against which the other systems are compared.

Figure 33 shows the acetate data. Error bars are shown for "auto" and are equal to 4ppmC (parts per million carbon), though all systems have the same error. Repeat analyses on individual samples were within this error range. All of the systems appear to undergo a rapid accumulation of acetate after initial inactivity, and the timing of each system's accumulation coincides with the ^{13}C-enrichment of IC shown in Figure 32. Again, data for "calcrete" are shown as a smoothed curve for comparison purposes.

Methane data are not shown. None of the systems produced any significant methane.

Discussion

Experiment 1

In system "meth", methane production was dominant and methanol appears to be the substrate of choice. Acetate production appears to be mainly due to organic matter decomposition, and $\delta^{13}C$ values of acetate confirm this. The slight enrichment of acetate versus DOC may be due to minor aceticlastic methanogenesis or other unknown processes consuming small amounts of acetate over time.

In system "meth-lim", both methane and acetate production were very high and sustainable over a long incubation period. The intermediate values of acetate $\delta^{13}C$ suggest variable sources. Acetate may be derived from both DOC decomposition and homoacetogenic production, the latter process having a large fractionation factor not unlike CO_2-reduction by methanogens (Gelwicks *et al.*, 1989).

System "meth-buff" confirms the presence of homoacetogenic bacteria that responded to the presence of abundant DIC by accumulating acetate rapidly. The low $\delta^{13}C$ values of acetate likewise confirm that the rapid accumulation of acetate was not from an organically-derived source. The low activity of methanogens, on the other hand, is curious and unexpected. One explanation is that they were partially inhibited by their inabilities to compete for CO_2/H_2 with homoacetogens. This does not explain why they did not revert to fermentive consumption of methanol that could have been the basis of a syntrophic relationship with DIC-hungry acetogens.

The carbon isotopic data for methane in systems "meth" and "meth-lim" are indicative of production from a single source. The distinct rise in $\delta^{13}C$ values for methane until methanol replenishment is strong indication of Rayleigh-type distillation.

Verification of this hypothesis is achieved by performing carbon mass balance calculations for methanol and deriving fractionation factors for the methanogenic practices. These calculations are to follow below.

Experiment 2

System "meth-cold" was prepared very similarly to system "meth-lim" of Experiment 1, but it behaved more like "meth-buff" because of low methanogenic activity. These results appear to corroborate previous findings that acetogens have a competitive advantage over methanogens for competitive substrates at low temperatures (Conrad *et al.*, 1989; Fey and Conrad, 2000). However, methane production was much more significant in system "trim-cold" both before and after the onset of aceticlastic methanogenesis. A possible explanation is that trimethylamine is exclusively a methanogenic substrate whereas it is conceivable that methanol is a competitive substrate for both groups of organisms, and hence methane production would be partially inhibited. While there is no direct evidence (here or in previous research) to substantiate methanol usage by acetogens, the substitution of one equivalent of CO_2 in the autotrophic reaction (4-2) would yield the following reaction:

$$CO_2 + CH_3OH + H_2 \rightarrow CH_3COOH + H_2O \qquad (4\text{-}8)$$

If such a reaction is possible by acetogens, it would help to explain the much lower sustained DIC concentrations in all of the systems containing methanol. The strong depletion of DIC is not seen in system "trim-cold".

As for DIC, the results hint at the possibility of Rayleigh-type distillation processes causing very short-lived enrichments in $\delta^{13}C_{IC}$ in system "trim-cold" (Figure 31). The much more gradual rise in $\delta^{13}C_{IC}$ values for system "acet-cold" may be related to minor homoacetogenic activity. This may be a good indication that incubation at slower rates is needed to study Rayleigh distillation processes. The low-concentration systems of Experiment 3 appear to achieve the desired result.

Experiment 3

Bacterial activity appears to have been most strongly favored in the (mostly) inorganic "0713-auto" system. Acetate accumulated and DIC became enriched in ^{13}C concurrently, generating a nice Rayleigh-type distillation curve. However, once acetate stopped accumulating, the enrichment of DIC likewise stopped. Very similar results were obtained for systems "0713-hetero" and "0713-control". The selective inhibition of methanogens in the latter system did not make a difference as methane did not accumulate beyond trace levels in all of the systems, but the similarity of results in "0713-hetero" and "0713-control" prove that the enrichment of DIC could only have been due to acetogenic processes, not to methanogenic processes. The one system inoculated with endostromatolite powder, "0713-calcrete", did not produce any results, indicating that the hand specimens are sterile.

It is unknown what caused the three active systems to cease acetate production. Aceticlastic methanogenesis is possible and was certainly witnessed in Experiment 2. Clearly, the results of this experiment support the acetogenic origin of ^{13}C-enrichment in endostromatolites, and moreover, if enrichment is to be sustained over time, acetate must be removed from the system before it can be consumed by other organisms and returned to the DIC pool. Thus it appears less likely that endostromatolites grew in closed-system conditions like the experiments reported herein.

Methanogenesis versus acetogenesis

Comparing the results of the incubation vessels in Experiment 1 and Experiment 2, the room temperature vessels of Experiment 1 produced more methane and more acetic acid than the refrigerated vessels of Experiment 2. Overall, more carbon accumulated as acetic acid than as methane. The ratio of acetic acid to methane was much greater for the cold systems. Figure 34 shows the ratio of acetic acid to methane expressed in units of carbon for selected incubation systems of both experiments. Methanogenesis is much

more adversely impacted at lower temperatures, and the results are similar to previous research (Conrad *et al.*, 1989; Wu *et al.*, 2001). The increase in the acetate:methane product ratio over time for all systems except "trim-cold" indicates that methanogenesis was more ephemeral than acetogenesis. The drop in the ratio for system "trim-cold" is related to the onset of acetrophic consumption. So the affinity of carbon toward acetic acid as an end-product of bacterial production is significant at all temperatures tested and is the dominant process at low temperatures. This result is consistent with the findings of Hines *et al.* (2001).

Rayleigh-type isotopic enrichments

The Rayleigh distillation equation is defined as follows:

$$R = R_o \bullet f^{(\alpha-1)} \qquad (4\text{-}9)$$

where R is the isotopic ratio of a compound being analyzed ($^{13}C/^{12}C$ in the case of carbon), R_o is the initial ratio (before reaction), f is the dimensionless residual amount of the reacting compound, and α is the isotopic fractionation factor. Methanogenesis and acetogenesis produce some of the largest isotopic fractionations of carbon known because bacteria strongly favour using ^{12}C over ^{13}C. Consequently, methanogenic and acetogenic substrates tend to accumulate ^{13}C over time, and this is how a Rayleigh-type enrichment is created.

Some of the experimental data show Rayleigh-like enrichments over time. For example, Figure 25 shows gradual increases in $\delta^{13}C$ of methane for two systems ("meth" and "meth-lim") until methanol was replenished after 50 days. Figure 31 depicts short-lived Rayleigh-like enrichments for IC, but biogenic CO_2 production eventually overwhelms the isotopic equilibrium of IC toward depleted values over time. Although direct isotopic measurements of methanol and trimethylamine could not be made, quantitative and isotopic data for the products of bacterial processes can be used to

generate isotopic mass balance equations from which the $\delta^{13}C$ composition of residual organic reactants for each system can be determined (see Appendix 3 for calculations).

Figure 34 shows the calculated $\delta^{13}C$ values of methanol over time for the 21°C systems of Experiment 1, derived from isotopic mass balance calculations. Data for the first 50 days of incubation are not included since replenishment of methanol occurred at this time and hence a portion of the substrate pool was not available to the bacteria. Most of the fractionation in systems "meth" and "meth-buff" occurred before the replenishment of methanol. System "meth-lim", on the other hand, continued to react and fractionate methanol for a longer period of time. The quantitative methanol data for this system is superimposed on the isotopic data to emphasize that the ^{13}C-enrichment of methanol coincides with steady methanol consumption, hence satisfying the conditions for a Rayleigh-type isotopic enrichment.

Using Equation 4-9 above, values of α are calculated for each set of data from system "meth-lim" where *f*, R and R_o are known. Figure 36 shows the data set for $\delta^{13}C$ of methanol versus *f*. To ensure the best possible fit of the Rayleigh enrichment curve, R_o was assumed to be unknown and Equation 4-9 was solved for R_o and α using the entire data set. The $\delta^{13}C$ of methanol had been previously analyzed from an aliquot taken directly from the reagent bottle; however, the starting $\delta^{13}C$ of the incubation systems could not be assumed to be equal to the previously-analyzed value of reagent methanol given the volatility of methanol and the presence of a headspace in the reagent bottle. Quantitative data for methanol was modeled to smooth out large variations in measured values, and the resulting curve in Figure 36 has calculated values of -42.4‰ for R_o and 0.970 for α. The former result closely matches the measured R_o of -42‰. The latter result for α is significantly different from published values of isotopic fractionation for autotrophic methanogenesis alone (0.934 at 25°C; Clark and Fritz, 1997). This is a good indication that more than one bacterial process is responsible for consuming methanol (as had been postulated from the results of Experiment 2), and it is possible to calculate estimates for the individual isotopic fractionation factors for each process.

Methane and acetic acid are the major end-products of bacterial processes in the incubation systems, and other sources and sinks of carbon are assumed to be small. The abundance of carbon in acetic acid (n_a) is expressed relative to carbon directed toward the sum of carbon in both acetic acid and methane. Data from Experiment 1 are used since the 21°C systems had the same substrate and temperature conditions. Instead of determining global averages of α and n_a for each incubation system, discrete values of α and n_a were calculated from each experimentally-derived value of *f* and R (R_o is assumed to be known and constant, in this case). The data are shown in Figure 37. Data from one of the systems from Experiment 2, "meth-cold", are also shown. A mixing curve (i.e. mixing of the discrete acetogenic and methanogenic reactions) to fit all of the Experiment 1 data was calculated as $\alpha = -0.0222\ n_a^2 + 0.0608\ n_a + 0.9455$. If global averages for α and n_a are used instead of discrete values (not shown), the mixing curve has nearly an identical equation and the fit of the curve to the data is nearly perfect (i.e. the coefficient of correlation, R^2, is greater than 0.999).

The endpoints of the mixing curve in Figure 37 provide the isotopic fractionation values for each bacterial process. For methanogenesis, $\alpha = 0.9455$, and for acetogenesis, $\alpha = 0.9841$. The former value is much closer to the published value of 0.934 for autotrophic methanogenesis at 25°C (Clark and Fritz, 1997). Hence methanol generates a fractionation of carbon not dissimilar to CO_2/H_2. It must be noted, however, that the methanogenic reaction of methanol can occur with and without hydrogen (see reactions 4-1 and 4-5 above). The experimentally calculated value of 0.9455 could thus represent a weighted average of two different methanogenic reactions. Given the results of Experiment 1, and in particular, the lack of methane production in system "meth-buff" in the presence of strong acetogenic activity, methanol fermentation by methanogens appears to be of marginal importance. Thus 0.9455 is probably a good estimation of hydrogenotrophic methane production from methanol (Reaction 4-3). The fractionation factor for acetogenesis is not nearly as meaningful as there is only indirect evidence pointing toward methanol conversion to acetate. Acetate from DOC decomposition

would tend to contribute enriched fractions that pull the calculated fractionation factor higher than previously published values (i.e. 0.942; Gelwicks *et al.*, 1989).

Data from system "meth-cold" plot along the mixing curve (Figure 14), so acetogenic processes do not seem to be impacted by low temperatures and hence continue to fractionate carbon despite the lack of competition from methanogenic processes. The impact of temperature on carbon fractionation by methanogenic processes could not be determined due to partial inhibition of methanogenesis at lower temperatures, hence providing a lack of data.

Not enough data were collected from the systems of Experiment 3 to perform carbon mass balance calculations and determine fractionation factors of the dominant processes.

Conclusions

Three sets of experimental incubations systems were created at different ambient temperatures. The first set of systems incubated at room temperature (~21°C) produced high levels of both methane and acetic acid. The second set incubated at low temperature in a refrigerator (~4°C) produced less of both products with a higher ratio of acetic acid to methane. The third set incubated at room temperature in the presence of low substrate concentrations also had a high ratio of acetic acid to methane produced. The bacteria used in these experiments were cultured from frozen soil collected from a periglacial limestone terrain where methane is being produced in low but significant quantities (Chapter 3). The limestone terrain hosts unique secondary deposits within fissures, called endostromatolites. Previous research invoked methanogenic processes as being responsible for endostromatolite formation and, in particular, the strong ^{13}C-enrichment trends found within growth columns. Evidence from the experimental incubations systems seems to contradict this assertion. Acetogenic bacteria were more active at cold temperatures and more active during low substrate availability. Isotopic results from the first two experiments also show that fractionation of carbon to form acetate changed very

little under different temperature conditions, proving that acetogens are inherently more suited to cold climate conditions.

^{13}C enrichment trends measured from secondary biogenic growths within limestone fissure (endostromatolites) are likely due to Rayleigh-type enrichment processes. Experimental incubation systems inoculated with cultured bacteria from periglacial limestone terrains have produced results amenable to the Rayleigh distillation model for isotopic fractionation. The experiments reported herein modeled the Rayleigh distillation curve on methanol as this substrate was preferentially consumed by methanogens and possibly acetogens. Residual methanol incurred a Rayleigh-type enrichment in ^{13}C as would be expected from a comparable autotrophic culture grown on CO_2/H_2. Future experiments with careful planning could produce the same results for modeling of DIC enrichment.

The fact that inorganic carbon did follow a sustained enrichment trend in the systems of the first two experiments is related to the organic-rich matrix. Rapid uptake of DIC by respiring bacteria and replenishment by fermentative microorganisms maintained DIC in close equilibrium with DOC, meaning that Rayleigh-type enrichments in DIC observed during initial bacterial growth were short-lived. For DIC enrichment to be sustainable, aceticlastic methanogenesis has to be marginalized. Previous research by Hines *et al.* (2001) is consistent with this hypothesis, i.e. that acetic acid is transiently accumulating in cold climate regions, implying that aceticlastic bacterial activity is not favourable at reduced temperatures. The experimental results from the enriched cultures demonstrate that methanogenic activity is almost completely inhibited at low temperature except in the presence of a non-competitive substrate like trimethylamine that is not representative of any compound found in natural periglacial systems. Only when such substrates are available do methanogens thrive and diversify their activities to include aceticlastic processes. In the recent geological past when climate was warmer in periglacial regions, greater groundwater circulation may have limited methanogenic processes from isotopically depleting the DIC pool within endostromatolite growth zones, allowing the enriched growth signal to occur under partially open conditions. This

factor of increased transport has been previously theorized to explain the ^{13}C-enrichment trends measured along endostromatolite growth columns.

Use of the Rayleigh isotopic fractionation model with experimental results for acetic acid and methane production generates experimental isotopic fractionation factors for methanogenesis ($\alpha = 0.946$) and acetogenesis ($\alpha = 0.984$). The fractionation factor for methanogenesis is not as low as previously published values for CO_2-reduction but is a good estimate of it. The fractionation factor for acetogenesis is a weighted average of several acetogenic processes including DOC decomposition that is not expected to have much fractionation related to it. The Rayleigh model calculations were very good at estimating the starting $\delta^{13}C$ of methanol (-42.4‰ VPDB calculated versus -42‰ VPDB measured on stock solution), proving that this model can be used with confidence for future research into evaluating the importance of various bacterial processes to carbon cycling.

Acknowledgements

This research project was funded by NSERC Research Grant 42590 to I.D.Clark and by a research bursary (PGS-B) provided to M. Marschner. Analyses were performed at the G. G. Hatch Stable Isotope Laboratories, Ottawa-Carleton Geosciences Centre, University of Ottawa, and we are most grateful to P. Middlestead, G. St. Jean, W. Abdi, and P. Wickham for their expertise and many suggestions. Additional facilities and materials were provided by D. Fortin to whom we are very thankful.

References

Alperin M J, Reeburgh W S (1985) Inhibition experiments on anaerobic methane oxidation. *Applied and Environmental Microbiology*. **50**: 940-945.

Baresi L (1984) Methanogenic cleavage of acetate by lysates of *Methanosarcina barkeri*. *Journal of Bacteriology*. **160**: 365-370.

Brock T D, Madigan M T, Martinko, J M, Parker J (1994). *Biology of Microorganisms (7th edition)*. Prentice Hall.

Chanton J P, Bauer J E, Glaser P A, Siegel D I, Kelley C A, Tyler C S, Romanowicz E H, Lazrus A (1995) Radiocarbon evidence for the substrates supporting methane formation within northern Minnesota peatlands. *Geochimica et Cosmochimica Acta*. **59**: 3663-3668.

Clark I, Fritz P (1997). *Environmental Isotopes in Hydrogeology*. Boca Raton, Lewis Publishers.

Clark I D, Lauriol B, Marschner M, Sabourin N, Chauret Y, Desrochers A (2004) Endostromatolites from permafrost karst, Yukon, Canada: paleoclimatic proxies for the Holocene hypsithermal. *Canadian Journal of Earth Sciences*. **41**: 387-399.

Conrad R, Mayer H-P, Würst M (1989) Temporal change of gas metabolism by hydrogen-syntrophic methanogenic bacterial associations in anoxic paddy soil. *FEMS Microbiology Ecology*. **62**: 265-274.

Department of Energy, Mines and Resources (Canada), *Aklavik – District of Mackenzie* (Geological Map 1517A). Surveys and Mapping Branch.

Dyke L D (1975). Structural investigations in Campbell Uplift, District of MacKenzie. *Geological Survey of Canada, Paper 75-1 (A)*, 525-532.

Ehrlich H L (1996) *Geomicrobiology (3rd edition)*. New York, Marcel Dekker Inc.

Gelwicks J T, Risatti B, Hayes J M (1989) Carbon isotope effects associated with autotrophic acetogenesis. *Organic Geochemistry*. **14**: 441-446.

Hines M E, Duddleston K N, Kiene R P (2001) Carbon flow to acetate and C_1 compounds in northern wetlands. *Geophysical Research Letters*. **28**: 4251-4254.

Klass D L (1984) Methane from anaerobic fermentation. *Science*. **223**: 1021-1028.

Krzycki J A, Kenealy W R, DeNiro M J, Zeikus J G (1987) Stable carbon isotope fractionation by *Methanosarcina barkeri* during methanogenesis from acetate, methanol, or carbon dioxide-hydrogen. *Applied and Environmental Microbiology*. **53**: 2597-2599.

Krzycki J A, Wolkin R H, Zeikus J G (1982) Comparison of unitrophic and mixotrophic substrate metabolism by an acetate-adapted strain of *Methanosarcina barkeri*. *Journal of Bacteriology*. **149**: 247-254.

Lansdown J M, Quay P D, King S L (1992) CH_4-production via CO_2 reduction in a temperate bog: A source of ^{13}C-depleted CH_4. *Geochimica et Cosmochimica Acta*. **56**: 3493-3503.

Lauriol B, Clark I (1999) Endostromatolites in the arctic: a paleohydrologic indicator. *Applied Geochemistry*. **14**: 775-785.

Lovley D R, Goodwin S (1988). Hydrogen concentrations as an indicator of the predominant terminal electron-accepting reactions in aquatic sediments. *Geochimica et Cosmochimica Acta*. **52**: 2993-3003.

Marschner M (2005) Methanogenic versus acetogenic reactions in periglacial groundwaters; implications for biogenic endostromatolite formation. (Chapter 3, this volume)

Marschner M, Clark I (2004) ^{13}C enrichments in periglacial biogenic carbonates may be due to acetogenic processes instead of methanogenesis. In: Water-Rock Interaction. Proceedings of the Eleventh International Symposium on Water-Rock Interaction WRI-11 , Saratoga Springs, NY, USA 27 June – 2 July (eds. Wanty, RB, Seal RR), 451-455.

Marschner M, Middlestead P, Clark I (2005). Using a simple high-performance liquid chromatography separation and fraction collection methodology to achieve compound-specific isotopic analysis for dissolved organic compounds. *Rapid Communications in Mass Spectrometry*. **19**: 261-268.

Martens C S, Kelley C A, Chanton J, Showers W J (1992) Carbon and hydrogen isotopic characterization of methane from wetlands and lakes of the Yukon-Kuskokwim delta, Western Alaska. *Journal of Geophysical Research.* **97**: 16,689-16,701.

Ritchie J C (1976) The Campbell Dolomite Upland near Inuvik, N.W.T. – A Unique Scientific Resource. *Musk-Ox*. **18**: 70-75.

St-Jean G (2003) Automated quantitative and isotopic (13C) analysis of dissolved inorganic carbon and dissolved organic carbon in continuous-flow using a total organic carbon analyser. *Rapid Communications in Mass Spectrometry*. **17**: 419-428.

Sugimoto A, Wada E (1993) Carbon isotopic composition of bacterial methane in a soil incubation experiment: Contributions of acetate and CO_2/H_2. *Geochimica et Cosmochimica Acta*. **57**: 4015-4027.

Whiticar M J Faber E, Schoell M (1986) Biogenic methane formation in marine and freshwater environments: CO_2 reduction vs acetate fermentation- Isotope evidence. *Geochimica et Cosmochimica Acta*. **50**: 693-709.

Woltemate I, Whiticar M J, Schoell M (1984) Carbon and hydrogen isotopic composition of bacterial methane in a shallow freshwater lake. *Limnology and Oceanography*. **29**: 985-992.

Wu X L, Chin K J, Stubner A, Conrad R (2001) Functional patterns and temperature response of cellulose-fermenting microbial cultures containing different methanogenic communities. *Applied Microbiology and Biotechnology*. **56**: 212-219.

Table 4.1: Summary of Experimental System Contents

EXPERIMENT 1

Vessel ID	culture media	C- bearing substrates	T (°C)
"meth"	10g/L soil powder "broth" (see text)	0.36M methanol (0.11 mol in 304.5 mL total)	21
"meth-lim"	10g/L soil powder "broth" (see text)	0.36M methanol and ~4 grams crushed limestone	21
"meth-buff"	10g/L soil powder "broth" (see text)	0.40M methanol and 0.05M $NaHCO_3$	21

EXPERIMENT 2

Vessel ID	culture media	C- bearing substrates	T (°C)
"meth-cold"	10g/L soil powder "broth" (see text)	0.21M methanol and ~4 grams crushed limestone	4
"acetic-cold"	10g/L soil powder "broth" (see text)	0.07M acetic acid & ~4 grams crushed limestone	4
"trim-cold"	10g/L soil powder "broth" (see text)	0.02M trimethylamine-HCl & ~4g crushed limestone	4

EXPERIMENT 3

Vessel ID	culture media	C- bearing substrates	T (°C)
"0713-auto"	De-ionized water	0.33M sodium bicarbonate + crushed limestone	21
"0713-hetero"	10g/L soil powder "broth" (see text)	0.32M sodium bicarbonate + crushed limestone	21
"0713-control"	10g/L soil powder "broth" (see text)	0.32M sodium bicarbonate + crushed limestone	21
"0713-calcrete"	10g/L soil powder "broth" (see text)	0.32M sodium bicarbonate + powdered endostromatolite "IC-2" (described in Chapter 3)	21

Table 4.2: Physical properties of incubation media components

REAGENT	**Formula**	**Purity**	$\delta^{13}C$ (‰ VPDB)
methanol	CH_3OH	0.9999	-42
acetic acid	CH_3CO_2H	>0.998	-38.02
sodium bicarbonate	$NaHCO_3$	1	-4.8
trimethylamine hydrochloride	$(CH_3)_3N{\bullet}HCl$	>0.98	-38.2
limestone	$CaCO_3 \pm MgCO_3$	N/A	N/A

Chapter 5

Summary and Conclusions

Endostromatolites are biogenic secondary carbonate deposits occurring within limestone fissures in Canada's permafrost regions. Their oxygen isotopic signals have been used as paleotemperature indicators from being in equilibrium with meteoric waters during emplacement over thousands of years since the last ice age ended some 13,000 years ago. Their ^{13}C-enriched isotopic signals indicate bacterial involvement from microorganisms capable of selectively reacting substrate molecules containing isotopically lighter carbon and thus enriching the residual dissolved inorganic carbon (DIC) with ^{13}C. The presence of these bacteria in the original depositional setting infers that conditions must have been anoxic and saturated. The widespread distribution of endostromatolites within exposed limestone outcrops suggests that the required conditions were ubiquitous in past periglacial environments. Present-day permafrost regions are too cold and too arid to support the widespread growth of these deposits. Weathering processes and deeper groundwater circulation in temperate regions tend to favour the development of vadose-zone karst, and so this is why endostromatolites are yet to be found outside of cold-climate regions.

This thesis has attempted to determine the processes responsible for creating the ^{13}C-enriched isotopic signals from endostromatolites by evaluating the biogenic processes of natural bacterial colonies obtained from periglacial soil within limestone terrains. Over the course of the past 7+ years, several field- and lab-based projects were launched to determine what organisms were responsible for creating the enriched secondary deposits and to infer how they were created. It is easy to forget that many of the tools used to achieve these purposes were not always available. New analytical instrumentation had to be acquired and new methodologies had to be developed. Even routine analyses were not always routine due to instrument unavailability and other technical problems. The results presented by this thesis represent some of the best achievements from experiments in working with unpredictable natural bacterial communities.

Here are some of the outcomes and conclusions, described briefly, that this investigation has produced:

- Compound Specific Isotopic Analysis (CSIA) is achieved for short-chain fatty acids in pure solutions and complex matrices. Using carbon-free carrier solvents with an existing High-Precision Liquid Chromatography (HPLC) instrument and a fraction collector, up to 100% recovery of individual compounds was achieved without affecting the integrity of these compounds in preparation for isotopic analysis on a wet-oxidation TIC-TOC Analyzer configured to an isotope ratio mass spectrometer (IRMS). Results were within the analytical error (±0.3‰) of the IRMS, thus lending a high degree of confidence to results of later experiments with bacterial incubation systems. This methodology needed to be established so that individual organic compounds produced from experimental cultures could be characterized isotopically rather than treating dissolved organic matter (DOM) as a whole.
- A new microdrilling technique for recovering and analyzing small carbonate samples for $\delta^{13}C$ and $\delta^{18}O$ was tested and validated. Three endostromatolite hand specimens showing good internal preservation were cut into thin and thick sections and sampled along individual growth columns. The thin sections proved to be too thin, but thick sections generated isotopic data that replicates previous findings where $\delta^{13}C$ is shown to be greater along endostromatolite growth columns compared to the host rock.
- A simple Rayleigh-type enrichment model was used to show how DIC in solution with active methanogenic and acetogenic bacteria becomes gradually enriched in ^{13}C over time. It is carbonate precipitating from enriched DIC that creates the isotopic signals measured in endostromatolite growth columns. The model predicts greater fractionation of DIC per equivalent of DOC (dissolved organic carbon) reacted by acetogenic bacteria compared to methanogenic bacteria, despite homoacetogenesis having less affinity for ^{12}C than methanogenic CO_2-reduction. Under closed system conditions, a strong potential exists for DIC

to become radiogenically "old" as acetogenesis preferentially puts limestone-derived DIC into solution.

- Field data from groundwaters in a periglacial limestone terrain where endostromatolites are found within outcrop fissures show that present-day conditions are not conducive to processes theoretically believed to have created endostromatolites. Methane is a ubiquitous product in anaerobic waters above permafrost, but $\delta^{13}C$ values do not show enrichments in high-methane waters, nor is acetate available in any appreciable quantity. Inhibited transport combined with the high availability of DOC may be responsible for encouraging bacterial activities that add ^{13}C-depleted DIC to solution. Eh values were higher than expected due to abundant sulphate in the sample waters, showing that methanogenesis is not inhibited by sulphate and that electromotive potential may not be a suitable measurement for predicting bacterial activities occurring in surface waters above permafrost.
- Some of the field conditions were mimicked in bacterial incubation experiments using cultured bacteria derived from frozen soil collected from the field site. Specifically, DIC enrichment was short-lived as negative feedback signals held DIC in closer isotopic equilibrium with DOC. Use of certain substrates (i.e. methanol) produced very distinct Rayleigh-type enrichments in the reactants, and these results were used with the Rayleigh model to calculate fractionation factors for methanogenic and acetogenic processes in the incubation systems. Methanogenic reduction of methanol strongly favours the production of $^{12}CH_4$ with a fractionation similar to CO_2-reduction.
- The bacterial incubation experiments tested many different conditions for growth. Acetogenesis was strongly favoured in the presence of DIC and limestone and appeared to have a competitive advantage over methanogenesis at cold temperatures. When substrates were limited, slow accumulation of acetate was concurrent with a gradual ^{13}C enrichment in DIC, complementing previous theoretical considerations that acetogens may be responsible for enrichment trends in endostromatolites.

- Aceticlastic methanogenesis was witnessed in bacterial incubation systems where methanogenesis was not inhibited by competitive uptake of substrates by acetogens. For DIC to maintain enriched $\delta^{13}C$ values, acetate must remain unavailable to methanogens. Partially-open conditions can achieve this, though this would likewise have the result of curtailing further enrichment of DIC. Endostromatolites bearing linear $\delta^{13}C$ signals along growth columns could indicate partially-open conditions and thus limit the usefulness of the Rayleigh distillation model in describing ^{13}C-enrichment processes for fissure deposits.

Further research is proposed to investigate the "openness" of endostromatolite growth systems. Dating paleoclimate events from ^{18}O data obtained from endostromatolites hinges on understanding the openness of these systems and hence the relative contributions of limestone from the host rock versus radiogenically active carbon from outside sources. Acetogenesis appears to increase contributions of radiogenically "old" carbon from limestone to the DIC pool, thereby affecting how ^{14}C age dates from endostromatolites are interpreted, though transport rates of products in and out of limestone fissure systems is equally important yet largely unknown. Some of the closed-system incubation experiments performed for this investigation could be repeated to determine the reproducibility of the results and to collect data for ^{18}O. This thesis has focused exclusively on carbon isotope systematics, but given the large fractionation incurred in methanogenic and acetogenic processes, and given that there is an even greater molecular mass difference between ^{18}O and ^{16}O compared to ^{13}C and ^{12}C, isotopic fractionation of oxygen may be at least as significant as fractionation of carbon in many of the processes observed. New methodologies for analyzing $\delta^{18}O$ of discrete compounds would have to be proposed and validated, but a preliminary investigation focusing on the ^{18}O-composition of water in a closed system incubation would elucidate if there are significant feedback signals that would skew interpretation of $\delta^{18}O$ data from being a clear paleotemperature signal. With the results of the repeated closed-system experiments, further experimentation with open-system incubation systems can be proposed to determine bacterial response under conditions which may more closely resemble the setting of endostromatolite emplacement.

FIGURE 1

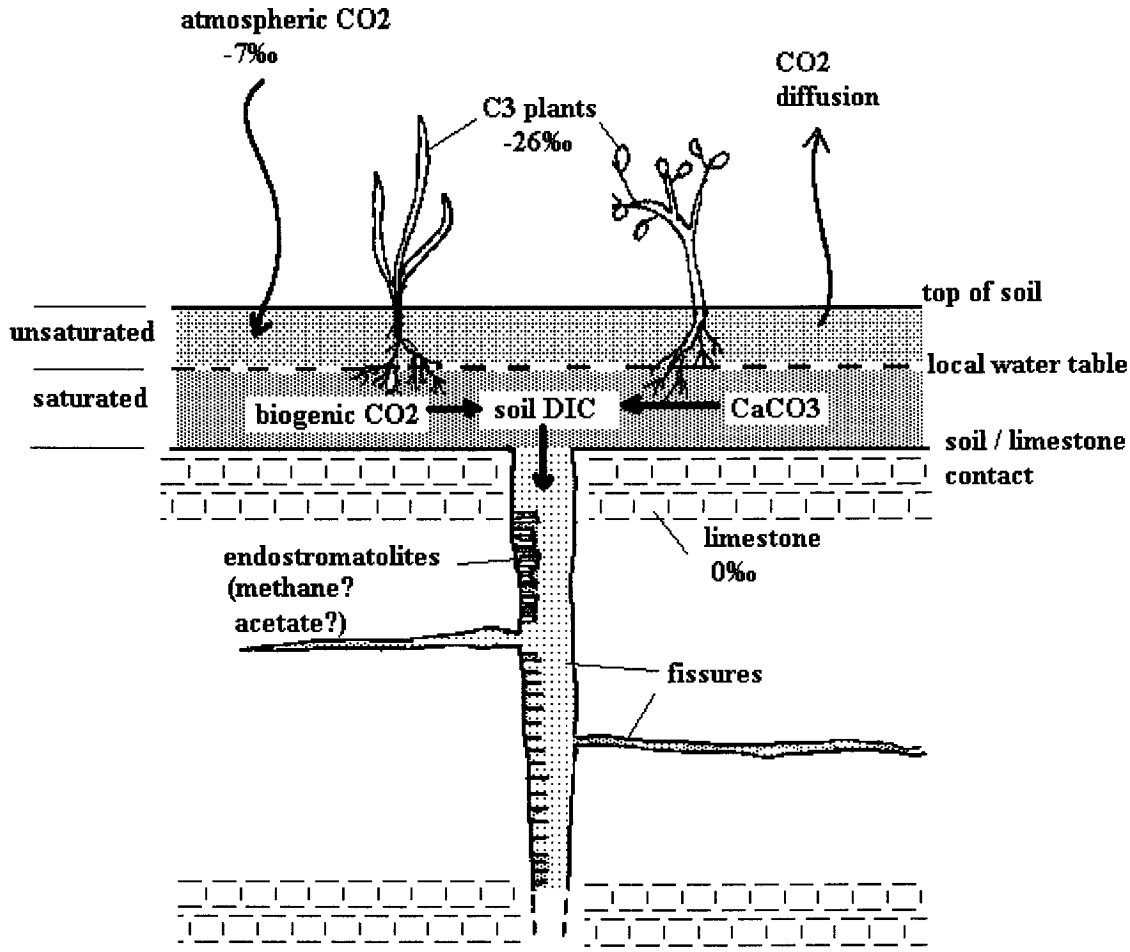

Figure 1: Conceptual model of the original environment in which endostromatolite growth took place. No drawn to scale. See Chapter 1 (Introduction) for explanations of the various processes shown. It is believed that bacterial processes within the fissure created ^{13}C-depleted products and thus enriched the residual DIC pool.

FIGURE 2

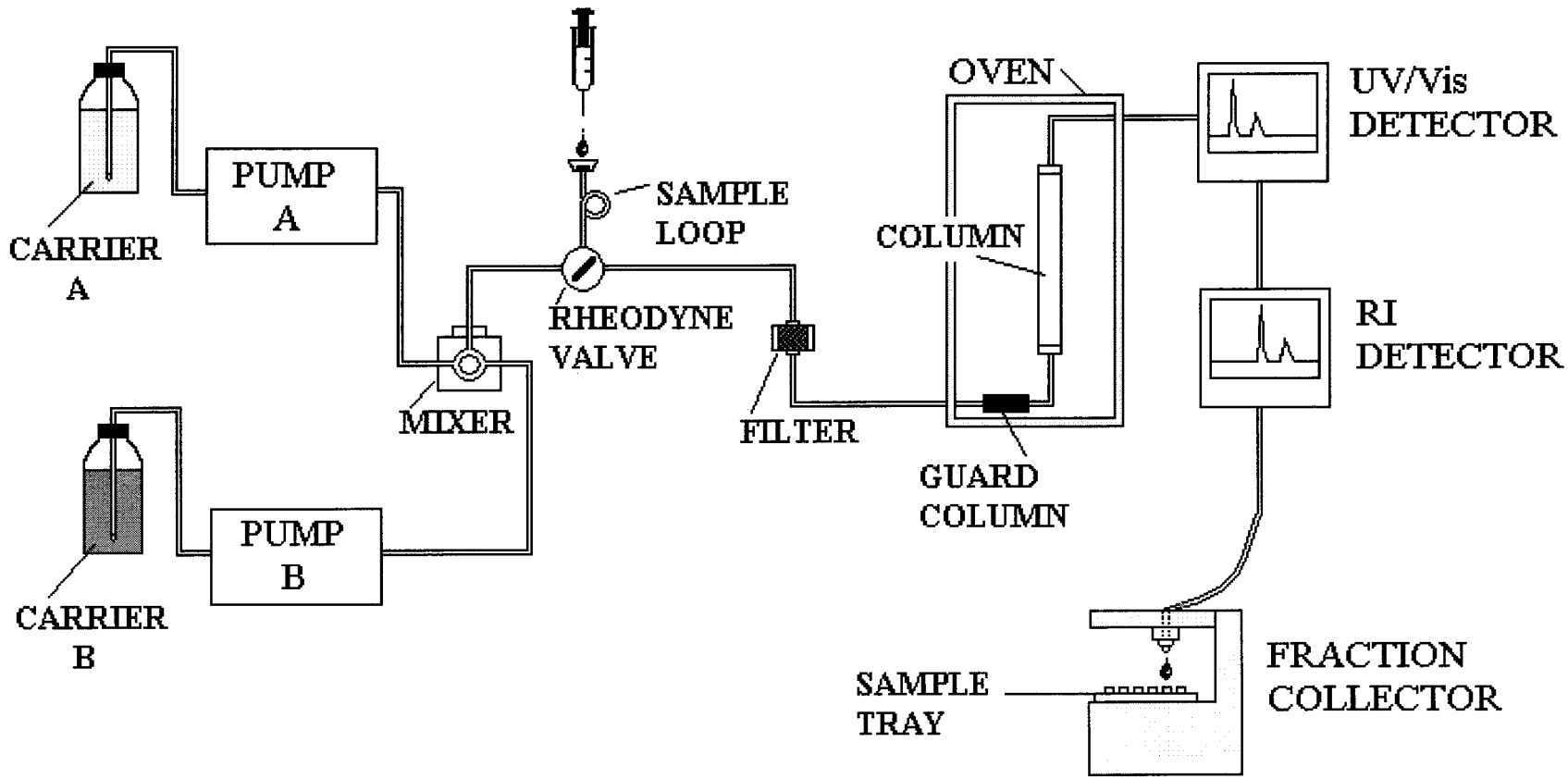

Figure 2: Schematic diagram showing HPLC components along flowpath. Not shown are electrical connections to the chromatography system manager (CSM) and the data capturing software (PowerStream 2.0).

FIGURE 3

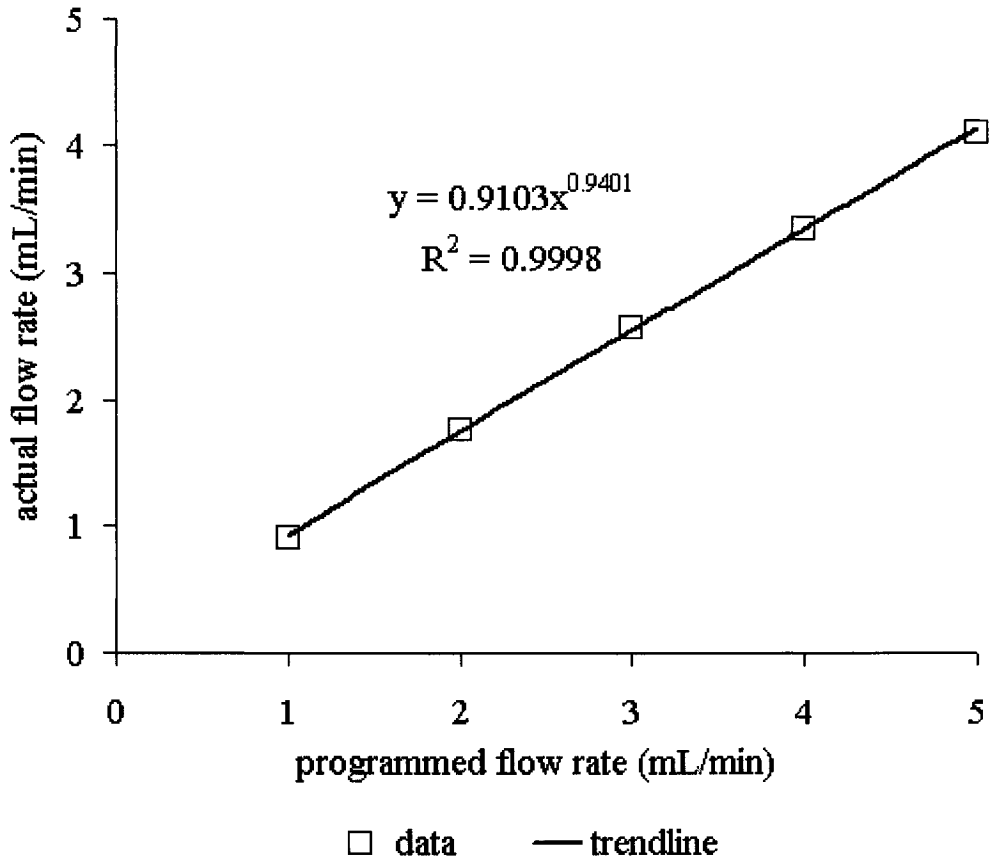

Figure 3: Calculated (actual) flow rates versus programmed flow rates for the dual-piston HPLC pumps.

FIGURE 4

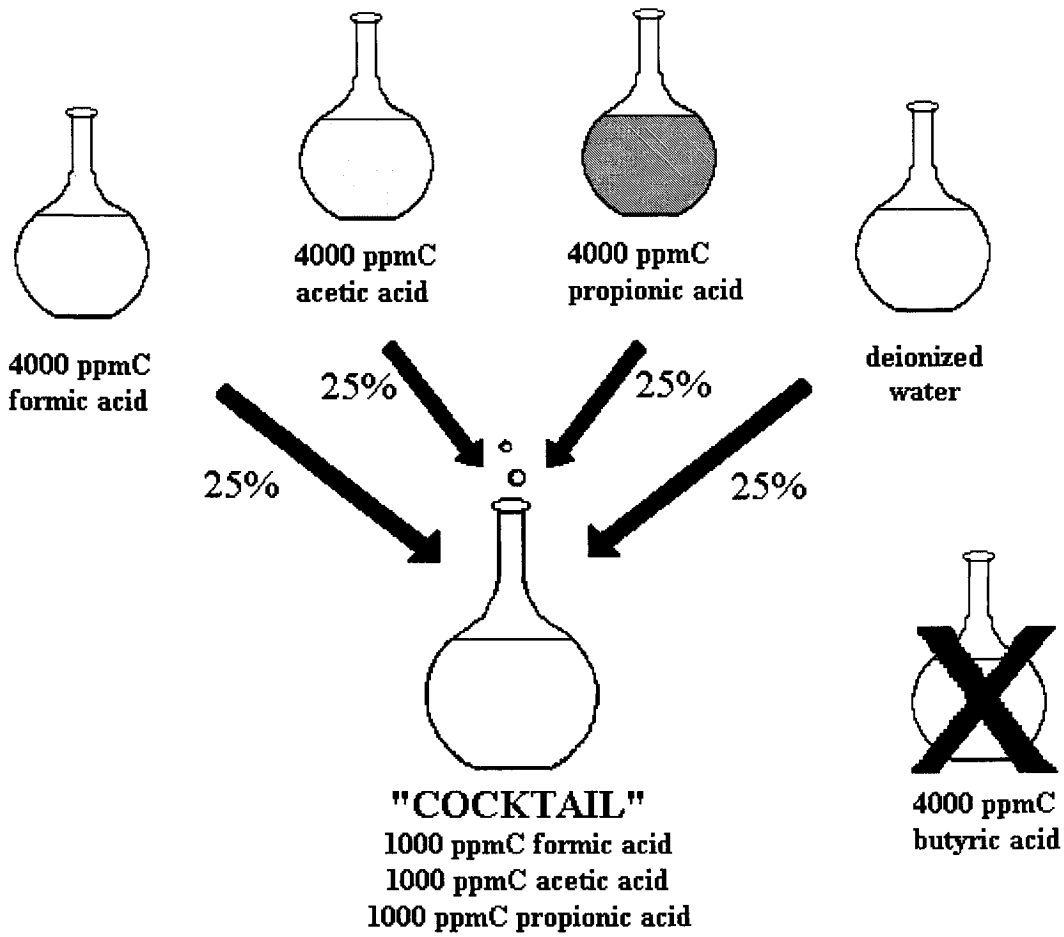

Figure 4: Standard mixture "cocktail" is made from one part of each of the first three fatty acid standards, plus one part deionized water in lieu of butyric acid

FIGURE 5

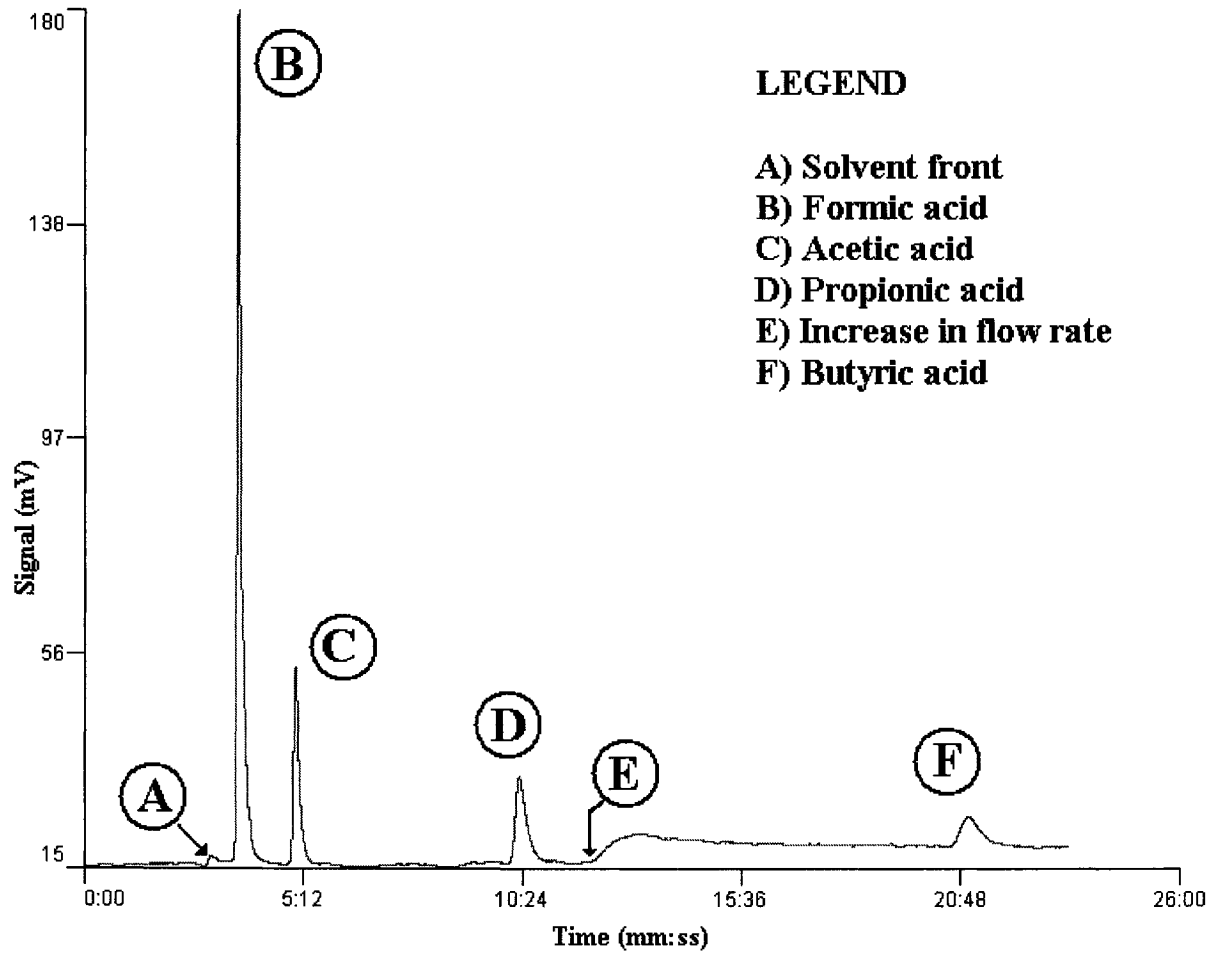

Figure 5: Typical HPLC chromatogram of fatty acid separation using 10^{-3} M phosphoric acid. A programmed flow rate of 3.0mL per minute was used in conjunction with the larger CSC Tribute column and a 1.0mL sample loop.

FIGURE 6

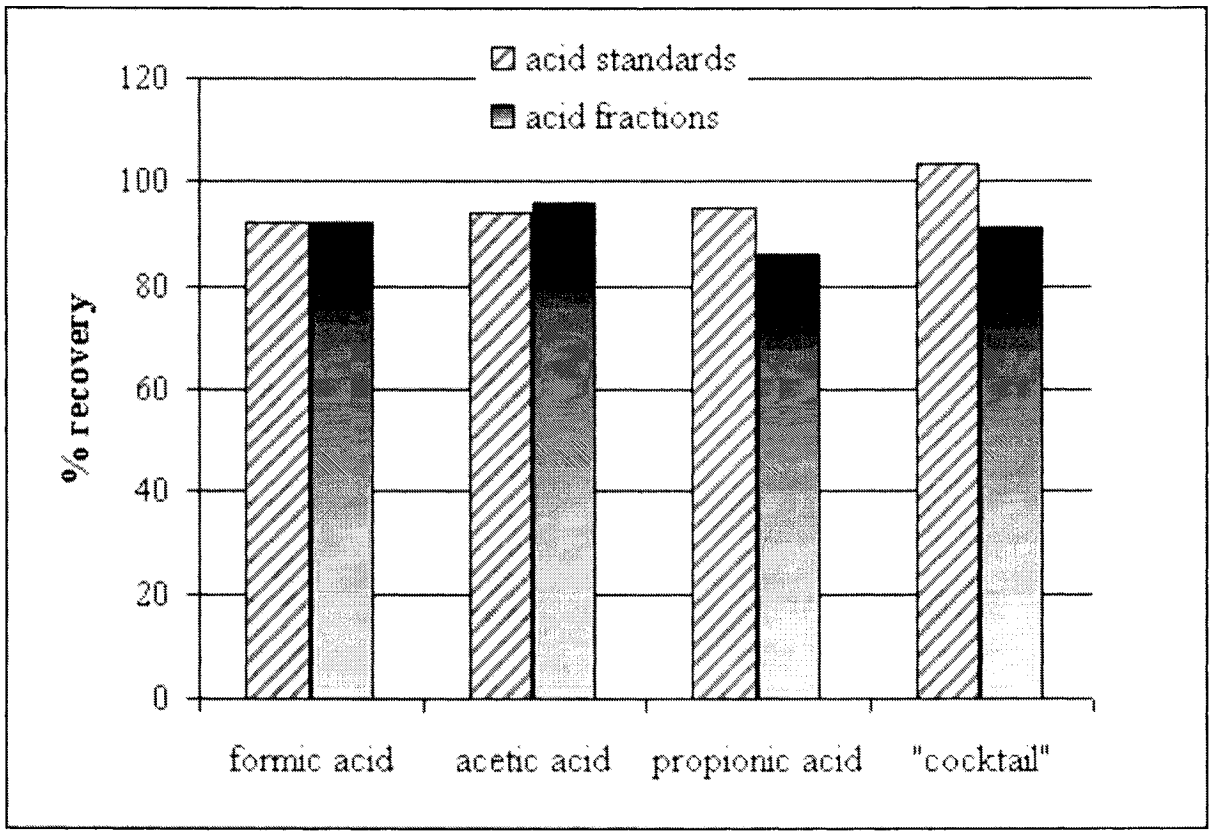

Figure 6: TIC/TOC quantitative data for standard acids and fractions derived by extraction of peaks on the HPLC.

FIGURE 7

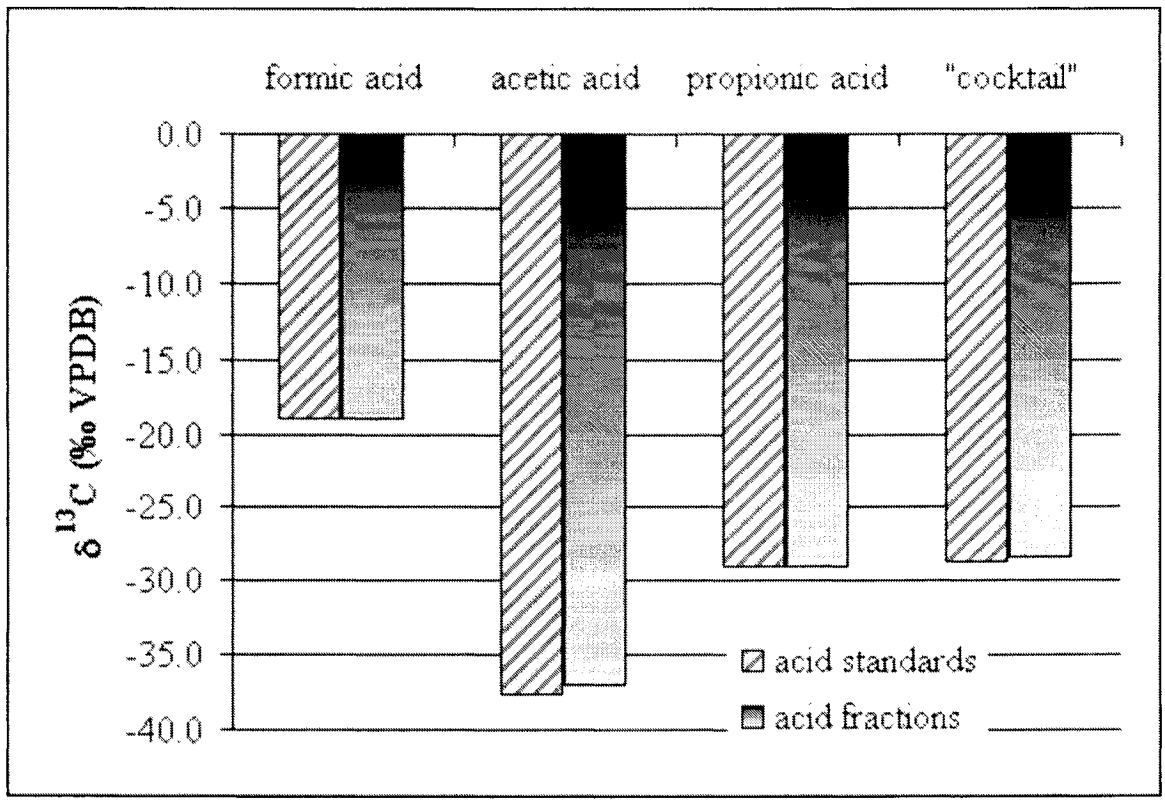

Figure 7: ^{13}C isotopic data for the standard organic acids prior to and subsequent to HPLC separation and extraction.

FIGURE 8

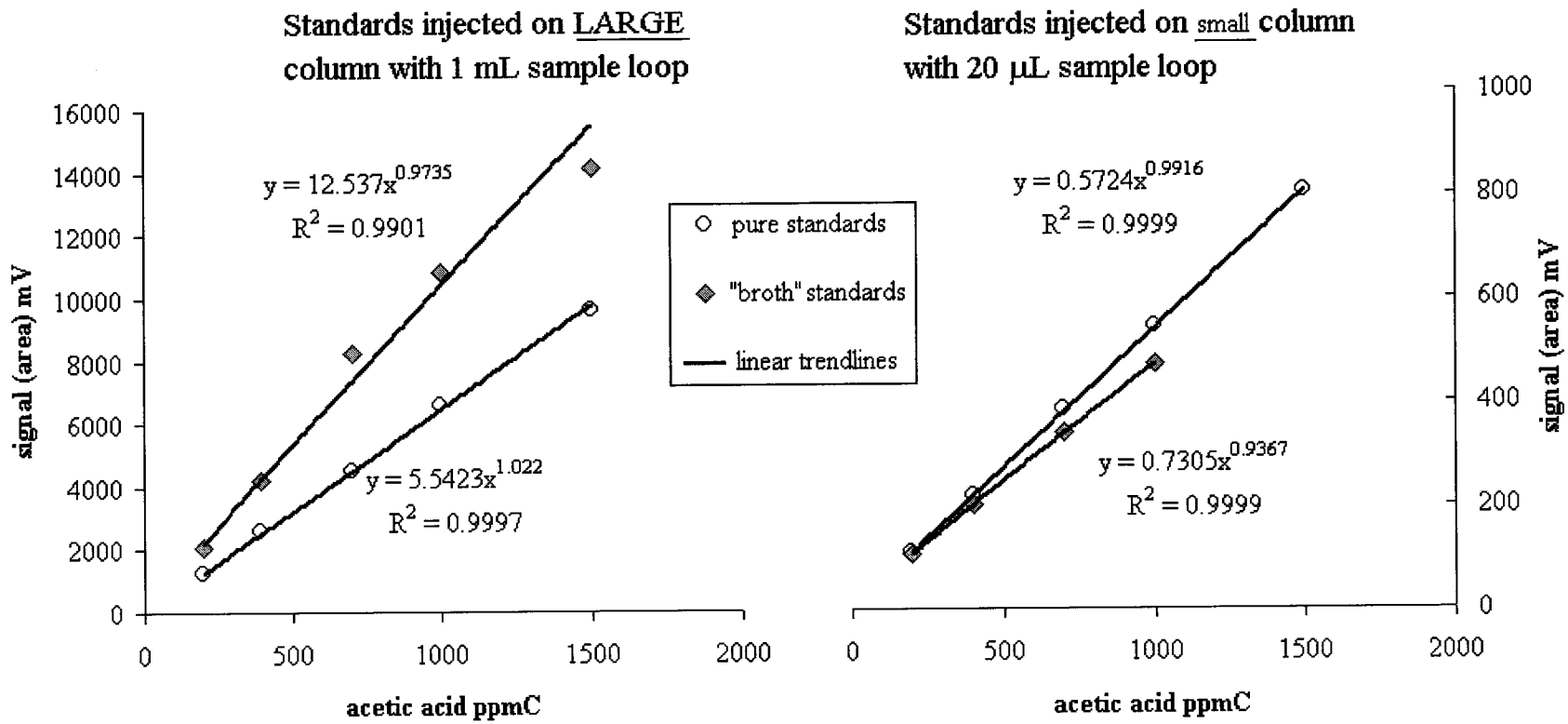

Figure 8: Comparison of the calibration curves for the acetic acid standards prepared in deionized water and soil "broth".

FIGURE 9

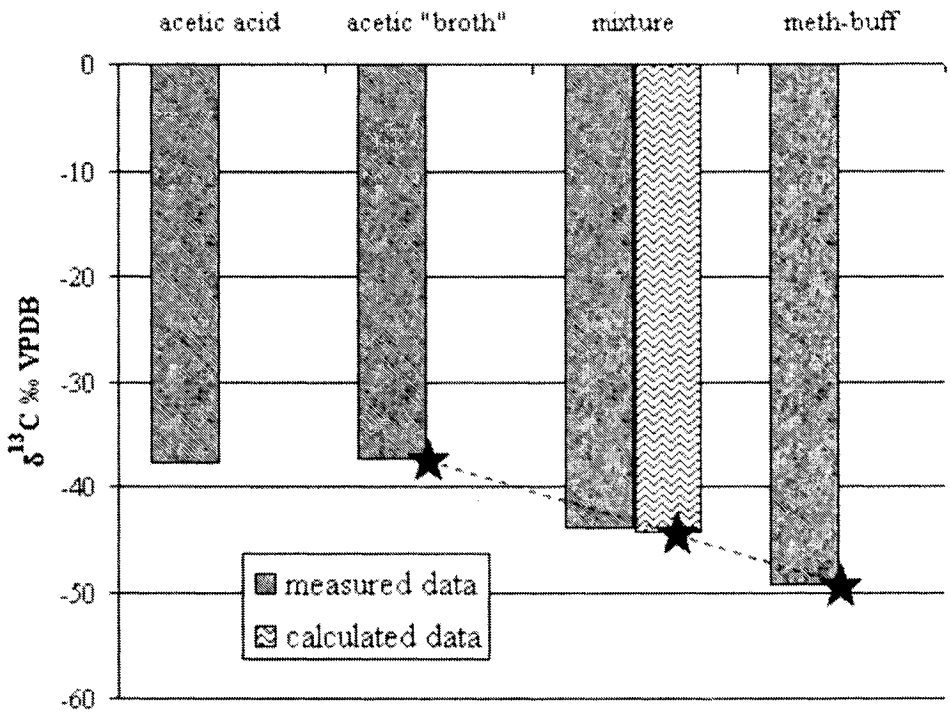

Figure 9: ^{13}C-isotopic comparison of acetic acid fractions extracted from two distinct end-members and a mixture made from them. The dashed line representing a mixing curve and the black stars representing components of the mixing curve are drawn on the graph for visual representation only.

FIGURE 10

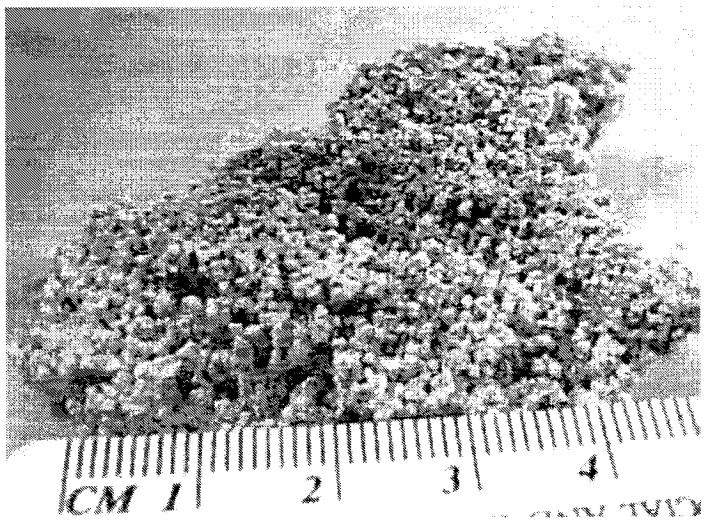

Figure 10: An example of an endostromatolite "crust" taken from the surface of an exposed limestone fissure. This view shows the typical *cauliflower* texture of the tops of clustered growth columns forming a thick, continuous layer. The fissure where this sample formed must have been quite wide because there is no evidence of stunted growth from contact with the opposite side of the fissure.

FIGURE 11

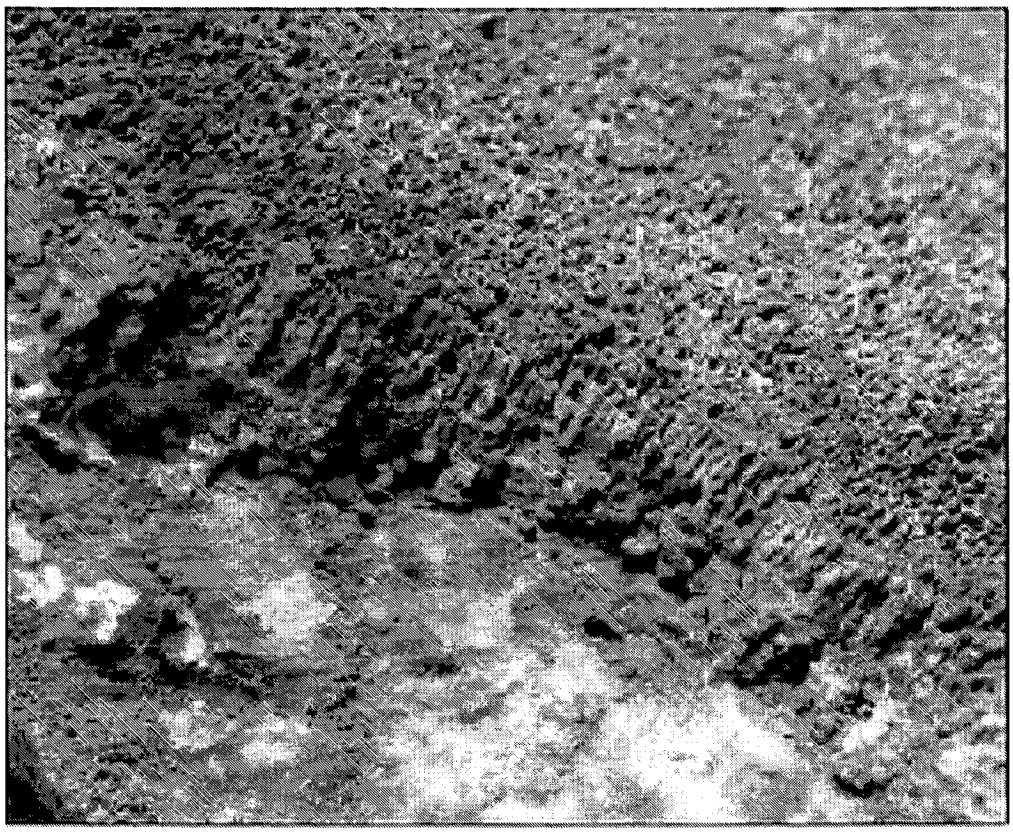

Figure 11: Clustered endostromatolite growth columns grow orthogonally to the surface of the limestone host rock (exposed in foreground). The scale of this picture is unknown. Photo courtesy I. Clark.

FIGURE 12

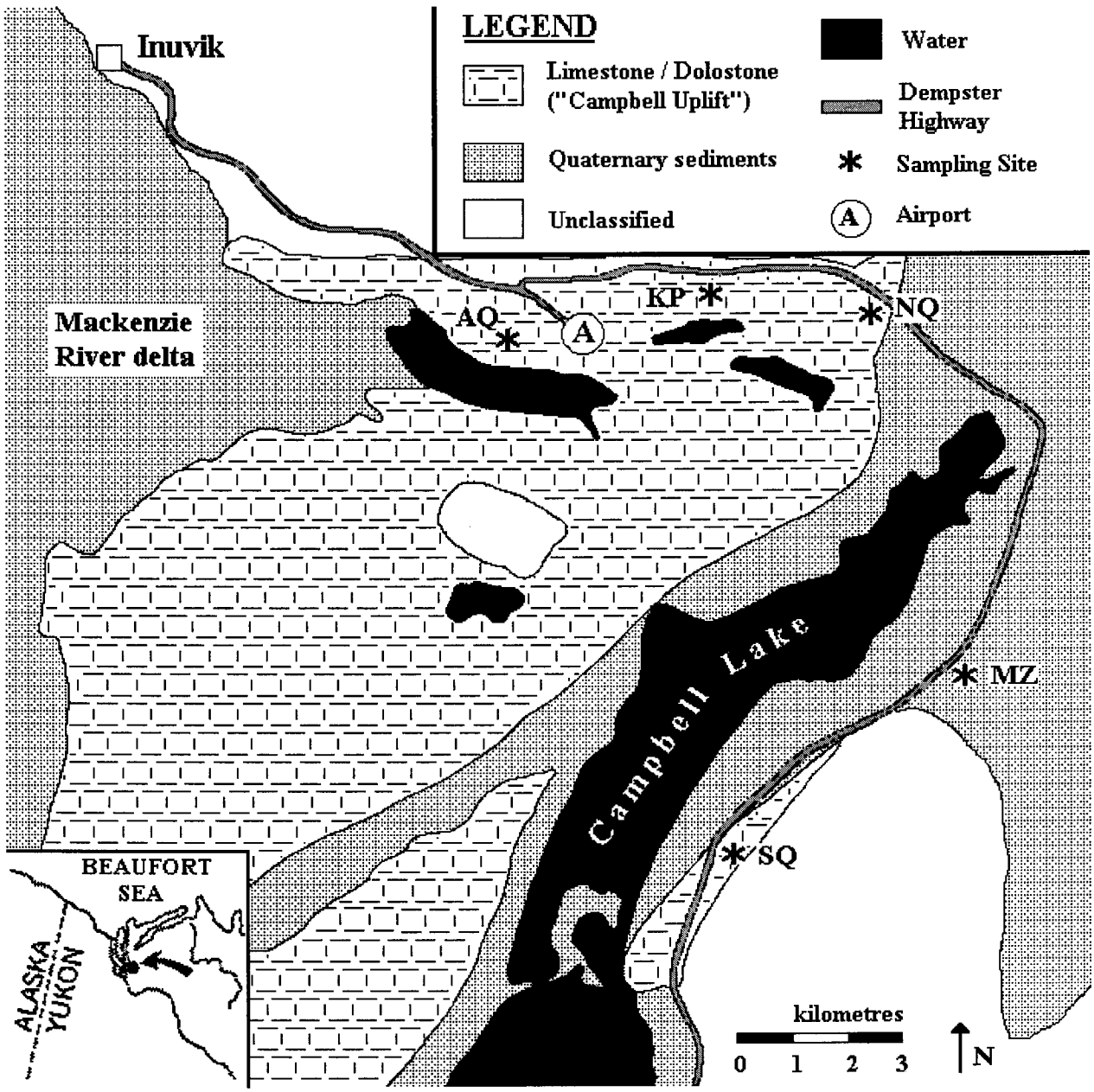

Figure 12: Drawing of field area to the south and east of Inuvik, N.W.T. Geological data are based on Geological Map 1517A, Department of Energy, Mines and Resources (Canada). Small-scale inset based on Ritchie (1976). Actual field monitoring sites are denoted by (*) and abbreviations are as follows: AQ = "Airport Quarry"; NQ = "North Quarry"; SQ = "South Quarry"; KP = "Kokelj's Peat" ; MZ = "Manmade site".

FIGURE 13

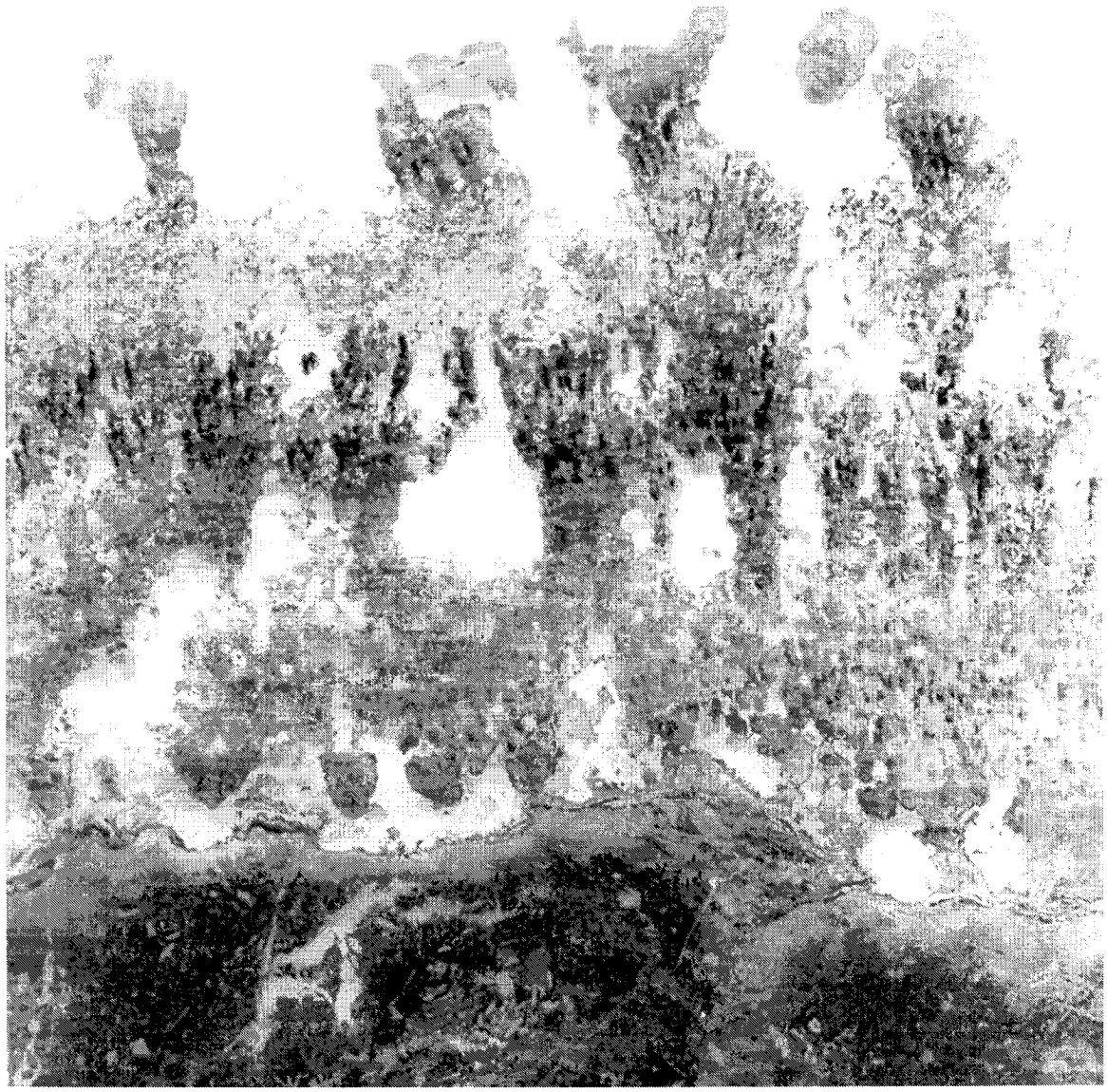

Figure 13: Sample "O-1" as shown in thin section. Field of view is approximately 26mm wide. Notice the highly variable sizes and shapes of growth columns from bottom to top. This particular sample must have undergone several stages of growth. Also note the sharp contact surface with the host rock where the typical basal layer of endostromatolite deposits is conspicuously absent.

FIGURE 14

Figure 14: Sample "O1-east" as shown in thin section. Field of view is 28mm wide. Exceptional preservation similar to the previous sample is evident, especially in the thick basal layer. No alteration rim at the contact with the host rock is evident. Instead, there is a thin, clear cement layer between the host rock and endostromatolite, indicating that the calcrete must have been attached to the fissure face.

FIGURE 15

Figure 15: Sample "IC-4" as seen in thin section. Field of view is 30mm wide. Individual columns are not discernible and the endostromatolite deposit appears to have a uniform texture throughout. The basal layer is thinner than the previous example with subdued light and dark banding. Notice the brachiopod fossil mould on the far right side. It is occluded with endostromatolite growths.

FIGURE 16

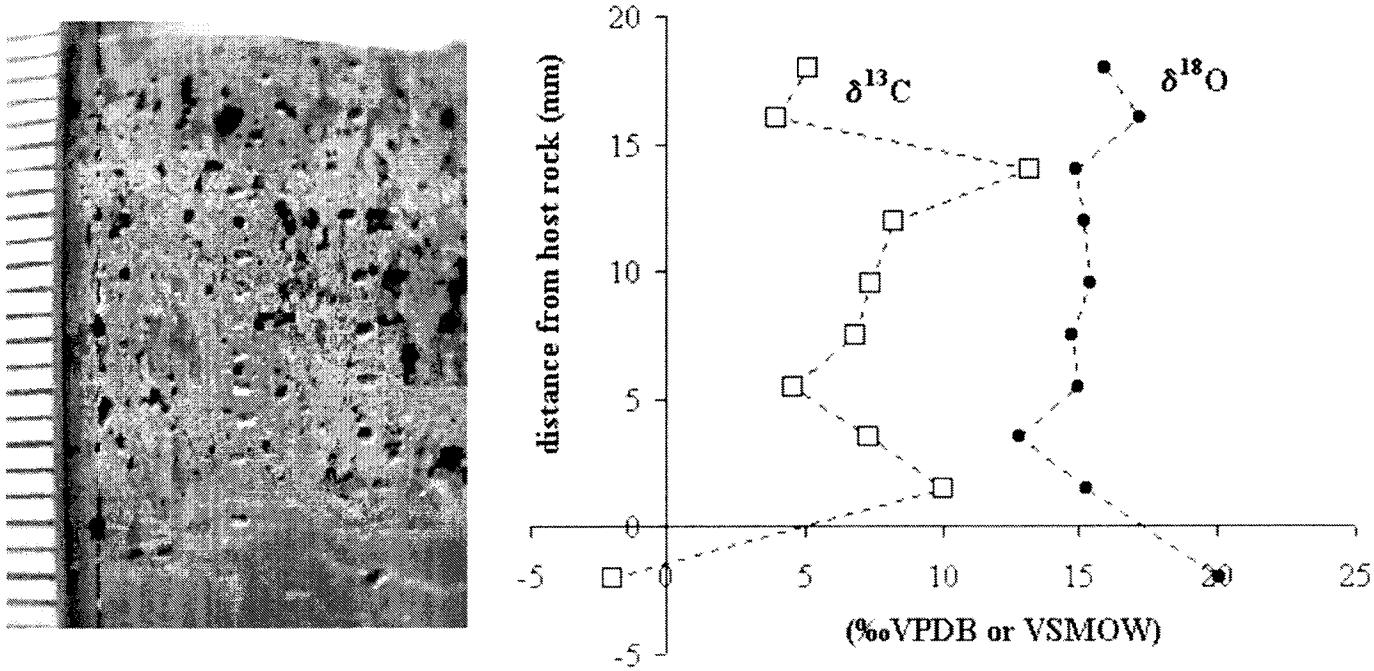

Figure 16: Carbon and oxygen isotopic data for endostromatolite sample **O-1**. At left is an image of the actual thick section after microsample drilling took place. Two sets of holes were drilled. The isotopic data in the chart to the right are for the second set. Data from the first set were lost due to instrument malfunction. The scale bar in the image at left has divisions of 1mm.

FIGURE 17

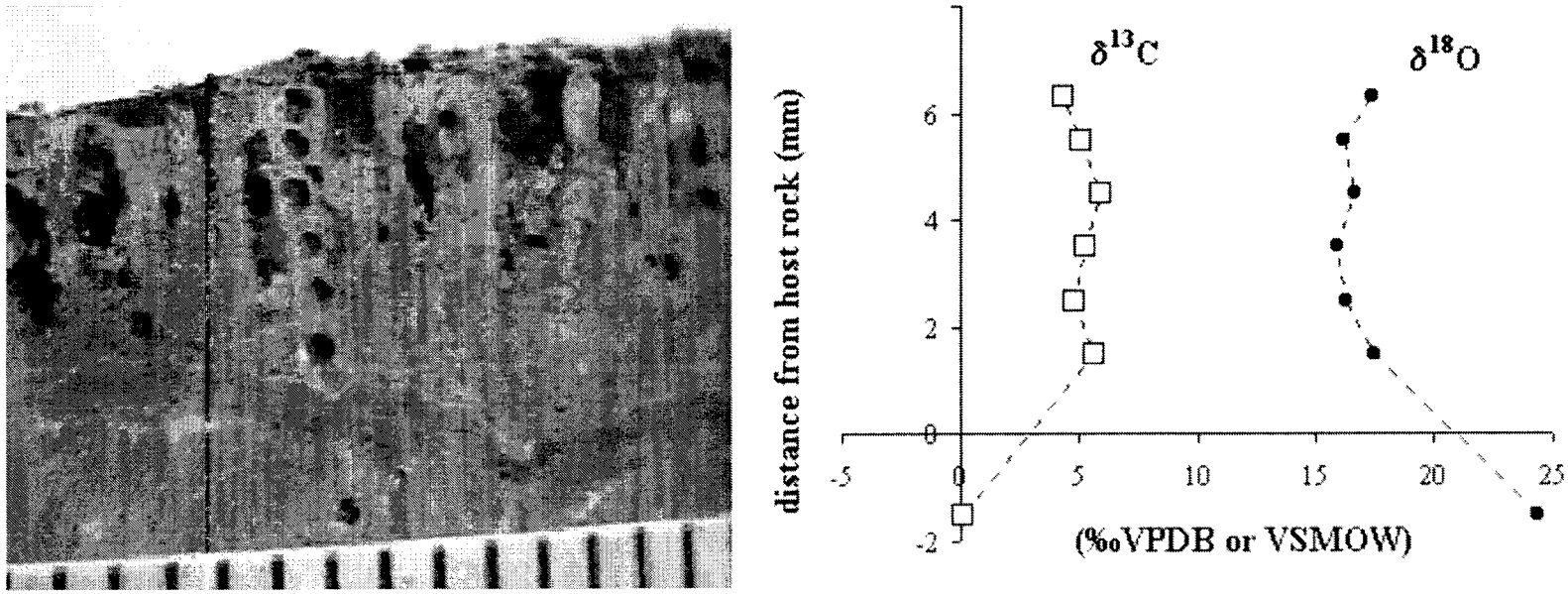

Figure 17: Carbon and oxygen isotopic data for endostromatolite sample **O1-east**. At left is an image of the actual thick section after microsample drilling took place. Two sets of holes were drilled. The isotopic data in the chart to the right are for the set shown (previously this section was drilled outside of the field of view). Data from the first set were lost due to instrument malfunction. The scale bar in the image at left has divisions of 1mm.

FIGURE 18

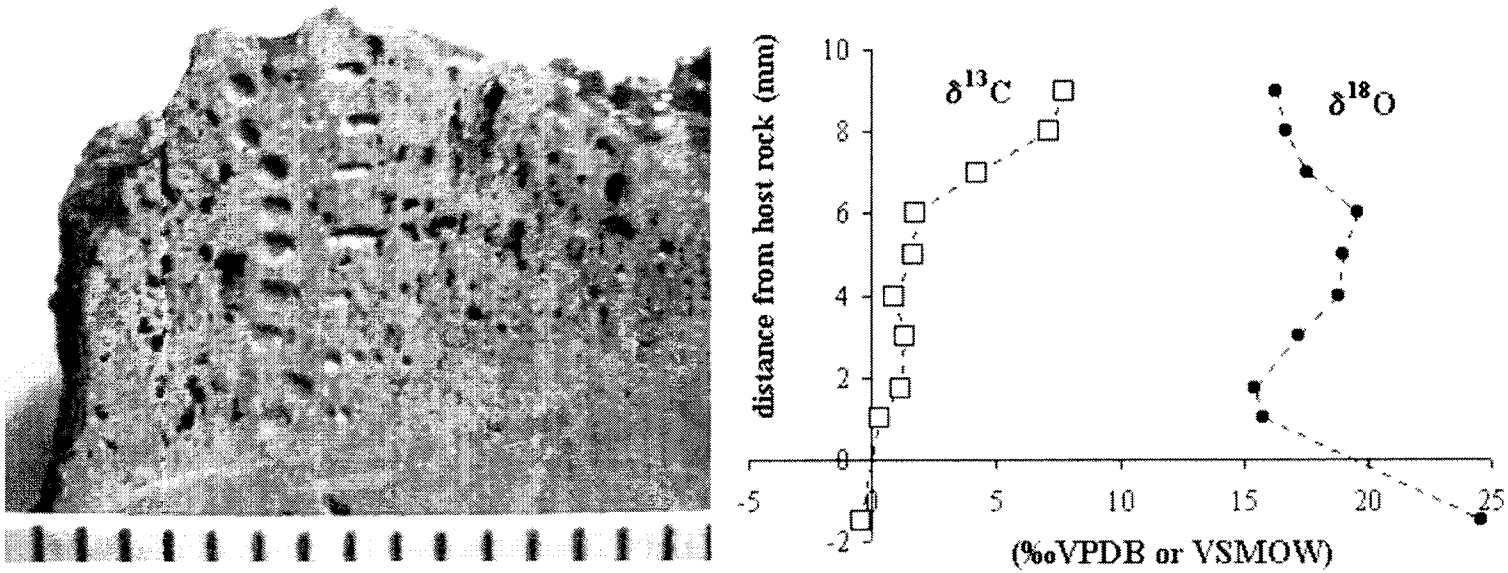

Figure 18: Carbon and oxygen isotopic data for endostromatolite sample **IC-4**. At left is an image of the actual thick section after microsample drilling took place. Two sets of holes were drilled. The isotopic data in the chart to the right are for the round holes on the left. Data from the first set were lost due to instrument malfunction. The scale bar in the image at left has divisions of 1mm.

FIGURE 19

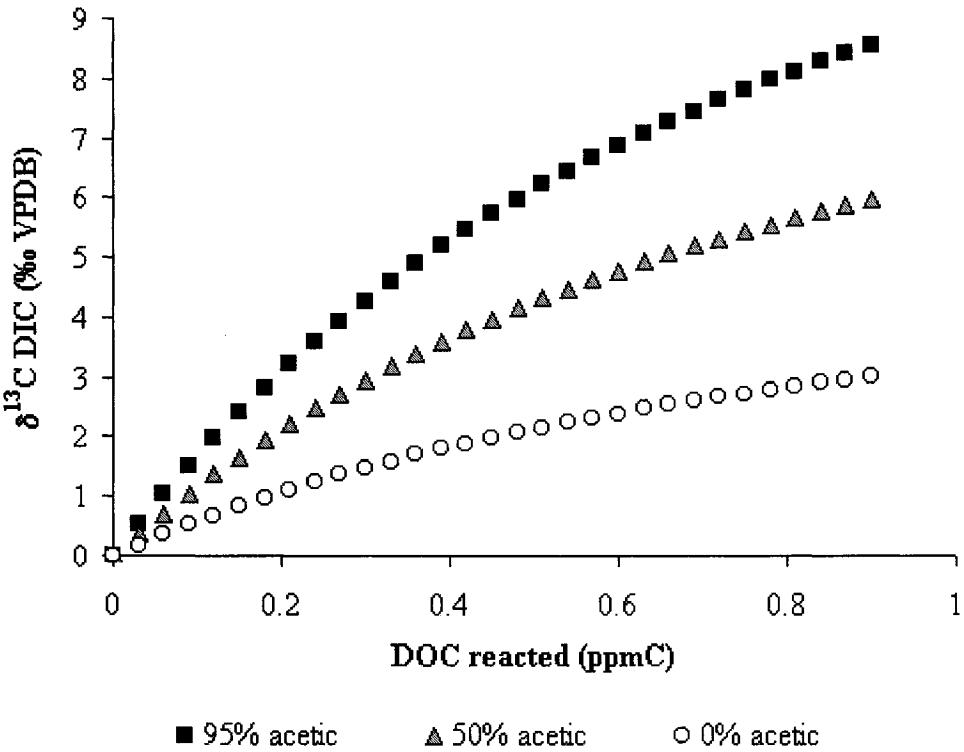

Figure 19: The carbon isotopic evolution of DIC in a saturated theoretical limestone fissure system where the starting DIC concentration is 1.2ppmC and 0.03ppmC aliquots of DOC are reacted stoichoimetrically (see Appendix 1). The DIC is subsequently reacted by a consortium of methanogenic and acetogenic bacteria. Even though acetogenesis is not as efficient as methanogenesis at reacting $^{12}CO_2$ versus $^{13}CO_2$, the limitations on methanogenesis posed by H_2 restriction allow greater DIC enrichment versus DOC consumption over time.

FIGURE 20

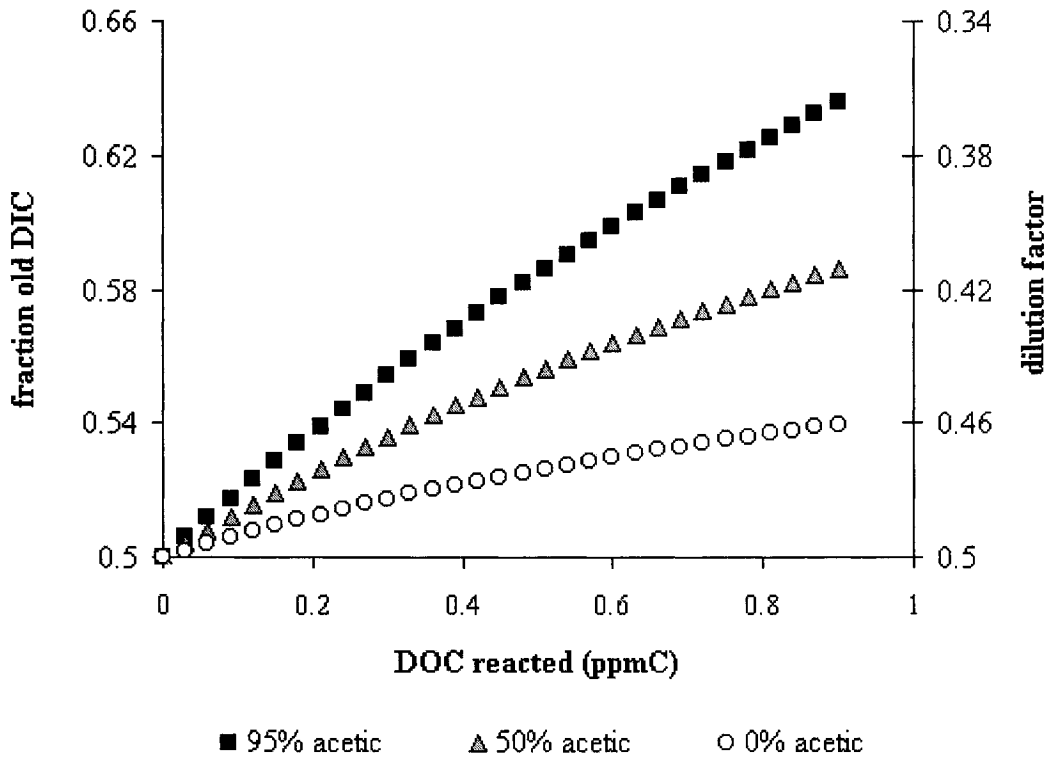

Figure 20: The evolution of DIC in a saturated theoretical limestone fissure system where the starting DIC has a dilution factor of 0.5. Subsequent bacterial reactions using the products of DOC decomposition enrich the DIC in "old carbon" from the limestone, but acetogenesis produces a much stronger contribution of limestone to groundwater DIC as long as acetate is not reacted by methanogenesis.

FIGURE 21

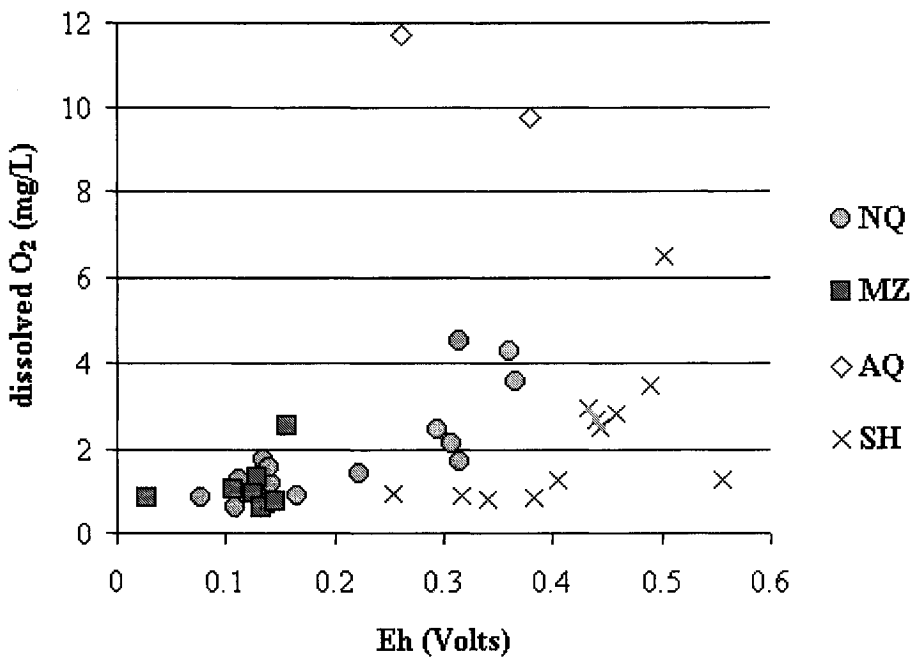

Figure 21: Dissolved oxygen versus Eh values for samples collected during the 2000 field season.

FIGURE 22

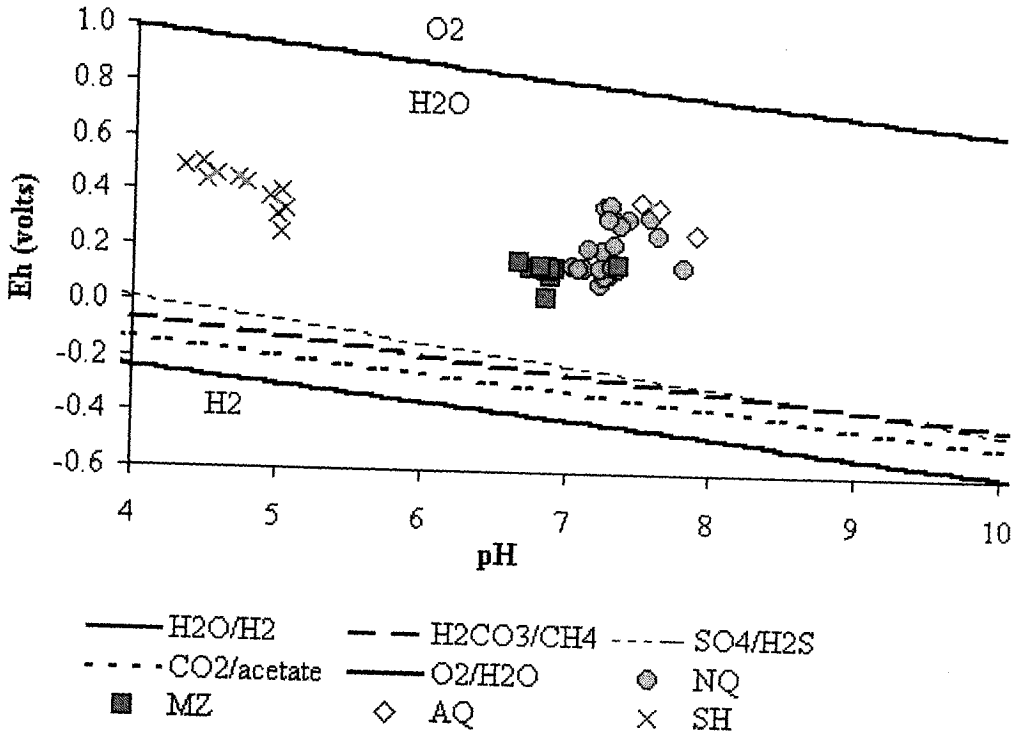

Figure 22: Eh versus pH data from the 2000 field samples plotted against calculated stability fields for various redox pairs (at 25°C).

FIGURE 23

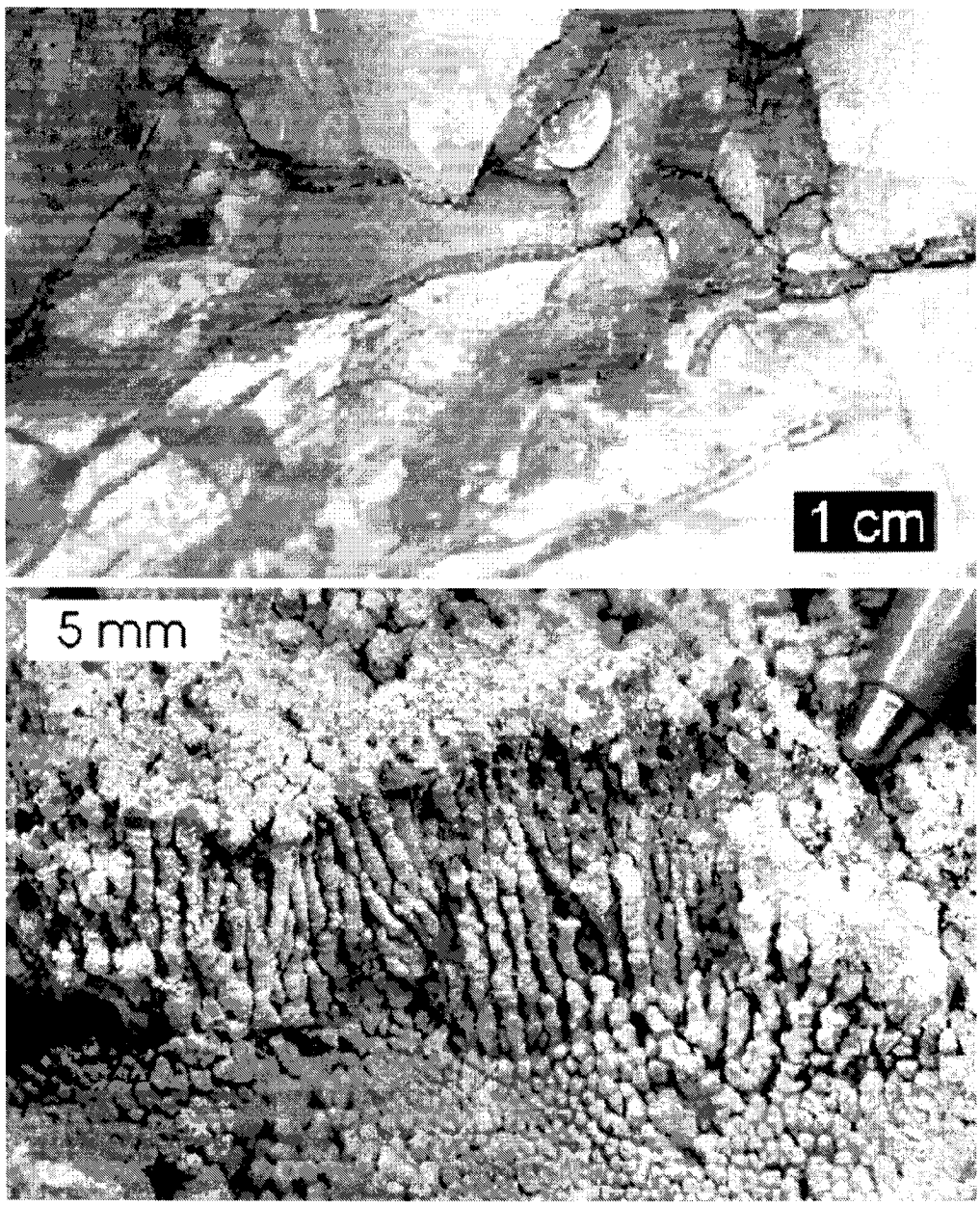

Figure 23 Images of endostromatolite deposits. The upper picture shows an actual outcrop (quarter is for scale) with endostromatolites lining the many fractures terminating at the outcrop surface. Lower picture is a closeup of the clustered growth columns from these fracture-filling deposits. From Marschner and Clark (2004).

FIGURE 24

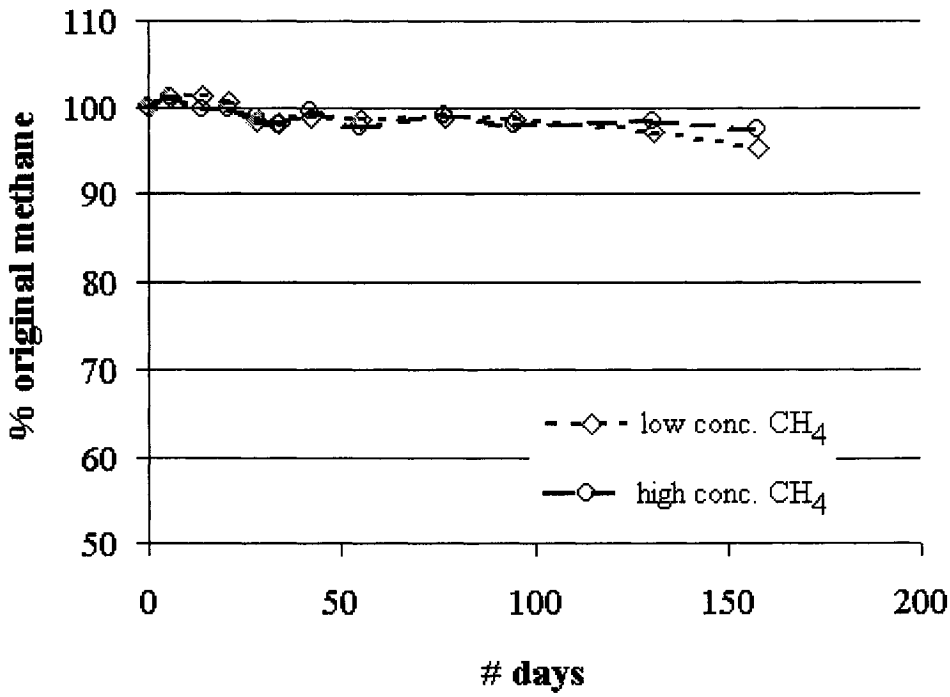

Figure 24 Experimental data showing the resistance of septa jars to leaks. Each jar was injected with a known quantity of methane and was tested regularly against freshly-prepared standards. The starting concentrations of the low- and high-CH_4 concentration vessels were 3.4 x 10^3 ppmV and 8.5 x 10^3 ppmV, respectively Data are not corrected for losses incurred from sample removal.

FIGURE 25

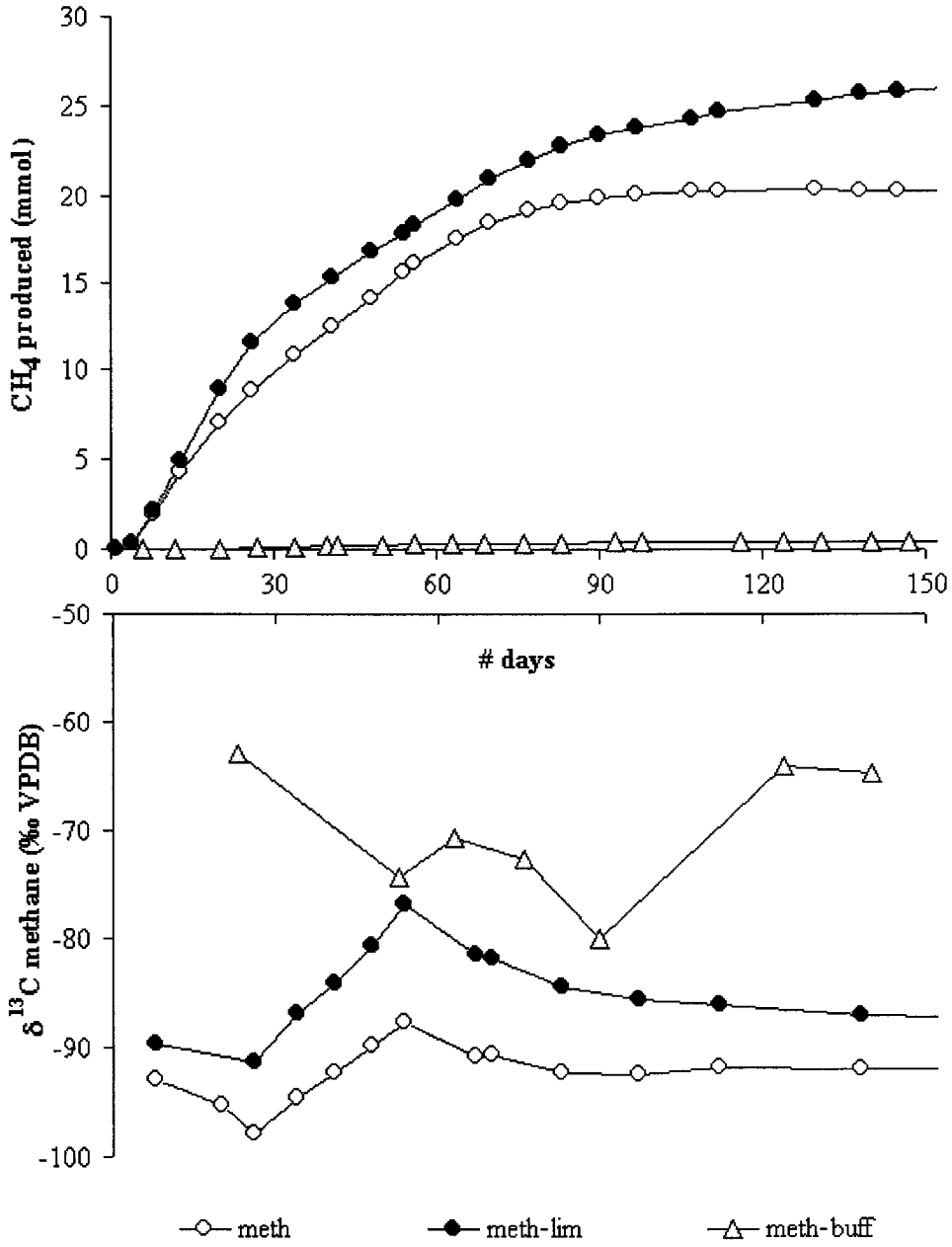

Figure 25 Methane data for Experiment 1 (Chapter 4) incubation systems. The top graph shows quantitative data, and the bottom graph shows isotopic data over the same period. Units on the abscissa axis for the top graph are in millimoles (mmol) which represent the total amount of methane produced, not a concentration. The carbon isotopic data in the lower graph are expressed in ‰ notation relative to the universal Vienna Pee-Dee Belemnite standard (VPDB). The data in both graphs are corrected for methane lost by sample removal and thus represent total experimental levels of methane, not merely instantaneous amounts in the incubation vessels at the time of analysis.

FIGURE 26

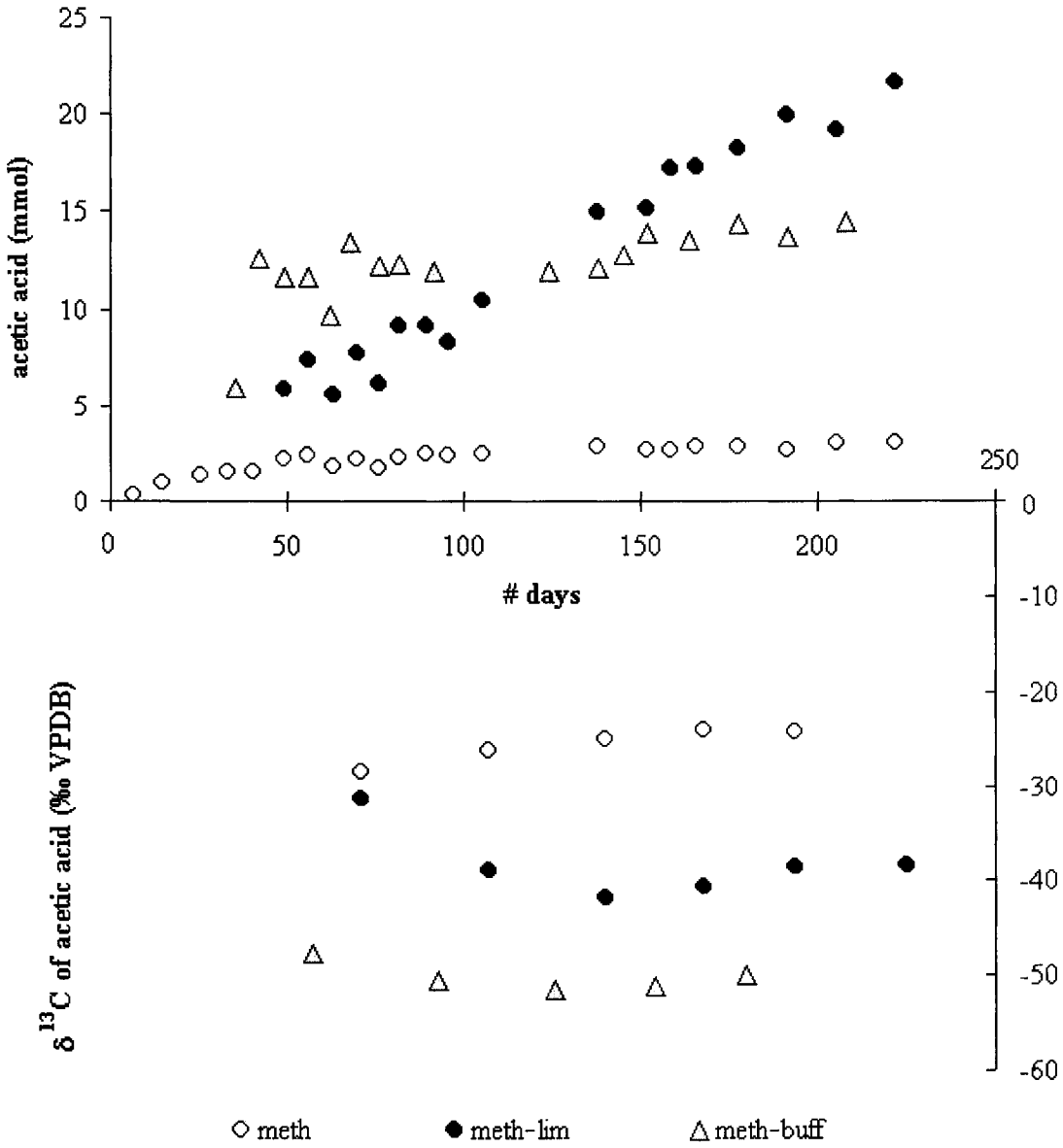

Figure 26 Acetic acid data for Experiment 1 (Chapter 4) incubation systems. The top graph shows quantitative data for combined protonated and deprotonated acetic acid, and the bottom graph shows isotopic data over the same period. Units on the abscissa axis for the top graph are in millimoles (mmol) which represent the total amount of acetic acid produced, not a concentration. The carbon isotopic data in the lower graph are expressed in ‰ notation relative to the universal Vienna Pee-Dee Belemnite standard (VPDB). The data in both graphs are corrected for acetic acid lost by sample removal and thus represent total experimental levels of acetic acid, not merely instantaneous amounts in the incubation vessels at the time of analysis.

FIGURE 27

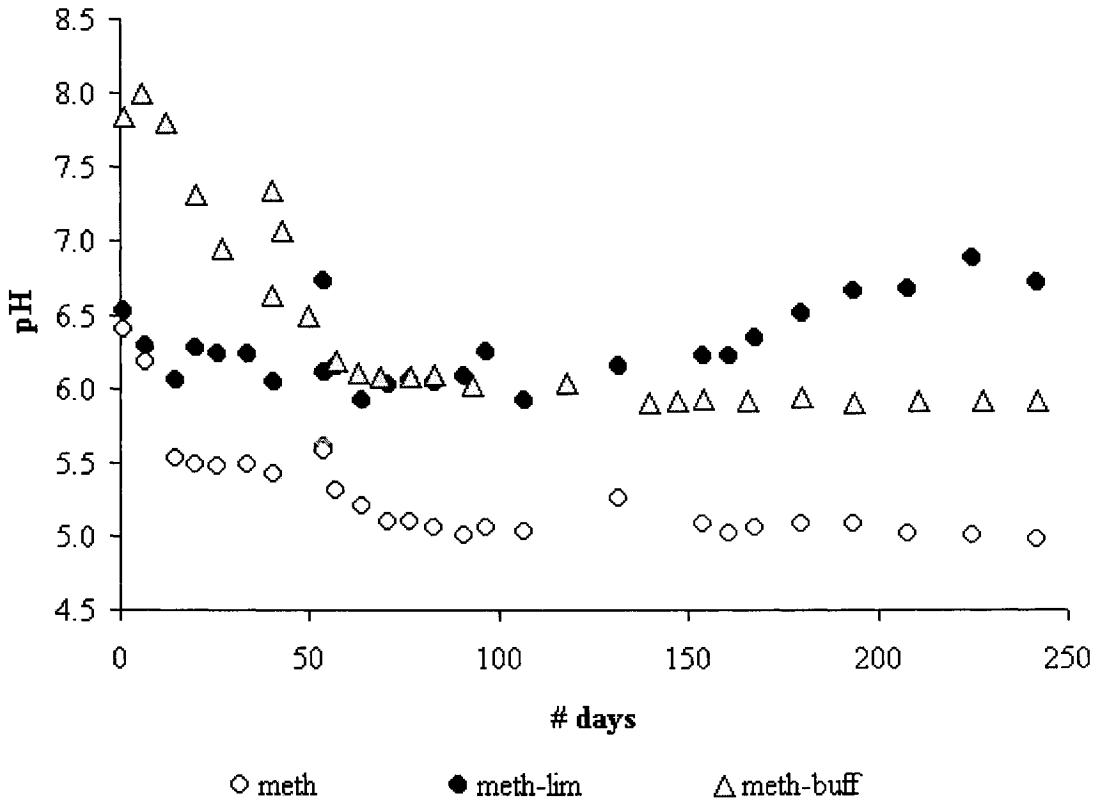

Figure 27 pH data for Experiment 1 (Chapter 4) incubation systems. Measurements were made on unfiltered microsamples with a standard non-refillable probe calibrated against buffered stock solutions with pH values of 7.01 and 4.00.

FIGURE 28

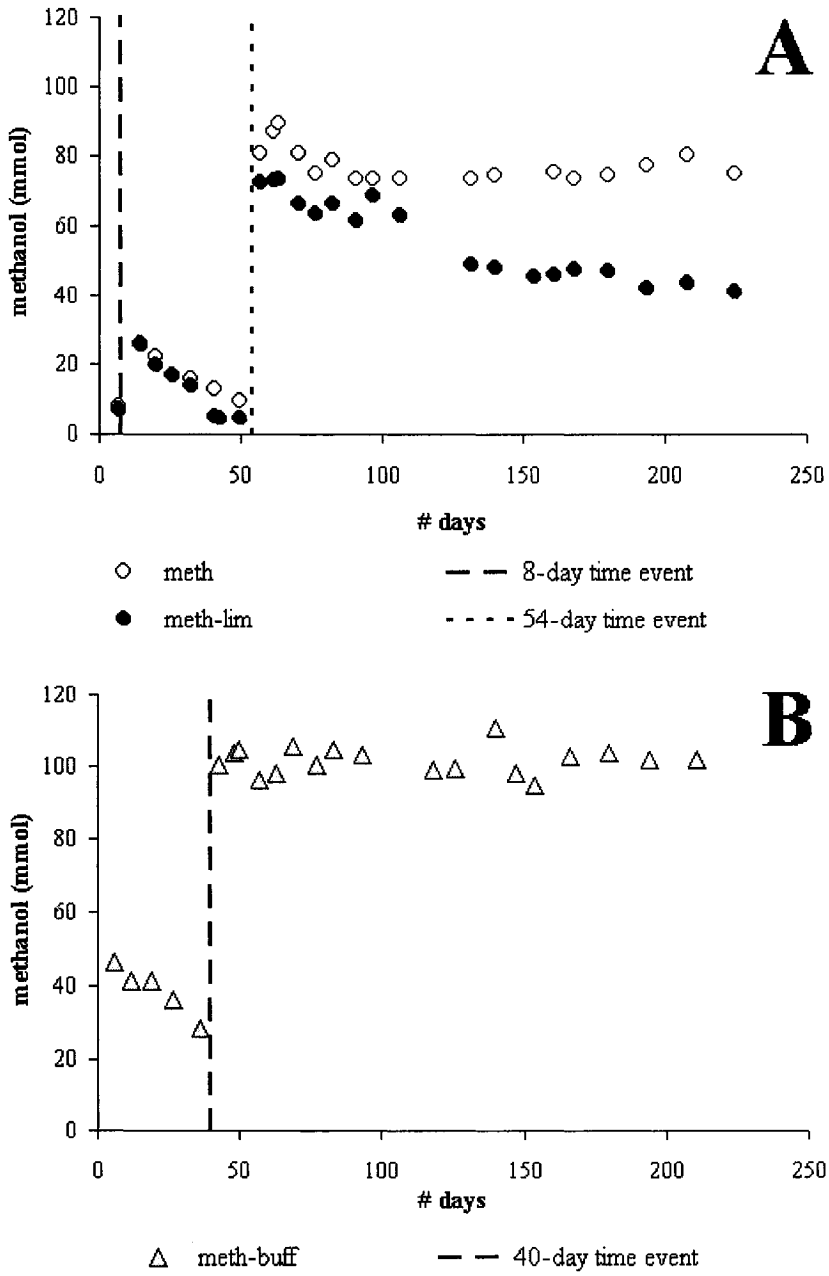

Figure 28 Methanol data for Experiment 1 (Chapter 4) incubation systems. Units on the abscissa axis for the top graph are in millimoles (mmol) which represent the total amount of methanol which can be experimentally accounted for, not a concentration. The data in the graph are corrected for methanol lost by sample removal and thus represent total experimental levels of methanol, not merely instantaneous amounts in the incubation vessels at the time of analysis. Only quantitative data are available for methanol because a suitable analytical method for isotopic determination was not developed prior to the onset of incubation.

FIGURE 29

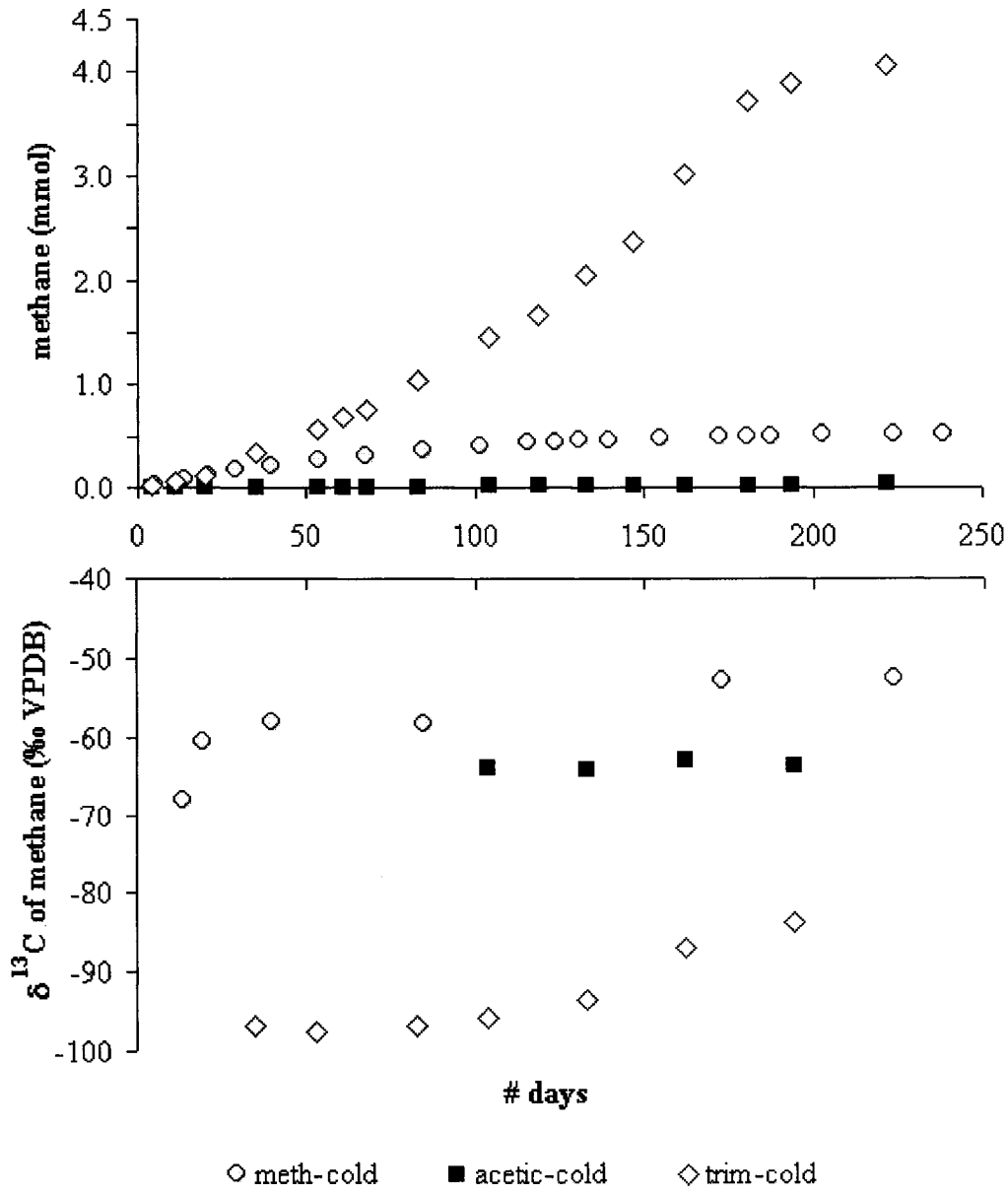

Figure29 Methane data for Experiment 2 (Chapter 4) cold incubation systems. The top graph shows quantitative data and the bottom graph shows isotopic data over the same period. Units on the abscissa axis for the top graph are in millimoles (mmol) which represent the total amount of methane produced, not a concentration. The carbon isotopic data in the lower graph are expressed in ‰ notation relative to the universal Vienna Pee-Dee Belemnite standard (VPDB). The data in both graphs are corrected for methane lost by sample removal and thus represent total experimental levels of methane, not merely instantaneous amounts in the incubation vessels at the time of analysis.

FIGURE 30

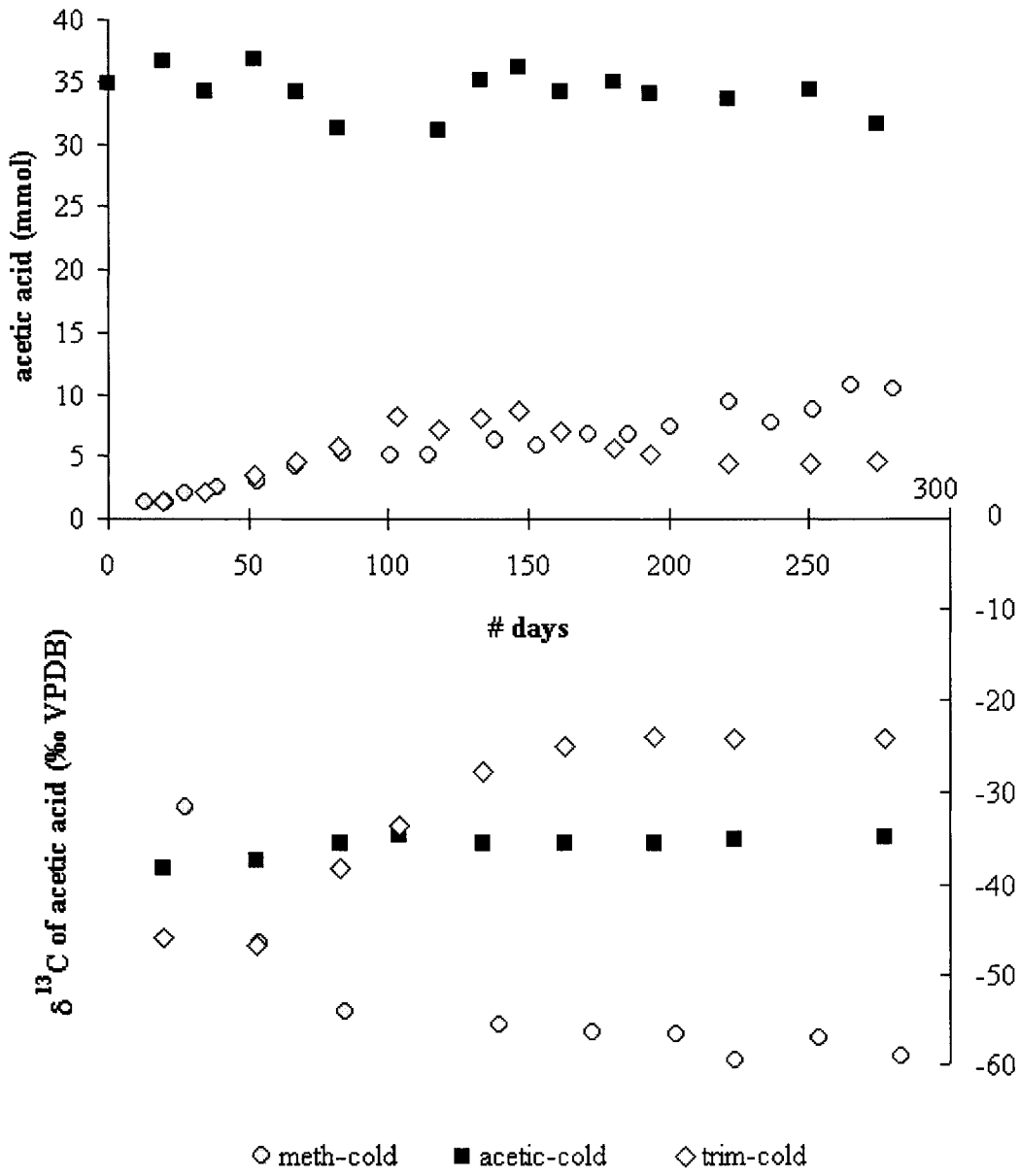

Figure 30 Acetic acid data for Experiment 2 (Chapter 4) cold incubation systems. The top graph shows quantitative data for combined protonated and deprotonated acetic acid, and the bottom graph shows isotopic data over the same period. Units on the abscissa axis for the top graph are in millimoles (mmol) which represent the total amount of acetic acid produced, not a concentration. The carbon isotopic data in the lower graph are expressed in ‰ notation relative to the universal Vienna Pee-Dee Belemnite standard (VPDB). The data in both graphs are corrected for acetic acid lost by sample removal and thus represent total experimental levels of acetic acid, not merely instantaneous amounts in the incubation vessels at the time of analysis.

FIGURE 31

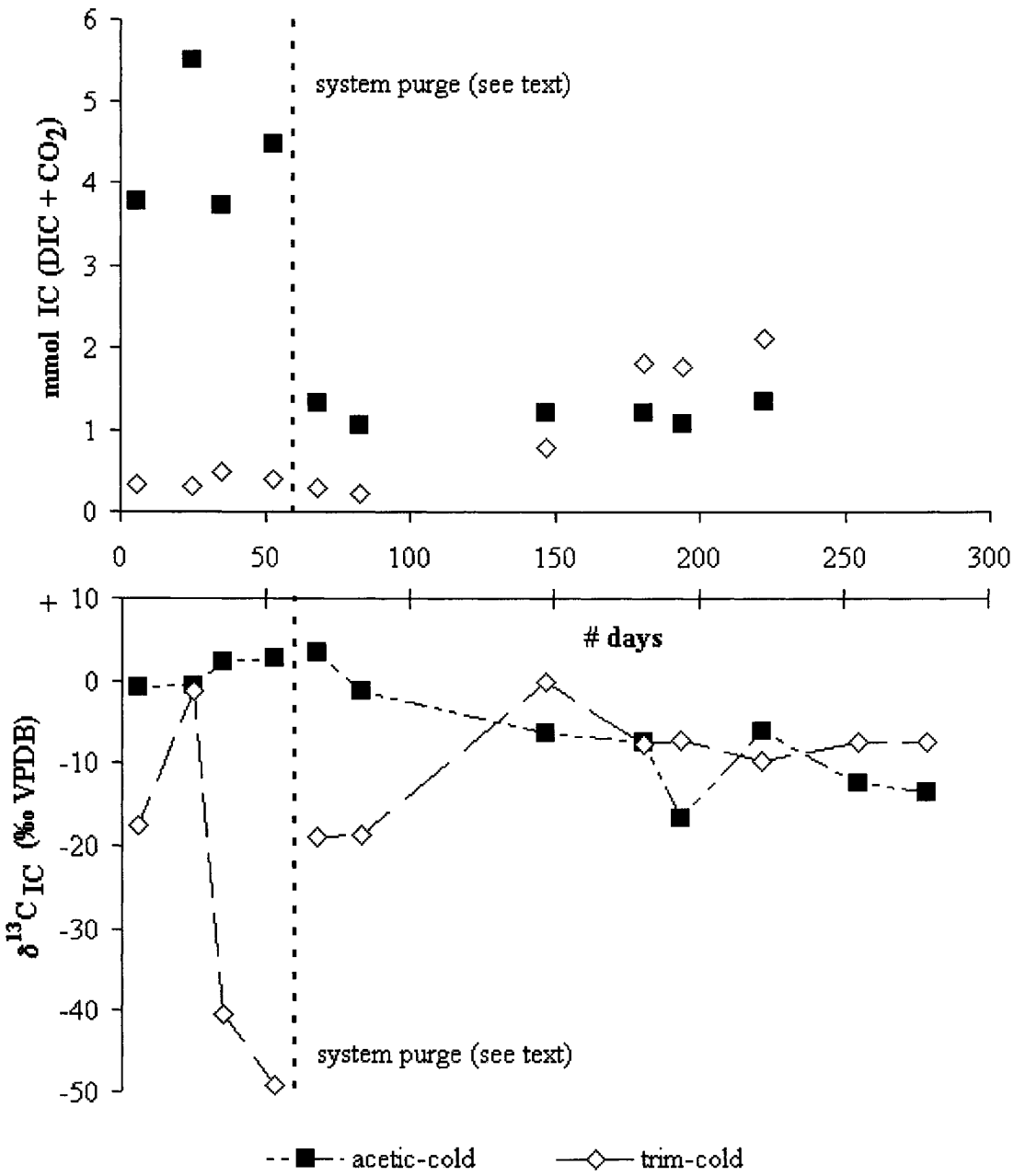

Figure 31 IC (inorganic carbon) data for Experiment 2 (Chapter 4) cold incubation systems. The top graph shows quantitative data (*i.e.* discrete amounts) and the bottom graph shows isotopic data over the same period. After 60 days, the vessels were opened, purged, and resealed with new septa to avoid sample loss from coring due to repeated piercing. The data in both graphs are corrected for IC losses during sample removal and thus represent total experimental levels of IC, not merely instantaneous amounts in the incubation vessels at the time of analysis.

FIGURE 32

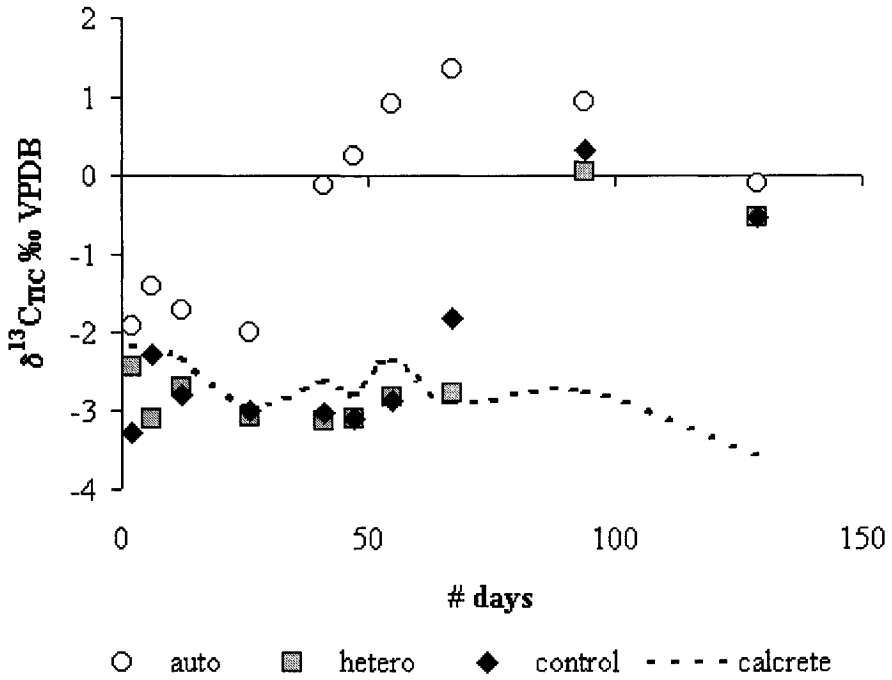

Figure 32 ^{13}C-isotopic data for IC for non-enriched closed-system incubation systems (Experiment 3, Chapter 4) using bacteria from a natural consortium collected from periglacial soil in a limestone terrain. IC is the sum of DIC and headspace CO_2.

FIGURE 33

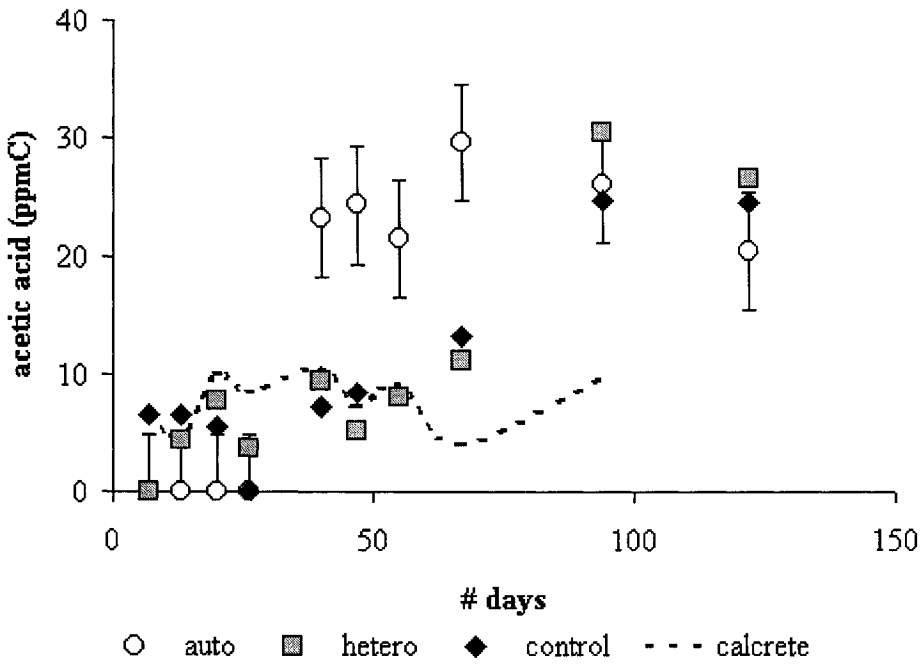

Figure 33 Quantitative data for acetate from non-enriched closed-system incubation systems (Experiment 3, Chapter 4) using bacteria from a natural consortium collected from periglacial soil in a limestone terrain.

FIGURE 34

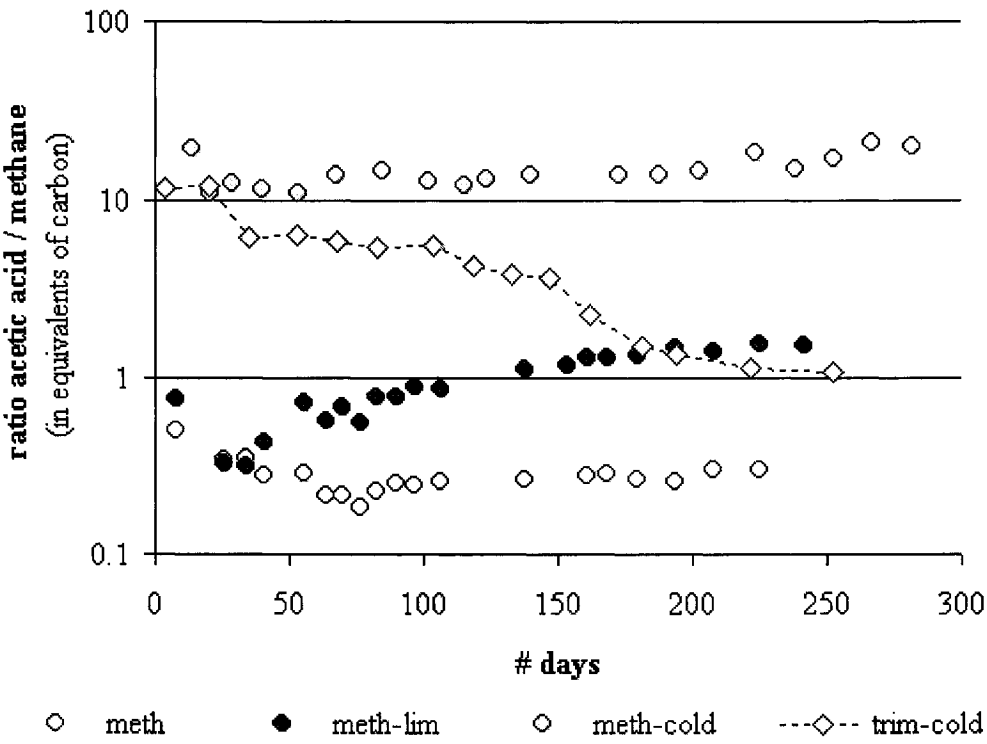

Figure 34 The ratio of acetic acid to methane (expressed in terms of equivalents of carbon) for various vessels in both experiments. Since acetic acid has two carbon atoms to just one for methane, the molar ratio can be derived by dividing results by 2. The trend toward acetic acid becoming a more important product as incubation time increases is evident in all vessels except "trim-cold" (see text for explanation).

FIGURE 35

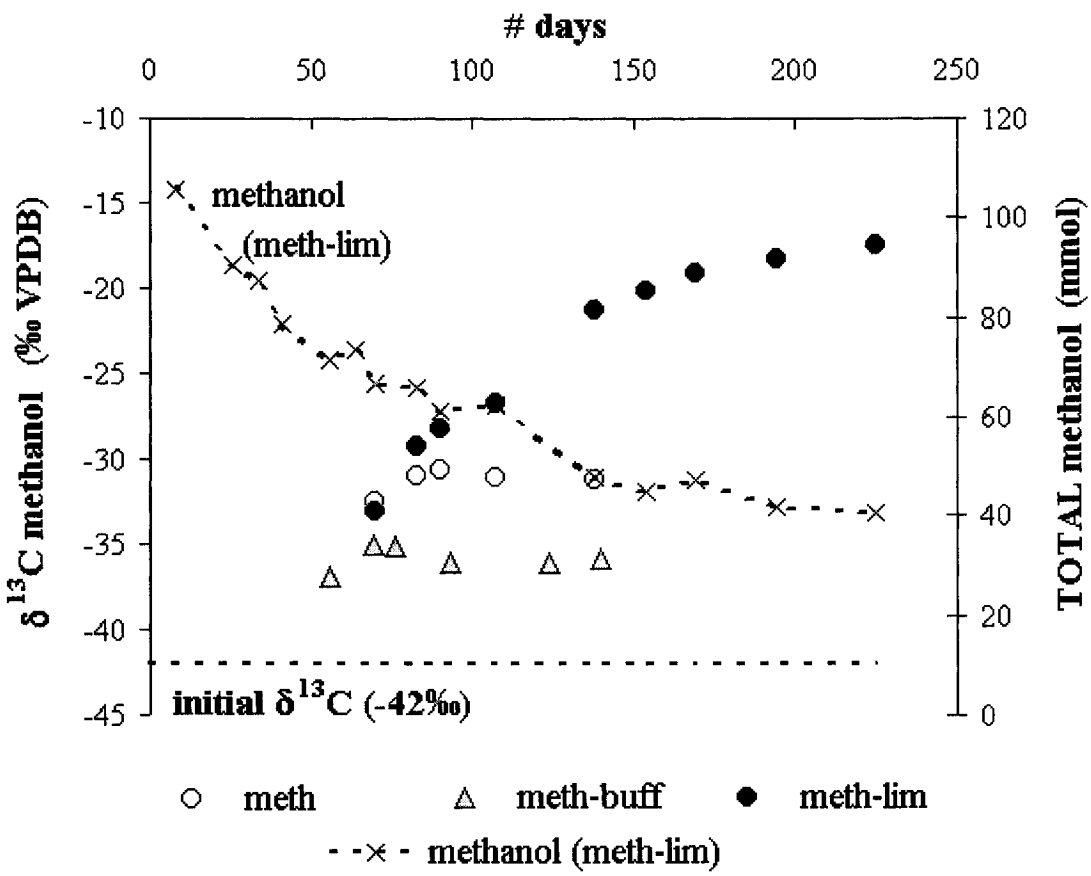

Figure 35 Calculated data for the isotopic enrichment of residual methanol over time in the incubation vessels of Experiment 1. Mass balance calculations using all measured data from major C-bearing reactants and products were used to derive the data. The original isotopic composition of methanol (-42‰ VPDB) is shown for visual reference.

FIGURE 36

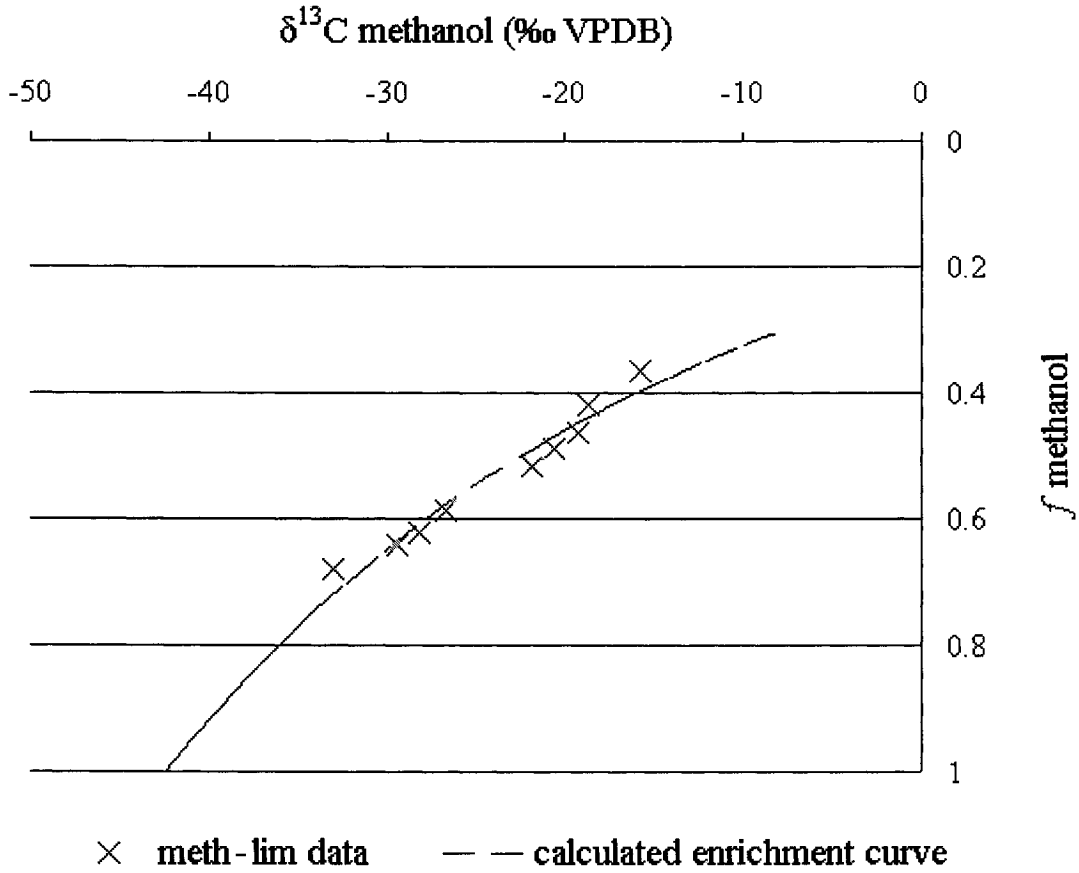

Figure 36 Calculated best-fit Rayleigh isotopic enrichment curve for the experimental data of incubation vessel "meth-lim". The Rayleigh model is based on Equation 4-7 (see text). Methanol is consumed and ^{12}C is preferentially removed, enriching the residual in ^{13}C.

FIGURE 37

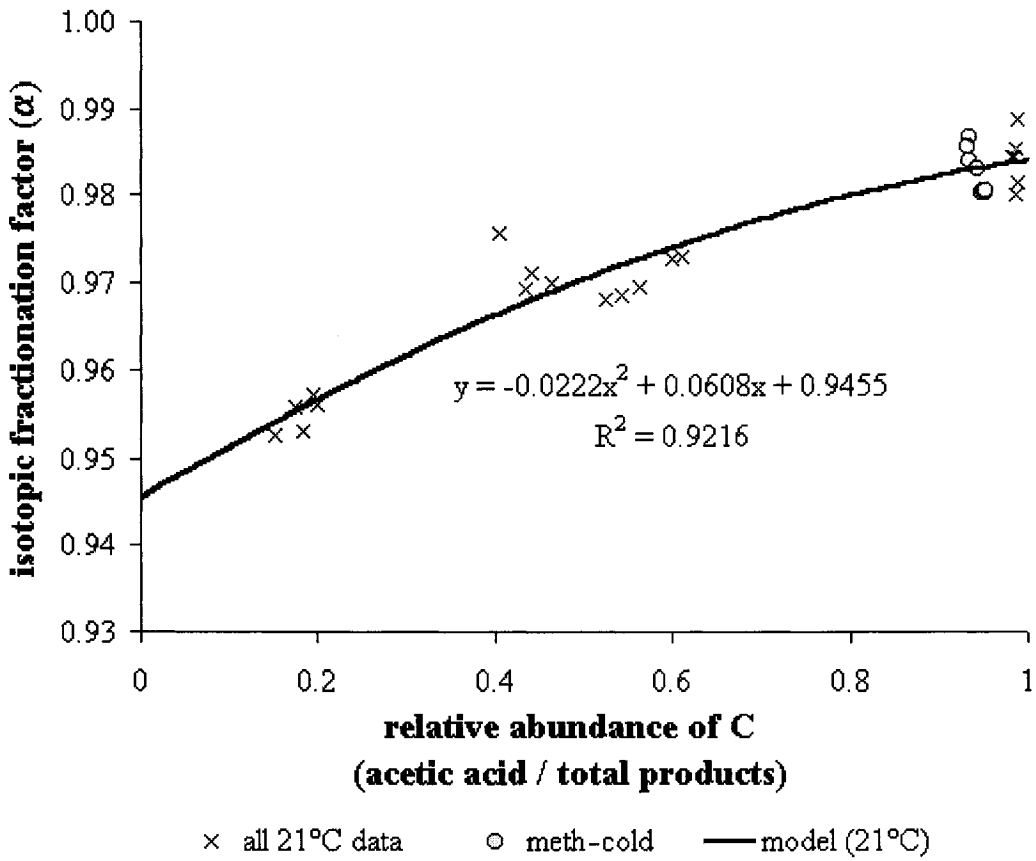

Figure 37 Calculated Rayleigh-model isotopic enrichment curve based on the relative abundance of acetic acid as a C-bearing product in bacterial reactions involving methanol from Experiment 1 (Chapter 4). The endpoints of the curve give predictions for the isotopic fractionation factor of two end-member reactions, methanogenesis and acetogenesis. The equation of the modelled curve is given in the diagram and the text.

Appendices

Appendix 1: Sample Calculations for Rayleigh Distillation Model

For this model, dissolved organic carbon (DOC) is reacted to form substrates for methanogenesis and acetogenesis in a saturated limestone fracture setting. The products of DOC decomposition are as follows (where CH_2O is the empirical formula denoting organic matter):

$$6CH_2O \rightarrow CH_3CH_2CH_2COOH + 2CO_2 + 2H_2$$

$$CH_3CH_2CH_2COOH + 2H_2O \rightarrow CH_3CH_2COOH + CO_2 + 3H_2$$

$$CH_3CH_2COOH + 2H_2O \rightarrow CH_3COOH + CO_2 + 3H_2$$

The overall reaction is:

$$6CH_2O + 4H_2O \rightarrow CH_3COOH + 4CO_2 + 8H_2$$

So it is apparent that H_2 and CO_2 are produced in a ratio of 2:1 . These two molecules serve as reactants for methanogenesis and acetogenesis as follows (respectively):

$$CO_2 + 4H_2 \rightarrow CH_4 + 2H_2O$$

$$2CO_2 + 4H_2 \rightarrow CH_3COOH + 2H_2O$$

It is also possible for methanogens to use acetic acid (CH_3COOH), but for this model, fermentative methanogenesis is assumed to be negligible and thus all methane production is via the CO_2-reduction pathway. Because acetogenic bacteria use H_2 and CO_2 in the ratio as it is produced, all DOC can be theoretically turned into acetate. Methanogens use H_2 and CO_2 in a 4:1 ratio, depleting molecular hydrogen in the system such that not all CO_2 can be reacted to form methane. All other competing bacterial processes which would consume H_2 are assumed to be inoperative in this model.

Several assumption are made for this model. The temperature is 4°C. The $\delta^{13}C$ of limestone is 0‰ VPDB and that of DOC is -26‰ VPDB. The $^{13}C/^{12}C$ ratio of international standard Vienna PeeDee Belemnite (VPDB) is 0.0111796. The fractionation constant ($\alpha_{methane}$) for CH4 derived from CO_2 is approximately 0.927 based on values from Clark and Fritz (1997) (see complete references at end of Chapter 3). The fractionation constant (α_{acet}) for acetic acid derived from CO_2 is 0.941 (based on results published by Gelwicks *et al* (1989). Because methanogenesis and acetogenesis are using the same products and because both processes are assumed to be occurring concurrently in the system, the overall fractionation factor (α_{both}) is estimated by a linear calculation, i.e.

$$\alpha_{both} = \frac{n_{acet} \times \alpha_{acet} + (1 - n_{acet})/2 \times \alpha_{CO2}}{(1 + n_{acet})/2}$$

Where n_{acet} is the fraction of DOC-derived CO_2 that is consumed via acetogenesis. The model is run using several different values of this variable.

Because the rates of the bacterial processes in the actual settings are unknown, we assume that DOC-derived CO_2 equilibrates isotopically with dissolved inorganic carbon (DIC). The initial DIC concentration is 1.2 ppmC (parts per million carbon).

Isotopic mixing of any two components A and B is calculated as follows:

$$R_{mix} = \frac{n_A \times f^{13}C_A + n_B \times f^{13}C_B}{n_A \times f^{12}C_A + n_B \times f^{12}C_B}$$

where:

$$f^{13}C_A = \frac{R_A}{1+R_A}$$

and

$$f^{12}C_A = 1 - f^{13}C_A \quad \frac{1}{1+R_A}$$

R is the $^{13}C/^{12}C$ ratio of a given component.

DOC is added to the system in 0.03ppmC "blocks". According to the reactions above, DOC decomposition will release 0.02ppmC CO_2 and 0.01ppmC acetic acid. The acetic acid reacts with the limestone and releases 0.005ppmC DIC to the DIC pool:

$$CaCO_3 + CH_3COOH \leftrightarrow Ca^{2+} + HCO_3^- + CH_3COO^-$$

The CO_2 equilibrates isotopically with the DIC pool before being reacted by bacteria.

The Rayleigh Distillation equation is as follows:

$$R = R_o \bullet f^{(\alpha-1)}$$

where R is the isotopic ratio of a compound being analyzed ($^{13}C/^{12}C$ in the case of carbon), R_o is the initial ratio (before reaction), f is the dimensionless residual amount of the reacting compound, and α is the isotopic fractionation factor (in this case it is α_{both} as shown earlier). For the model, f is based on the entire DIC pool, even though just a small portion of it is reactive as CO_2. Carbon dioxide is a weak acid that reacts with limestone in a disproportionation reaction as follows:

$$CaCO_3 + CO_2 + H_2O \leftrightarrow Ca^{2+} + 2HCO_3^-$$

Because pH effects in the model system are assumed negligible, the above reaction is reversible, and overall, all of the CO_2 from DOC decomposition remains available to the bacteria as long as there is hydrogen (H_2) to react.

So preferential consumption of $12CO_2$ by both kinds of bacteria enriches the residual DIC pool in ^{13}C. The enrichment increases with every 0.03ppmC "block" of DOC added to the system. The DIC pool grows larger over time for two reasons. Leftover CO_2 reacts with limestone to form 2 equivalents of DIC for every equivalent of unused CO_2. Acetic acid also liberates limestone-derived DIC in a 1:1 ratio. The calculations take into account the obvious fact that acetic acid has two carbons.

The model is run for three different values of n_{acet} : 0.95, 0.50, and 0.

The "age" of the DIC can also be calculated from the model. These calculations are easy as they are simply weighted averages. Although the system is "closed", water in contact with limestone has DIC that is typically 50% derived from the limestone and 50% from atmospheric CO_2. Limestone is sparingly soluble in the presence of water. The starting DIC concentration of 1.2ppmC is close to saturation for the dissolution of $CaCO_3$ in contact with pure water. Limestone dissolution is greatly enhanced by CO_2. Atmospheric CO_2 has $\delta^{13}C$ values around -7‰ VPDB, so when dissolves, hydrolizes and deprotonates, the resulting DIC is not much different from the straight dissolution of 0‰ limestone. So it is justifiable to have a starting DIC that is 50% "new" in the theoretical system. CO_2 from the atmosphere contains ^{14}C, a radiogenic isotope that is used for carbon dating. Limestones of geological age contain no ^{14}C. Age dating requires knowledge of carbon inputs into a source material. The theoretical model shows that disproportionate amounts of "old" limestone DIC are released to solution.

Appendix 2: Tables of Field Data for Chapter 3

Table 3.1: Site names and details of monitoring stations

Site name	Explanation
NQ (general)	Active limestone quarry on the northern end of the Campbell Uplift, southeast of Inuvik. The outcrop is a localized topographic high. Talus from quarrying covers some areas at the base of the slope, and most of the sampling was done within the talus area. NQ-1, -2, -3 were set up in a line extending away from outcrop on debris-covered talus slope. NQ-4 was located off to the side where the talus gives way to vegetation. NQ-P was located off to the side in the bushes
NQ-1	25 cm of rock talus overlies a 10 cm porous organic soil and a dense layer of clay beneath the soil. Piezometer appears to tap the soil at 30 cm depth. Lots of flow.
NQ-2	10 cm of rock rubble overlies 20 cm of woody organic-rich soil and underlying clay extends down to permafrost (~50 cm depth). Piezometer taps soil at 25 cm depth. Good flow.
NQ-3	6-10 cm of rock rubble overlies 10 cm organic soil and 35 cm clayish soil. Flow of water through organic soil was very slow. Piezometer appears to have penetrated clay
NQ-4	10-15 cm soil overlies 25 cm clay. Flow from organic soil was rapid, but piezometer extended down into clay.
NQ-P	30 cm of organic soil overlies permafrost. Piezometer reached down to permafrost. Flow was ephemeral
MZ (general)	A man-made site. Soil and gravel were deposited here to make a pathway leading to a construction site. A stream draining the material and adjacent wooded area flows along the pathway from east to west. A tributary flowing over carbonate-rich mud enters the stream at a culvert.
MZ-1	On the rock rubble-covered shore of the stream.. Limestone rubble covers 20-25 cm root-rich soil, 15-20 cm clay-rich soil, and a gravel-filled till. Piezometer depth not measured.
MZ-2	On the delta where the drainage channel fans out. Silty clay extends to 50+ cm depth with roots penetrating entire span. Piezometer depth unknown
MZ-RF	Runoff from the drainage channel. Flow occurs on top of silty clay, so ability of water to penetrate surface and enter subsurface flow appears minimal.
MZ-stream	The main stream flowing next to the built-up pathway.
SH (general)	The shale site. On a topographic high to the south of eastern "oulier" limestone outcrop related to the Campbell Uplift. Outcrops appear highly weathered. Sampling was done mainly in an area located between an exposed outcrop and a shallow but extensive pond.
SH-1	Midway between the shaley outcrops and pond. Debris-rich soil extends down to unknown depth. Debris is gravel- and cobble-sized shale fragments.
SH-2	Close to the edge of the pond. Shale fragments in soil are small, flaky. Piezometer depth 50-55 cm.
SH-puddle	Standing water lying between SH-1 and SH-2.

Table 3.1 (cont'd)

Site name	Explanation
SH-pond	The pond adjacent to SH-2. White precipitated salts along shore are widespread.
AQ (general)	The "airport quarry", located to the west of the Inuvik Airport. A southward flowing stream receives runoff from a quarry to the west and a vegetated slope to the east. The stream flows next to a pathway built up with quarry materials.
AQ-1	A piezometer is installed in the slope to the east of the stream where runoff is discharging from beneath the vegetation layer. The soil is organic-rich.
AQ-2	Similar to AQ-1, but located more upslope.
KP	Dubbed "Kokelj's Peat". This location is a flat marshy area less than 100 metres away from the Dempster Highway. The seasonal depth of thawing in permafrost is measured here within ice wedges. While there are no carbonate rock outcrops visible at the surface, the area receives inputs of lime dust from the highway every time a vehicle passes at high speed on the highway on dry days.
KP-1	A piezometer is inserted 30cm into the thawed soil horizon atop an ice wedge.
KP-surface	Stading water atop the soil in the ice wedge scar.
KP-lake	The lake proximal to the ice wedge monitoring station.
SQ	The "South Quarry" located in a limestone "outlier" exposure south and east of the main Campbell Uplift. The rock faces exhibit much rust-coloured staining from weathering of iron-bearing minerals. A stream follows along the roadway leading into the quarry, draining the vegetated sloping lands surrounding the quarry. The quarry itself is essentially dry with no runoff near the surface. No monitoring was done at this site.

Table 3.2A: Data from June-July 2000 Field Collection, Inuvik, NWT

sample ID	collection date	pH	T (°C)	Eh (V)	diss. O_2 (mg/L)	alkalinity (mg/L HCO3)	E.C. (mS)	salinity (‰)	TDS (mg/L)	CH_4 (mmol/L)	DIC (mmol/L)	$\delta^{13}C_{DIC}$ (‰ VPDB)
NQ-1	June 20 2000	**7.81**		**0.15**		349				2.90E-02	6.08	-15.05
NQ-1	June 21 2000	**7.03**		**0.14**		285				3.43E-02	5.86	-14.89
NQ-1	June 24 2000	7.29	14	0.11	1.25	334	0.69	0.3	3.30E+02	5.19E-02	6.69	-15.63
NQ-1	June 26 2000	7.34	15.9	0.14	1.56	462	0.75	0.4	3.63E+02		7.04	-15.58
NQ-1	June 28 2000	7.24	12.6	0.13	0.90	484	0.78	0.4	3.72E+02	9.37E-02	7.38	-15.84
NQ-1	June 30 2000	7.30	11	0.17	0.89	462	0.75	0.4	3.58E+02	8.07E-02	7.13	-15.58
NQ-1	July 3 2000	7.22	10	0.08	0.86	505	0.79	0.4	3.73E+02	1.73E-01	7.76	-15.44
NQ-1	July 5 2000	7.25	14.2	0.11	0.62	499	0.76	0.4	3.66E+02	1.27E-01	7.74	-15.16
NQ-1	July 7 2000	7.11	11.7	0.14	0.71	487	0.78	0.4	3.76E+02	1.66E-01	7.71	-15.03
NQ-2	June 20 2000	7.24		**0.20**		277				1.04E-02	5.64	-15.20
NQ-2	June 21 2000	**7.62**	13	0.26		278				8.50E-03	5.30	-15.02
NQ-2	June 24 2000	7.34	14.4	0.31	2.14	295	0.53	0.3	2.58E+02	1.56E-02	5.93	-15.49
NQ-2	June 26 2000	7.42	16.5	0.32	1.68	409	0.72	0.3	3.47E+02		6.18	-15.53
NQ-2	June 28 2000	7.37	11	0.29	2.46	406	0.75	0.4	3.55E+02	2.18E-02	6.48	-15.59
NQ-2	June 30 2000	7.32	11.8	0.22	1.40	408	0.73	0.3	3.47E+02	7.00E-02	6.28	-14.66
NQ-2	July 3 2000	7.35	9.7	0.14	1.72	432	0.74	0.3	3.47E+02	3.88E-02	6.56	-15.08
NQ-2	July 5 2000	7.22	15.7	0.14	0.78	446	0.71	0.3	3.43E+02	5.72E-02	6.79	-15.05
NQ-2	July 7 2000	7.31	14.4	0.14	1.20	450	0.69	0.3	3.32E+02	4.09E-02	6.87	-14.92
NQ-3	June 20 2000	7.08		**0.13**		479					9.52	-16.74
NQ-3	June 21 2000	**7.14**	9	0.20		400				4.98E-02	7.68	-16.59
NQ-4	June 24 2000	6.90	14.9	0.14	1.53	523	1.02	0.5	4.91E+02	8.06E-02	7.07	-13.89
NQ-4	June 26 2000					891					10.41	-15.43

162

Table 3.2A (cont'd)

sample ID	collection date	pH	T (°C)	Eh (V)	diss. O_2 (mg/L)	alkalinity (mg/L HCO_3)	E.C. (mS)	salinity (‰)	TDS (mg/L)	CH_4 (mmol/L)	DIC (mmol/L)	$\delta^{13}C_{DIC}$ (‰ VPDB)
NQ-P	June 21 2000	7.57	13	0.33		149				1.39E-05	2.73	-13.67
NQ-P	June 24 2000	7.26	10.4	0.36	4.30	169	0.32	0.1	1.50E+02	1.48E-05	2.82	-13.51
NQ-P	June 26 2000	7.30	9.6	0.37	3.60	157	0.31	0.1	1.45E+02		2.68	-13.60
NQ-P	June 28 2000	7.28	7.6	0.31	4.53	164	0.34	0.2	1.59E+02	0.00E+00	2.64	-13.89
MZ-stream	June 30 2000	6.80	9.1				0.15	0.1	6.90E+01			
MZ-stream	July 3 2000	6.90	8.9				0.17	0.1	8.10E+01			
MZ-stream	July 5 2000	7.26	10				0.19	0.1	8.90E+01			
MZ-stream	July 7 2000	7.02	8.1				0.20	0.1	9.20E+01			
MZ-1	June 21 2000	7.35	9	0.15		183				2.34E-02	3.69	-16.24
MZ-1	June 28 2000	6.89	8.9	0.13	1.33	244	0.73	0.3	3.43E+02	2.19E-02	4.07	-16.10
MZ-1	June 30 2000	6.85	7.9	0.03	0.87	321	1.21	0.6	5.72E+02	3.28E-02	5.12	-16.07
MZ-1	July 3 2000	6.88	7.8	0.11	1.05	433	1.70	0.8	8.12E+02	3.75E-02	6.99	-16.09
MZ-1	July 5 2000	6.75	11.3	0.13	0.72	435	1.93	1.0	9.40E+02	2.73E-02	6.62	-13.93
MZ-1	July 7 2000	6.66	10	0.16	2.53	337	1.51	0.8	7.32E+02	2.44E-02	6.36	-14.61
MZ-2	June 30 2000	6.91	11.2	0.14	0.72	473	2.57	1.3	1.28E+03	1.43E-03	8.07	-12.63
MZ-2	July 3 2000	6.85	8.8	0.13	0.96	489	2.48	1.2	1.20E+03	1.56E-03	8.19	-12.72
MZ-2	July 5 2000	6.88	11.2	0.13	0.63	469	2.47	1.2	1.21E+03	1.49E-03	8.05	-12.47
MZ-2	July 7 2000	6.81	10.6	0.15	0.77	474	2.42	1.2	1.18E+03	1.19E-03	8.13	-12.30
MZ-runoff	June 30 2000	6.97	11.8				2.64	1.3	1.30E+03			
MZ-runoff	July 3 2000	7.56	14.3			453	2.39	1.2	1.18E+03			
MZ-runoff	July 5 2000	7.65	19.7			412	1.53	0.8	7.54E+02		6.45	-1.85
MZ-runoff	July 7 2000	7.47	18.8			423	2.26	1.1	1.13E+03		6.78	-1.90
AQ-1	June 21 2000	7.62	5.1	0.36		162				0.00E+00	2.77	-10.93
AQ-1	June 24 2000	7.51	4.9		11.50	171	0.68	0.3	3.14E+02		2.91	-10.69
AQ-1	June 26 2000	7.50	7.4	0.38	9.72	198	0.72	0.3	3.39E+02		3.15	-10.76

Table 3.2A (cont'd)

sample ID	collection date	pH	T (°C)	Eh (V)	diss. O_2 (mg/L)	alkalinity (mg/L HCO_3)	E.C. (mS)	salinity (‰)	TDS (mg/L)	CH_4 (mmol/L)	DIC (mmol/L)	$\delta^{13}C_{DIC}$ (‰ VPDB)
AQ-2	June 26 2000	7.74	6.8		10.87	143	0.64	0.3	2.97E+02	0.00E+00	2.22	-11.16
AQ-2	June 28 2000	7.89	6.7	0.26	11.70	158	0.67	0.3	3.12E+02	6.70E-05	2.25	-10.91
SH-1	June 26 2000	3.69	20.8	0.56	1.26		6.25	3.3	3.29E+03		1.42	-6.04
SH-1	June 28 2000	4.72	14.8	0.44	2.48		8.49	4.6	4.55E+03	4.28E-04	3.37	-8.09
SH-1	June 30 2000	4.35	12.5	0.49	3.46		8.71	4.7	4.63E+03		3.00	-8.22
SH-1	July 3 2000	4.49	13.2	0.44	2.68		7.40	4.0	3.90E+03	4.27E-04	3.38	-8.33
SH-1	July 5 2000	4.77	17.2	0.43	2.95		7.82	4.3	4.20E+03	4.70E-04	3.46	-7.33
SH-1	July 7 2000	4.56	14.1	0.46	2.84		7.6	4.1	4.06E+03	4.65E-04	4.10	-7.63
SH-puddle	June 26 2000	3.95	18.9									
SH-puddle	June 28 2000	3.95	16.1				8.32	4.5	4.46E+03			
SH-puddle	June 30 2000	3.94	12.7				8.54	4.6	4.53E+03			
SH-puddle	July 3 2000	3.79	18.6				7.95	4.4	4.29E+03			
SH-puddle	July 5 2000	3.92	20.5				8.37	4.6	4.53E+03			
SH-puddle	July 7 2000	3.93	14.9				7.61	4.1	4.07E+03			
SH-2	June 26 2000	4.46	17.9	0.50	6.50		10.06	5.6	5.52E+03	3.77E-04	2.57	-4.83
SH-2	June 28 2000	5.01	14	0.40	1.25		8.20	4.4	4.37E+03	3.76E-04	3.18	-4.88
SH-2	June 30 2000	5.05	12.5	0.34	0.81		7.85	4.2	4.15E+03		3.22	-4.74
SH-2	July 3 2000	4.94	13.5	0.38	0.86		6.72	3.6	3.54E+03	4.01E-04	3.17	-4.59
SH-2	July 5 2000	5.02	14.8	0.25	0.95		6.89	3.7	3.65E+03	4.46E-04	3.02	-4.66
SH-2	July 7 2000	4.99	13.4	0.32	0.89		6.31	3.4	3.30E+03	4.77E-04	2.86	-4.39
SH-pond	June 26 2000	4.68	21.6									
SH-pond	June 28 2000	4.71	18.3				4.90	2.6	2.55E+03			
SH-pond	June 30 2000	4.79	12.3				4.99	2.6	2.55E+03			
SH-pond	July 3 2000	4.61	16.3				4.77	2.5	2.46E+03			
SH-pond	July 5 2000	4.71	19.2				4.95	2.6	2.57E+03			
SH-pond	July 7 2000	4.61	14.8				4.82	2.5	2.48E+03			

Table 3.2B: Explanation of measured parameters occurring in Table 2A

Parameter	Explanation
T	Temperature in degrees Celcius. Measured with ATP probe attached to pH meter
Eh	Electromotive potential in volts. Measured with a silver-silver chloride electrode and corrected to Eh by adding (220 – 0.72*(T °C))/1000 volts.
Diss O_2	Dissolved diprotic oxygen. Measured with a specialized probe (see text).
alkalinity	The sum of deprotonated bases that can be titrated with strong acid. In carbonate waters, most alkalinity is from HCO_3.
salinity	The amount of dissolved salts per unit water. Measured with an electrical conductivity probe.
E.C.	Electrical Conductivity in milliSiemens per centimetre. Measured with an electrical conductivity probe (which also gave results as salinity and total dissolved solids).
TDS	Total Dissolved Solids in milligrams per litre. Measured with an electrical conductivity probe.
CH_4	Total dissolved methane in millimoles per litre. See text for explanation.
DIC	Dissolved Inorganic C arbon in milligrams per litre. Measured in a glass vacuum line after cryogenic extraction and purification.
$\delta^{13}C_{DIC}$	The $^{13}C/^{12}C$ of DIC expressed in permil (‰) notation relative to international standard VPDB.
Log PCO_2	Partial pressure of CO_2 expressed as a logarithm. Calculated from DIC, pH, and T.

Table 3.3: Geochemical Data for 2000 Field Samples

Sample ID	Date collected	aCa (mmol/L)	aCO_3 (mmol/L)	Sat. Index
NQ-1	June 21 2000	2.09E+00	1.64E-03	-0.06
NQ-1	June 24 2000	2.30E+00	3.45E-03	0.31
NQ-1	June 28 2000	2.29E+00	4.31E-03	0.40
NQ-1	June 30 2000	2.42E+00	4.52E-03	0.44
NQ-1	July 3 2000	2.88E+00	3.98E-03	0.45
NQ-1	July 5 2000	2.48E+00	4.72E-03	0.48
NQ-1	July 7 2000	2.28E+00	3.14E-03	0.26
NQ-2	June 24 2000	2.27E+00	3.47E-03	0.31
NQ-2	June 28 2000	3.57E+00	4.60E-03	0.61
NQ-2	June 30 2000	2.18E+00	4.29E-03	0.37
NQ-2	July 3 2000	2.41E+00	4.58E-03	0.43
NQ-2	July 5 2000	2.27E+00	4.11E-03	0.40
NQ-2	July 7 2000	2.46E+00	4.92E-03	0.50
NQ-3	June 21 2000	3.61E+00	2.55E-03	0.35
NQ-4	June 24 2000	3.37E+00	2.23E-03	0.30
NQ-P	June 24 2000	1.31E+00	1.52E-03	-0.31
NQ-P	June 28 2000	1.08E+00	1.44E-03	-0.43
MZ-1	June 21 2000	1.15E+00	1.95E-03	-0.26
MZ-1	June 28 2000	1.68E+00	8.78E-04	-0.45
MZ-1	June 30 2000	2.99E+00	1.00E-03	-0.14
MZ-1	July 3 2000	4.78E+00	1.39E-03	0.20
MZ-1	July 5 2000	5.33E+00	1.12E-03	0.17
MZ-1	July 7 2000	4.51E+00	7.02E-04	-0.11
MZ-2	June 30 2000	8.33E+00	1.71E-03	0.55
MZ-2	July 3 2000	8.51E+00	1.44E-03	0.47
MZ-2	July 7 2000	5.49E+00	1.40E-03	0.28
AQ-1	June 24 2000	1.57E+00	2.30E-03	-0.09
AQ-2	June 26 2000	1.38E+00	3.46E-03	0.05
AQ-2	June 30 2000	1.43E+00	5.35E-03	0.25

Table 3.3 (cont'd)

Sample ID	Date collected	aCa (mmol/L)	aCO_3 (mmol/L)	Sat. Index
SH-1	June 26 2000	7.19E+00	4.48E-10	-6.04
SH-1	June 28 2000	6.79E+00	9.01E-08	-3.79
SH-1	June 30 2000	6.94E+00	1.32E-08	-4.63
SH-1	July 3 2000	6.74E+00	2.92E-08	-4.30
SH-1	July 5 2000	6.57E+00	1.28E-07	-3.64
SH-1	July 7 2000	6.39E+00	5.09E-08	-4.07
SH-2	June 26 2000	7.29E+00	2.37E-08	-4.32
SH-2	June 28 2000	6.71E+00	3.08E-07	-3.27
SH-2	June 30 2000	6.69E+00	3.52E-07	-3.22
SH-2	July 3 2000	9.48E+00	2.21E-07	-3.27
SH-2	July 5 2000	6.61E+00	3.21E-07	-3.25
SH-2	July 7 2000	7.01E+00	2.49E-07	-3.35

Note: "a" denotes activity. For example, "aCa" is the activity of Ca^{2+} ions in solution, where activity is calculated from the ionic strength of solution.
The saturation index is expressed as the logarithm of the activity product of Ca^{2+} and CO_3^{2-} versus the solubility product of $CaCO_3$. A value of 0 denotes saturation; a value above 0 indicates supersaturation; and a value below 0 denotes undersaturation.

Table 3.4: Field Data from 2003 Collection Season

Sample ID	Date Collected	pH	T (°C)	Eh (V)	diss. O_2 (mg/L)	alkalinity (mg/L HCO3)	DIC (mg/L)	log PCO_2	$[CH_4]$ (mmol/L)	TOC (ppmC)	$\delta^{13}C$ DIC (‰ VPDB)	$\delta^{13}C$ CH_4 (‰ VPDB)
NQ-1R	June 18 2003	7.16	9.0		2.25				4.24E-02	11.3	-18.6	-65.8
NQ-1R	June 20 2003	7.15	7.6	0.24	0.96	280	324	-1.67	3.69E-02	10.3	-17.5	-66.0
NQ-2R	June 23 2003	7.16	12.0	0.41	3.00	200	230	-1.83	1.48E-04	10.0	-15.0	-38.4
NQ-P2	June 18 2003									44.0		
MZ-1	June 18 2003	7.08	4.3	0.22	1.63				7.49E-03	11.3	-19.6	-71.0
MZ-1	June 20 2003	7.10	4.4	0.17	1.06	375	441	-1.50	9.61E-03	10.2	-20.7	-71.5
MZ-1	June 23 2003	7.01	5.6	0.16	1.20	327	399	-1.47	7.40E-03	11.3	-19.1	-72.0
MZ-2R	June 18 2003	7.02	5.0		1.45				4.61E-04	12.6	-17.9	-51.0
MZ-2R	June 20 2003	6.97	5.5	0.18	1.12	419	519	-1.32	4.38E-04	12.5	-17.8	-57.8
MZ-2R	June 23 2003	6.90	6.3	0.15	0.84	397	508	-1.27	5.28E-04	11.5	-16.4	-58.9
MZ-stream	June 18 2003	8.03	4.3	0.42	11							
MZ-stream	June 20 2003	7.96	4.4		10.1							
MZ-stream	June 23 2003	7.72	5.0		9.19	33	34	-3.18				
KP-1	June 23 2003	5.14	6.4	0.42	0.63						-27.2	
KP-1-surface	June 23 2003	6.02	7.9		3							
KP-lake	June 23 2003	7.64	15.4		8.4	76	79	-2.73				
SQ-stream	June 19 2003	7.23	2.9		11.8	11	12	-3.16		26.3		
SQ-1	June 19 2003	7.47	2.1		11.9	15	16	-3.26		30.0		
AQ-stream	June 20 2003	8.09	5.9		11.1	210	213	-2.74				

Table 3.5: Geochemical Data for 2003 Field Samples (a denotes activity)

Sample ID	date collected	aCa mmol/L	aFe mmol/L	aMg mmol/L	aMn mmol/L	aNa mmol/L	aSO_4 mmol/L	$aHCO_3$ mmol/L	aCO_3 mmol/L	SI ($CaCO_3$)
NQ-1R	June 20 2003	4.19	0.00	0.74	1.80E-02	0.40	3.61	4.51	1.18E-03	0.07
NQ-2R	June 23 2003	4.21	0.00	0.76	0.00E+00	0.42	3.81	3.20	9.66E-04	0.01
MZ-1	June 20 2003	3.50	0.25	1.75	3.45E-02	0.67	4.33	6.08	1.25E-03	0.00
MZ-1	June 23 2003	3.54	0.22	1.72	3.24E-02	0.64	4.35	5.50	9.53E-04	-0.11
MZ-2R	June 20 2003	4.51	0.11	2.15	2.52E-02	0.82	5.47	7.02	1.04E-03	0.04
MZ-2R	June 23 2003	4.59	0.13	2.18	2.56E-02	0.85	5.79	6.85	8.81E-04	-0.03
MZ-stream	June 23 2003	0.34	0.00	0.16	0.00	0.05	0.19	0.53	6.74E-04	-1.28
KP-lake	June 23 2003	0.62	0.00	0.23	0.00E+00	0.13	0.13	1.23	1.67E-03	-0.57

Note: "a" denotes activity. For example, "aCa" is the activity of Ca^{2+} ions in solution, where activity is calculated from the ionic strength of solution.
The saturation index is expressed as the logarithm of the activity product of Ca^{2+} and CO_3^{2-} versus the solubility product of $CaCO_3$. A value of 0 denotes saturation; a value above 0 indicates supersaturation; and a value below 0 denotes undersaturation.

Appendix 3: Calculations for quantitative mass balance

When $CO_{2(g)}$ dissolves in water, it reacts as a weak acid to form carbonate via the following reactions:

$$CO_{2(g)} \leftrightarrow CO_{2(aq)} \quad (i)$$

$$CO_{2(aq)} + H_2O \leftrightarrow HCO_3^- + H^+ \quad (ii)$$

$$HCO_3^- \leftrightarrow CO_3^{2-} + H^+ \quad (iii)$$

The equilibrium constants (k) for the above reactions are expressed as follows:

$$k_{CO_2} = \frac{[CO_{2(aq)}]}{P_{CO_2}} \quad (iv)$$

$$k_1 = \frac{[H^+] \times [HCO_3^-]}{[CO_{2(aq)}]} \quad (v)$$

$$k_2 = \frac{[H^+] \times [CO_3^{2-}]}{[HCO_3^-]} \quad (vi)$$

Square brackets [] denote molar concentrations, and P_{CO_2} is the partial pressure of CO_2 (in atmospheres). Values of k_{CO_2}, k_1 and k_2 are temperature-dependent. Consult Clark and Fritz (1997) for equations used to derive k values from temperature.

[DIC] is the sum of all dissolved protonated and deprotonated species of carbonate, i.e.

$$[DIC] = [CO_{2(aq)}] + [HCO_3^-] + [CO_3^{2-}] \quad (vii)$$

The relative proportion of each dissolved species of carbonate is expressed versus [DIC] using sigma notation as follows:

$$\sigma_o = \frac{[CO_{2(aq)}]}{[DIC]} = \frac{[CO_{2(aq)}]}{[CO_{2(aq)}] + [HCO_3^-] + [CO_3^{2-}]} \quad (viii)$$

$$\sigma_1 = \frac{[HCO_3^-]}{[DIC]} = \frac{[HCO_3^-]}{[CO_{2(aq)}] + [HCO_3^-] + [CO_3^{2-}]} \quad (ix)$$

$$\sigma_2 = \frac{[CO_3^{2-}]}{[DIC]} = \frac{[CO_3^{2-}]}{[CO_{2(aq)}]+[HCO_3^-]+[CO_3^{2-}]} \quad (x)$$

Sigma values can be expressed in terms of $[H^+]$, k_1 and k_2 alone. This is accomplished by rearranging Equations (*v*) and (*vi*) and substituting into Equation (*vii*). For example, rearranging Equation (*v*) for $[CO_{2(aq)}]$ produces:

$$[CO_{2(aq)}] = \frac{[H^+]\times[HCO_3^-]}{k_1} \quad (xi)$$

Rearranging Equation (*vi*) for $[CO_3^{2-}]$ produces:

$$[CO_3^{2-}] = \frac{k_2 \times [HCO_3^-]}{[H^+]} \quad (xii)$$

Substituting Equations (*xi*) and (*xii*) into (*vii*), we get:

$$[DIC] = \frac{[H^+]\times[HCO_3^-]}{k_1} + [HCO_3^-] + \frac{k_2 \times [HCO_3^-]}{[H^+]}$$

Dividing both sides by $[HCO_3^-]$, we get:

$$\frac{[DIC]}{[HCO_3^-]} = \frac{[H^+]}{k_1} + 1 + \frac{k_2}{[H^+]}$$

$$= \frac{[H^+]^2 + k_1 \times [H^+] + k_1 \times k_2}{k_1 \times [H^+]}$$

Sigma value σ_1 is the reciprocal:

$$\frac{[HCO_3^-]}{[DIC]} = \sigma_1 = \frac{k_1 \times [H^+]}{[H^+]^2 + k_1 \times [H^+] + k_1 \times k_2} \quad (xiii)$$

We can similarly derive σ_o and σ_2. The final equations will be:

$$\frac{[CO_{2(aq)}]}{[DIC]} = \sigma_o = \frac{[H^+]^2}{[H^+]^2 + k_1 \times [H^+] + k_1 \times k_2} \quad (xiv)$$

and

$$\frac{[CO_3^{2-}]}{[DIC]} = \sigma_2 = \frac{k_1 \times k_2}{[H^+]^2 + k_1 \times [H^+] + k_1 \times k_2} \quad (xv)$$

From Equations (*xiii*) to (*xv*), it is apparent that $\sigma_o + \sigma_1 + \sigma_2 = 1$, a condition which must hold true.

The experimental incubations systems are prepared in gas-tight septa jars which contain both an aqueous phase and a gaseous headspace. The amount of $CO_{2(g)}$ in the headspace must be accounted for when describing IC (since IC is defined as the sum of DIC and $CO_{2(g)}$).

Knowing [DIC] and pH, $[CO_{2(aq)}]$ is calculated from Equation (*xiv*) and P_{CO_2} is calculated from Equation (*iv*). Assuming that headspace CO_2 behaves as an ideal gas, the Ideal Gas Law can be applied:

$$P \times V = n \times R \times T \quad (xvi)$$

where P is the gas pressure (in atmospheres), V is the headspace volume (in litres), n is the number of moles, R is the ideal gas constant (= 0.08206 L•atm/K•mol), and T is temperature in degrees Kelvin. Rearranging Equation (*xvi*) to solve for the headspace $CO_{2(g)}$ concentration expressed as a molar quantity, we get:

$$[CO_{2(g)}] = \frac{n}{V_h} = \frac{P_{CO_2}}{R \times T} \quad (xvii)$$

In equation (*xvii*), P_{CO_2} is the partial pressure of CO_2 and is identical to the same term in Equation (*iv*). The headspace volume is denoted as V_h; the volume of aqueous phase will be denoted as V_a. Under standard conditions (i.e. T = 273.15K), the product of RT is 22.4. Since the incubation experiments were performed at an ambient room temperature of approximately 294K, the product of RT becomes 24.1 for our calculations.

A useful way of expressing the relative distribution of IC between the headspace and the aqueous phase is with a partitioning coefficient, D_c:

$$D_c = \frac{n_{CO_2}}{n_{DIC}} \quad (xviii)$$

where n denotes a discrete molar quantity of IC. The amount of carbon in each phase is simply the concentration multiplied by the phase volume:

$$n_{CO_2} = [CO_2] \times V_h \quad (xix)$$

$$n_{DIC} = [DIC] \times V_a \quad (xx)$$

The sum $V_h + V_a$ is equal to a constant, V_t, which is the volume of the incubation vessels. So Equation (*xx*) can be substituted as follows:

$$n_{DIC} = [DIC] \times (V_T - V_h) \quad (xxi)$$

Substituting Equations (*xix*) and (*xxi*) into Equation (*xviii*) produces:

$$D_c = \frac{[CO_{2(g)}] \times V_h}{[DIC] \times (V_T - V_h)} \quad (xxii)$$

$[CO_{2(g)}]$ is known from Equation (*xvii*), so substituting into Equation (*xxii*) yields:

$$D_c = \frac{P_{CO_2} \times V_h}{[DIC] \times 24.1 \times (V_T - V_h)} \quad (xxiii)$$

To derive an expression for D_C that is completely quantitatively independent, P_{CO_2} and [DIC] need to be removed. This is accomplished first by substituting for P_{CO_2} using Equation (*iv*):

$$D_c = \frac{[CO_{2(aq)}] \times V_h}{k_{CO_2} \times [DIC] \times 24.1 \times (V_T - V_h)} \quad (xxiv)$$

From Equation (*xiv*), we know that $[CO_{2(aq)}] / [DIC]$ is equal to σ_o, and sigma values are dimensionless, so Equation (*xxiv*) simplifies to:

$$D_c = \frac{\sigma_o \times V_h}{k_{CO_2} \times 24.1 \times (V_T - V_h)} \quad (xxv)$$

Now, let's look at calculations for isotopic mass balance.

Isotopic data are expressed in per-mil notation (‰) as follows:

$$\delta^{13}C_X = \left[\frac{R_X - R_{VPDB}}{R_{VPDB}}\right] \times 1000 \text{ ‰} \quad (xxvi)$$

where R is the ratio of $^{13}C/^{12}C$ for any compound X. R_{VPDB} is the ratio of the international Vienna Pee-Dee Belemnite standard against which all samples are reported (with $\delta^{13}C_{VDPB} = 0$ ‰). R_{VPDB} is equal to 0.011 179 6.

Fractionation factors for isotopic exchange are denoted by alpha values (α) as follows:

$$\alpha_{X-Y} = \frac{R_X}{R_Y} = \frac{1000 + \delta_X}{1000 + \delta_Y} \qquad \text{(xxvii)}$$

where X and Y are two different chemical species. For instance, in the hydration and deprotonation of $CO_{2(aq)}$ (shown in Equation (*ii*) of Appendix 1, above), X would represent HCO_3^- and Y would represent $CO_{2(aq)}$. Isotopic fractionation is temperature-dependent. Clark and Fritz (1997) provide equations relating temperature and α_{X-Y} values for many reactions involving organic and inorganic carbon compounds.

Calculations using equations in Appendix 1 show how inorganic carbon species are distributed versus pH in closed systems containing both aqueous and gaseous phases. The calculations allow us to described IC quantitatively on the entire system, not just one phase. Describing IC isotopically requires using both the calculations from Appendix 1 and Equations (*xxvi – xxvii*) above. For instance, if a headspace gas sample is analyzed for $\delta^{13}C_{CO_{2(g)}}$ and the pH of the aqueous phase is measured, sigma values (σ_o, σ_1, σ_2) and the partitioning coefficient D_c can be used to calculate the relative amounts of dissolved carbonate species (i.e. $CO_{2(aq)}$, HCO_3^-, CO_3^{2-}) present in the aqueous phase, and α_{X-Y} values from Clark and Fritz (1997) can be used with Equation (xxvii) to calculate $\delta^{13}C$ on each DIC component. Combining the $\delta^{13}C$ values of each inorganic carbon species to derive R_{IC} requires using the isotopic mixing equation:

$$R_{IC} = \frac{\sigma_o \times f^{13}C_{CO_{2(aq)}} + \sigma_1 \times f^{13}C_{HCO_3} + \sigma_2 \times f^{13}C_{CO_3} + D_c \times f^{13}C_{CO_{2(g)}}}{\sigma_o \times f^{12}C_{CO_{2(aq)}} + \sigma_1 \times f^{12}C_{HCO_3} + \sigma_2 \times f^{12}C_{CO_3} + D_c \times f^{12}C_{CO_{2(g)}}}$$

(*xxviii*)

where $f^{13}C$ and $f^{12}C$ are mole fractions of ^{13}C and ^{12}C, defined as follows:

$$f^{13}C_X = \frac{R_X}{1 + R_X} \qquad (xxix)$$

$$f^{12}C_X = 1 - f^{13}C_X = \frac{1}{1 + R_X} \qquad (xxx)$$

Converting R_{IC} into $\delta^{13}C_{IC}$ is achieved using Equation (xxvi) above.

Similar calculations are used for assessing the $\delta^{13}C$ of "residual methanol" in the enriched experimental incubation systems described in the text. For these calculations, acetic acid and methane are two major products of bacterial processes occurring in the systems, and methanol is the main substrate. It is possible that other substrates exist from which acetic acid and methane are produced (such as TIC). It is likewise possible that methanol is being reacted to other unknown products. For simplicity, "residual methanol" is defined as the methanol expected to be remaining in solution if no other processes other than acetic acid and methane formation from methanol are occurring. The mass balance equation for calculating the amount of residual methanol is:

$$n_{meth} = (n_{meth})_i - n_{CH_4} - n_{acetic} \qquad (xxxi)$$

Where n_X is a discrete quantity of compound X, and $(n_{meth})_i$ is the initial amount of methanol present at the onset of incubation. The isotopic mass balance equation is:

$$R_{meth} = \frac{(n_{meth})_i \times f^{13}C_{(meth)_i} + n_{CH_4} \times f^{13}C_{CH_4} + n_{acet} \times f^{13}C_{acet}}{(n_{meth})_i \times f^{12}C_{(meth)_i} + n_{CH_4} \times f^{12}C_{CH_4} + n_{acet} \times f^{12}C_{acet}} \qquad (xxxii)$$

Where $f^{13}C$ and $f^{12}C$ are once again the mole fractions of ^{13}C and ^{12}C.

Because there are no known reactions where methanol is an exclusive substrate in acetic acid formation, it would be logical to assume that the sum of the acetic acid and methane would be greater than the amount of residual methanol since other substrates are substituting for methanol. However, experimental measurements show the opposite to be true, i.e. there is a deficit of methanol. Incorporation of relatively ^{13}C-enriched carbon (from DOM and/or TIC) into acetic acid would tip the calculated isotopic result for residual methanol toward more depleted values. Furthermore, since there is a methanol deficit, we can assume that methanol is being consumed to produce unknown compounds, leaving a smaller residual methanol pool (which is measured). The $\delta^{13}C$ composition of that smaller pool is likely to be more enriched than the values calculated from Equation *xxxii* above given Rayleigh-type enrichments resulting from bacterial activity similar to methanogenic and acetogenic processes. So the isotopic mass balance calculations are shown to be conservative in estimating the isotopic composition of methanol.

The Rayleigh distillation equation is shown in Equation (4-12) in the text. Calculations using this equation are simple and do not need to be explained here.

Appendix 4

"Methanogenic versus acetogenic reactions in periglacial groundwaters; Early Incubation Experiments"

Abstract

Endostromatolites, periglacial carbonate features created by methanogenic and/or acetogenic activities, retain an ^{18}O record of paleoclimatic significance, and a characteristically enriched $\delta^{13}C_{calcite}$ values of up to +14‰ VPDB. Soil microorganisms from a periglacial carbonate terrain where endostromatolites outcrop were used to inoculate simple closed-system incubation experiments to determine the metabolic pathways involved in endostromatolite growth and their effect on residual DIC and secondary calcite. Quantitative geochemical and isotopic methods were used to characterize the major carbon-bearing reactants and products. Methanol and trimethylamine were preferred substrates for methane formation; acetate and formate failed to stimulate and sustain methanogenic activity. While access to inorganic carbon was limited in the incubation systems, methanogens used methanol as a substitute for CO_2 in the hydrogenotrophic reaction pathway, and acetogenic activity was reduced, though not completely inhibited. When TIC was not limited, acetogenic activity accelerated and methane production lagged.

Isotopic enrichments of residual TIC were observed in the initial stages of the carbonate-buffered acetogenic incubations but were short-lived as the lack of a solid carbonate phase in contact with the aqueous incubation systems allowed TIC to be turned over rapidly and maintained in closer isotopic equilibrium with ^{13}C-depleted organic matter. The systems became acidic due to the lack of pH buffering from limestone dissolution, but gaseous CO_2 release was not solely responsible for raising $\delta^{13}C_{TIC}$ from -3.0‰ to as high as +5.1‰ VPDB. Growth of endostromatolite columns in limestone fissures preserves a ^{13}C-isotopic enrichment signal that is believed to be the result of similar processes observed in the experimental incubation systems.

Introduction

Secondary carbonate within limestone fissures in Canadian periglacial terrains is a newly identified material that holds interesting paleoclimatic information (Lauriol and Clark, 1999). These deposits, referred to as *endostromatolites* for their growth within the rock mass and hidden from light, have been attributed to methanogenic activity on the basis of petrographic and isotopic evidence (Chauret, 2000; Lauriol and Clark, 1999). They originate within saturated talik that developed on southern exposures of bedrock during past hypsithermal events. Having been deposited in equilibrium with meteoric waters during the late Pleistocene and early Holocene, their $\delta^{18}O$ composition has been used to interpret paleoclimatic conditions of the recent geologic past (Clark *et al.*, 2003).

Isotopic studies of carbon reveal that endostromatolites are enriched in ^{13}C compared to the host rock, and the degree of enrichment increases away from the growth surface. Lauriol and Clark (1999) have examined the isotopic systematics of inorganic carbonate precipitation in periglacial environments, and they conclude that the origin of this material is biogenic. They invoke methanogenic activity as a process potentially responsible for the ^{13}C enrichments. Other evidence of direct bacterial involvement includes banded microstructures within growth columns (see Figure i). Their growth model holds that during warmer periods and permafrost degradation, groundwaters infiltrating through soil and vegetation would carry organic carbon into rock fractures. This source of carbon and the saturated porosity in the subsurface supported methanogenic bacteria.

This investigation presents preliminary experimental results into the association of endostromatolites with active carbon-fractionating bacterial populations. Northern wetlands are an important source of biogenic methane to the global atmospheric budget (Chanton *et al.*, 1995; Lansdown *et al.*, 1992; Martens *et al.*, 1992). During a hydrological investigation of discharge waters along the Big Fish River catchment, located in the Richardson Mountains, N.W.T. (see Clark *et al.*, 2001), soil and water samples were collected for use in experimental incubations. The bacterial populations in

modern natural materials taken from limestone terrains where endostromatolites once grew should have many similarities to the microorganisms that lived within the fissures. Past climate improvement likely permitted more widespread water circulation, transporting soil organics and DOC (dissolved organic carbon) from the vegetated surface down through zones of talik. Exposure and erosion of the outcrops have since terminated growth within the fissures. Climate deterioration since deposition has allowed expansion of permafrost and decreased groundwater circulation. A strong potential for anaerobic bacterial activity within talik and the saturated overlying active layer exists. It is our purpose to use modern natural materials in methane-generating periglacial limestone terrains for determining the biogeochemical mechanisms for growth of endostromatolite. The experiments reported herein will establish some preliminary characteristics of the microbiological communities in our soil samples, and this information will be used as a basis for planning ongoing research.

Methodology

This work integrates field sampling of groundwaters in permafrost carbonate terrain with microcosm experiments undertaken in the laboratory at the University of Ottawa. In both settings, a suite of geochemical parameters was monitored, including pH, temperature, [CH_4], [DIC] (dissolved inorganic carbon), [DOC] (dissolved organic carbon), and $\delta^{13}C_{DIC}$. Square brackets [] denote concentration.

For clarity, dissolved inorganic carbon is expressed as the sum of aqueous carbonate species:

$$n_{DIC} = n_{CO_{2(aq)}} + n_{HCO_3^-} + n_{CO_3^{2-}}$$

(where *n* represents the amount of the given species, usually in moles). Total inorganic carbon ("TIC") is herein used to denote the sum of aqueous n_{DIC} and $n_{CO_{2(g)}}$, the amount of carbon dioxide present in gaseous headspace in contact with aqueous solutions. When no gaseous phase is in contact with a liquid, $n_{DIC} = n_{TIC}$. References to inorganic carbon ("IC") are qualitative and do not imply any particular phase or amounts

of a certain phase. All aqueous samples analyzed for DIC were filtered with filter paper of 0.45 μm pore size.

Field Sampling

In June 1997, a block of unfrozen organic-rich soil was cut from the active layer of the study area near Big Fish River, N.W.T. (68° 18' N; 136° 18' W). A description of the geomorphology and geology of the site, and the geochemistry of groundwaters at the site, is given by Clark *et al.* (2001). The intact block, measuring approximately 40cm by 25cm by 15cm, was preserved in a plastic Tupperware dish sealed with packing tape around all sides of the lid. Water samples were pumped into large plastic jugs manually with plastic tubing attached to a large disposable syringe at one end. The materials were kept refrigerated slightly above freezing upon delivery to the laboratory facilities. While aseptic conditions were not strictly maintained for the sampling protocol, minimal handling of the soil after collection ensured adequate sample integrity with minimal contamination. As a precaution, soil samples for use in the incubation experiments described below were removed with sterilized metal tools from the centre portions of the intact block.

Incubation Experiment #1

The purpose of the first experiment was to create incubation systems inoculated with soil from the field sample collected above and to determine the potential of several carbon-bearing substrates to sustain methanogenic cultures. The main variable analyzed on the systems was methane concentration to determine how much methane was produced and how quickly it was produced (i.e. the time derivative of production). Incubation of the soil organisms involved using anaerobic growth media containing essential nutrients and growth substrates suited to methanogenic bacteria (Table I). Four substrates (shown in **BOLD** in Table I) were provided individually by adding a certain amount to four separate vessels. A fifth vessel was given half the amount of each substrate plus 2-bromoethanesulfonic acid (BES) to a final concentration of 10 gL^{-1} to inhibit methanogenesis. Ten grams of wet soil was used to inoculate the media in each

250mL jar directly. Final volumes of slurry were 110 mL, leaving a residual nitrogen headspace of 140 mL per jar. The clear glass jars were sealed tightly with silica-gel septa liners under open-top caps.

Incubation Experiment #2

The second experiment sought to determine how the presence/absence of inorganic carbon would impact substrate usage and to determine the effects on the $\delta^{13}C$ of the residual DIC (i.e. would the presence of IC affect methanol usage by methanogens and/or other bacteria present?) The cultures were prepared with a modified media recipe (Table I). Two litre glass vessels were used to store the inoculated systems. One litre of autoclaved growth media in each vessel was inoculated with 50g of wet soil plus 7.6mL of methanol (99.94% pure). The vessels had dual openings to permit easy access and removal of aqueous and gaseous samples (see Figure ii). To prevent possible diffusion of oxygen into the closed systems in the event of gas leakage, the vessels were stored in an anaerobic chamber with an atmosphere of less than 5% each H_2 and CO_2 in a balance of N_2. The chamber temperature was maintained at 25°C. Oxygen levels in the chamber were monitored using a methylene blue indicator solution that is sensitive to concentrations as low as 10ppmV (D. Fortin, personal communication).

In total, three different incubation systems were prepared. One system was not given inorganic carbon (as $NaHCO_3$) as a buffering reagent; this system was called vessel A. Another system was initially prepared with $NaHCO_3$ to a concentration of 4.0 $g \cdot L^{-1}$ (48 mM), and this system was called vessel B. Autoclaving of the buffered solution caused a decrease in dissolved inorganic carbon (DIC) by CO_2 release. The actual starting concentration of DIC in vessel B was measured to be 35 mM (samples were taken before DIC in solution was able to establish an equilibrium P_{CO_2} in the headspace). A control system with incipient in-situ conditions identical to vessel A was created by adding BES methanogenic inhibitor to a concentration of 3.0 $g \cdot L^{-1}$, and this became vessel C. By selectively inhibiting methanogenic bacteria, the results of the closed

systems would show that differences between vessels A and B and changes over time in these systems were, in fact, due to differential methanogenic activities.

Analyses

Levels of inorganic carbon in the vessels and the isotopic composition of IC were determined regularly by monitoring DIC using the acid volatilization technique. Orthophosphoric acid was used to react aqueous samples under vacuum and thereby convert DIC to CO_2. CO_2 was separated and purified cryogenically on a vacuum line before being sealed in Pyrex tubes and analyzed for $\delta^{13}C$ on a SIRA-12 isotope ratio mass spectrometer (IRMS). Values of [DIC] were converted to n_{TIC}, the total inorganic carbon content of the entire vessel (taking into account both aqueous and gaseous phases) by using calculations based on the equilibrium constants for all IC phases summarized in Clark and Fritz (1997).

Headspace gases were sampled with air-tight glass syringes. Methane and methanol were quantitatively measured by injection of headspace samples into a gas chromatograph with a flame ionization detector (GC-FID). Methane concentrations were converted to discrete amounts for each vessel by taking into account the headspace volume, pressure, and losses of methane from sample removal. Solution pH was measured on small liquid aliquots exported from the anaerobic chamber. Fatty acid analyses were performed on a Beckman HPLC using a Bio-Rad organic acid analysis column at the facilities of the Department of Microbiology (College of Biological Science), University of Guelph.

At the time of the second experiment, a methodology for analyzing $\delta^{13}C$ of methane was still in development, and the reporting of $\delta^{13}C_{CH4}$ results is given in the discussion (section 4.0). The method used was gas chromatography – combustion – isotope ratio mass spectrometry (GC-C-IRMS), and the instrument used to perform analyses was a Finnigan MAT Delta Plus with a cryogenic precondensing interface for collecting small amounts of methane from gas sample volumes up to 100mL. While the

instrument's precision for identical replicate analyses is ± 0.3‰, manual injection of discrete samples with a glass air-tight syringe gave results with a standard error closer to ± 1.0‰.

Isotopic results are reported using delta notation in ‰ (permil) and are referenced to universal standard VPDB (Vienna Pee Dee Belemnite). The equation for calculating the delta value is:

$$\delta^{13}C_{sample} = \left[\frac{R_{sample} - R_{stnd}}{R_{stnd}} \right] \times 1000 \text{ ‰}$$

where R_{sample} and R_{stnd} are the $^{13}C/^{12}C$ isotopic ratios of the sample and of the standard, respectively.

Hydrogen (H_2) was not measured in the incubation systems. Previous research has shown that hydrogen is produced in natural systems by a variety of microorganisms involved in biogenic degradation in natural systems and that levels of hydrogen are maintained at low concentrations due to competitive usage by methanogens, sulphate reducers, and acetogens (see Brock *et al.*, 1994; Conrad *et al.*, 1989; Jones *et al.*, 1982). Interspecies hydrogen transfer (ISHT) is directly responsible for creating symbiotic dependence between respirers and organic fermentative bacteria, the result of which is that most hydrogen is turned over quickly and is hence not "visible" in natural systems. Conrad (1999) summarizes many hydrogen-producing and hydrogen-consuming processes in methanogenic systems.

Results

Experiment #1

Methane production results in the first set of experimental incubation vessels are shown in Table II. Only the systems containing either methanol or trimethylamine produced significant amounts of methane. Production in all vessels was relatively slow for the first 183 days. The methanol system initially had the highest methane output. Between 183 and 260 days, production in the trimethylamine system accelerated. The extended period of slow production before accelerated growth resulted in an infrequent sampling protocol. The vessels used to hold the closed systems for this experiment were subsequently determined to be diffusive to methane, so the apparent loss of methane from the headspace of the trimethylamine system after 344 days is due to gradual diffusion. Because of the lack of oxygen and any other possible oxidizing agents that could be used by respiring organisms in the vessels, loss of CH_4 due to methane oxidation is not a viable process. By contrast, the same decline in $[CH_4]$ over time is not evident in the methanol system where a maximum was not reached and methane concentration was highest at the end of the analytical period. Ebullitive methane release was not apparent in this vessel. Trace amounts of methane were formed in the presence of acetate and formate, comparable to the inhibited systems containing BES. Since the substrates were added in excessive amounts in all systems, the results of Table II are purely qualitative and represent no more than 10% of available substrate converted to CH_4.

Experiment #2

For the second experiment, methanol was chosen as the primary substrate; however, other carbon-bearing reagents in the media recipe (see Table I) may have also served as potential substrates for methane production and/or cell growth. Because of slow growth in the incubation systems of the first experiment, it appeared that methanol was the substrate that had the greatest effect on inducing methanogenic production. The selection of methanol is consistent with it being a natural degradational product of organic carbon, and would likely be available to methanogenic bacteria in natural systems.

The controlled variable for this set of incubations was the presence/absence of inorganic carbon. Incubation was allowed to continue over a period of more than 400

days. Within 3 days of inoculation, gas bubbles were observed being released from the sediment layer at the bottom of vessel A. The results of methane production appear in Figure iii. Vessel A underwent very rapid methane formation until a peak was reached in less than 60 days. By contrast, buffered vessel B underwent slower methane production, gradually increasing over time and peaking near the end of the incubation period, similar to the methanol system of Experiment #1. Control vessel C yielded negligible methane. The gradual decline of methane from vessel A after 60 days is attributed to diffusive loss overtaking the rate of production.

The production of CH_4 is not fully supported by methanol consumption (Figure iv). Buffered vessel B had consistently the lowest methanol concentration, followed by unbuffered vessel A and control vessel C. Because methanol was added in excess relative to the available headspace volume for CH_4 being released by methanol-degrading methanogens, methanol was never entirely consumed, and even vessel B's contents were never measured below 50% of the initial concentration ($6.0 g \cdot L^{-1}$). Most of the methanol consumption occurred within the first 100 days of incubation, before a GC-FID method could be established.

pH data are shown in Figure v. The initial pH of vessel B was higher than the unbuffered systems; it had a starting value of about 7.0 after inoculation, whereas the other systems started at values around 6.0 to 6.1. All three systems became more acidic shortly after the onset of incubation, dipping to as low as 4.99 in vessel A. After 40 days, all three systems established steady conditions, with vessel B maintaining a pH around 5.6, vessel A around 5.0, and vessel C in the vicinity of 5.2.

Results for inorganic carbon are shown in Figure vi. Most noticeable is the immediate decline of n(TIC) in vessel B after only a matter of days. Since n(TIC) values take into account partitioning of phases between the solution and the headspace, losses of TIC cannot be attributed to the shift of pH causing DIC to be protonated and shifted to the headspace as $CO_{2(g)}$. In the two unbuffered vessels, n(TIC) remained relatively low.

Carbon isotopic data for TIC are shown in Figure vii. The $\delta^{13}C$ of $NaHCO_3$ used in the media recipe (Table I) was measured to be -4.79‰ ± 0.02‰ VPDB (average of three measurements; error is the mean deviation of these measurements). Autoclaving of the growth media resulted in a small fractionation of DIC, and the actual measured starting value of $\delta^{13}C_{DIC}$ was -2.6‰ VPDB. Calculated starting values for TIC could not be determined because equilibrium with headspace CO_2 was not established yet immediately after inoculation. All other carbon-bearing reagents in solution were much more depleted compared to bicarbonate: methanol (-39.6‰); ammonium acetate (-38.1‰); and soil organic matter (-26‰± 0.5‰ VPDB; average of four measurements). The $\delta^{13}C_{TIC}$ results (Figure vii) show enrichment trends for all three vessels over different time frames. Vessel A evolved rapidly and the enrichment is short-lived. However, vessel B shows a distinct enrichment peak, reaching +5.1‰ VPDB after only two weeks. Control vessel C shows a prolonged enrichment trend that reached a peak of +1.4‰ VPDB. All three systems became depleted over time, reaching values almost as low as -30‰ with the exception of the control vessel, that evolved to -10‰ VPDB.

Quantitative chromatography of fatty acids was performed on two separate occasions, and the results were combined with results of other compound-specific analyses to establish a carbon budget for each vessel. The mass balance data are shown in Table III. Measured values are compared to starting concentrations to obtain a surplus/deficit of each species. Values for each compound are corrected for mass removed for sampling. Acetate was included in the media reagent recipe as an ammonium salt (see Table I). The chromatographic results show that acetate was consistently the most abundant fatty acid in solution with minor amounts of formic and propionic acids (short-chain fatty acids larger than acetate were detected but not standardized). Only acetate was included in the mass balances since other fatty acids were largely produced from the decomposition of DOC released from soil organic matter and thus represent a minor and unquantifiable carbon source.

By the first sampling period, the vessels had established quasi-steady state conditions with respect to pH (Figure v), *n*(TIC) (Figure vi), and methanol concentration

(Figure iv), so errors associated with combining results over a short sampling period are small. Net acetate production was evident in all three vessels, but much more so for vessel B than for the unbuffered vessels. The excess of acetate in vessel B was more than seven times greater than in either of the other two vessels. All three vessels registered surplus carbon budgets, though a close balance of reactants and products was established in the unbuffered vessels. By the second sampling period nearly eight months later, the large acetate surplus in vessel B had become much smaller, and minor acetate deficits were apparent in vessels A and C. The large carbon surplus in vessel B had become a significant deficit. The same pattern is evident in vessel C to a lesser extent. Vessel A maintained a carbon surplus, though the apparent increase in methanol concentration after eight months seems erroneous, and a measurement error is assumed to be responsible. A greater explanation of the results is given in the following discussion.

Discussion

Methanogenic reactions – theory

Previous research into natural and cultured methanogenic bacterial systems has shown two major reaction pathways to exist: CO_2-reduction and acetate fermentation (Whiticar *et al.*, 1986; Landsdown *et al.*, 1992; Jedrysek, 1995; Hornibrook *et al.*, 1997). CO_2-reduction occurs as follows:

$$CO_2 + 4H_2 \rightarrow CH_4 + 2H_2O \quad (1)$$

(Brock *et al.*, 1994). This reaction pathway can be more generally classified as *hydrogenotrophic methanogenesis* since partially reduced compounds can substitute for CO_2 (such as formate and methanol) (Ehrlich, 1996). For example, a hydrogenotrophic reaction utilizing methanol as carbon source would proceed as follows:

$$CH_3OH + H_2 \rightarrow CH_4 + H_2O \quad (2)$$

Acetate fermentation is a *methylation* or *disproportionation* reaction where both CO_2 and CH_4 are products:

$$CH_3CO_2H \rightarrow CO_2 + CH_4 \quad (3)$$

(Ehrlich, 1996). Other carbon-bearing substrates that can be fermented by methanogens include methylamine, methanol and formate; acetate is the only multicarbon compound

that can be used directly by methanogens. Fermentation of methanol is given by the following reaction:

$$4CH_3OH \rightarrow 3CH_4 + CO_2 + 2H_2O \quad (4)$$

Fermentation reactions are much less thermodynamically favourable than hydrogenotrophic reactions. A major source of hydrogen produced in natural systems is organic fermentation. Conrad (1999) has shown that organic fermentation is a source of both H_2 and lightweight carbon-bearing compounds that are essential precursors to methanogenesis in natural systems.

The isotopic composition of compounds evolved in methanogenesis has been studied extensively (*e.g.* Boehme *et al.*, 1996; de Graff *et al.*, 1996; Burke Jr. *et al.*, 1988; Balabane *et al.*, 1987; Krzycki *et al.*, 1987; Schoell, 1980; Fuchs *et al.*, 1979;. Silverman and Oyama, 1968). In general, the two reaction pathways are distinguished by the $\delta^{13}C$ of methane they produce. Whiticar *et al.* (1986) suggest that CO_2-reduction produces CH_4 with $\delta^{13}C$ between -110 and -60‰ VPDB and aceticlastic methanogenesis creates $\delta^{13}C_{CH4}$ usually between -65 and -50‰ VPDB. The large amount of variability in $\delta^{13}C$ of CH_4 derived from CO_2 is partially due to species-specific fractionation (Gelwicks *et al.*, 1994). Fractionation factors ($\alpha^{13}C_{CO_2\text{-}CH_4}$) measured on pure cultures yield values between 1.025 and 1.061 (Games *et al.*, 1978). Similarly, species-specific fractionation for acetate fermentative bacteria is anticipated (Gelwicks *et al.*, 1994), though intramolecular isotopic heterogeneity of acetate and side reactions such as methyl-group oxidation add uncertainty to the determination of fractionation during acetate consumption. Sugimoto and Wada (1993) obtained methane from incubated rice paddy soil with values as enriched as -33‰ VPDB, implying that very little fractionation between the methyl group of acetate and CH_4 occurs.

The large fractionation associated with biogenic CO_2 reduction enriches the residual DIC pool in ^{13}C over time. Boehme *et al.* (1996) demonstrated this for methanogenic marine sediments. This would appear to be a reasonable explanation for the measured isotopic enrichments in endostromatolite columns. A decrease in the partial pressure of CO_2 due to CO_2 uptake would favour inorganic carbonate precipitation:

$$2HCO_{3(aq)}^{-} + Ca^{2+}(aq) \leftrightarrow CO_2 + H_2O + CaCO_3 \quad (5)$$

(Clark and Fritz, 1997). In a theoretical system where the only source of IC is the dissolution of bedrock, autotrophic methanogenesis would cause the isotopic composition of precipitating carbonate phases to reach a ^{13}C-enriched steady state over time. The enrichment would be attenuated if organic matter decomposition, that releases ^{13}C-depleted CO_2, becomes a significant contributing source of IC to the IC pool available to methanogens. Fermentation of organic materials disproportionates carbon into CO_2 and reduced species (see Conrad, 1999). When an electron acceptor such as O_2 enters the system, proportionally more oxidized carbon is produced by heterotrophic respirers, with significant inputs of ^{13}C-depleted CO_2. Thus, ^{13}C-enrichment in endostromatolite columns would suggest highly anaerobic reducing in-situ growth conditions (i.e. an environment lacking electron acceptors).

Acetogenic reactions - theory

Homoacetogenesis occurs as follows:

$$2CO_2 + 4H_2 \rightarrow CH_3CO_2H + 2H_2O \quad (6)$$

$$(\Delta G°r = -78 \text{ kJ})$$

(Gelwicks *et al.*, 1989). If methanol can substitute for one equivalent of CO_2 in the above reaction, the resulting reaction would be:

$$CO_2 + CH_3OH + H_2 \rightarrow CH_3CO_2H + H_2O \quad (7)$$

$$(\Delta G°r = -69 \text{ kJ})$$

The standard Gibbs free energies of Reactions (6) and (7) above were obtained by using the values of Drever (1996). Both of these reaction are less thermodynamically favourable than hydrogenotrophic methanogenesis ($\Delta G°r = -131$ kJ for Reaction (1); $\Delta G°r = -112$ kJ for Reaction (2)). However, other variables are likely responsible for favouring acetogenesis over methanogenesis. For example, competition for H_2 favours acetogens over methanogens at lower temperatures (Conrad *et al.*, 1989). Heterotrophic acetogenesis, Reaction (7), consumes much less molecular hydrogen per equivalent of

acetate formed than homoacetogenesis, Reaction (6). Hydrogen in natural systems is maintained at low concentrations due to competitive microbial usage and to interspecies hydrogen transfer (ISHT) (see, for example, Conrad *et al.*, 1989). Consequently, at low H_2 levels, Reaction (4) would become thermodynamically unfavourable before the mixed substrate reaction in Equation (5). In addition, limited access to IC would put additional stress on the homoacetogenic pathway. Acetogenic activity was limited but not totally inhibited in vessel A due to a lack of IC. Chemical inhibition of methanogens in vessel C had no appreciable effect on acetogenic activity, so the reduced production by acetogens in vessels A and C was not exclusively due to competition for H_2.

The presence of methanol had a stimulatory effect on acetate production in contrast to other substrates tested (data not shown). The effect was even more pronounced in the presence of IC (see Table III). These results suggest the presence of a mixed acetogenic population or of at least one versatile organism capable of using both DIC and methanol.

Early acetogenesis and $\delta^{13}C_{DIC}$ enrichment – experimental evidence

Acetate production has contributed to acidity: CO_2-reduction alone would have induced the pH of the systems to increase. The acid dissociation constant (k_1) of acetate is 1.75×10^{-5} at 25°C, so it is a much stronger acid than carbonic acid ($k_1 = 4.45 \times 10^{-7}$ at 25°C) (Skoog *et al.*, 1994). It would appear logical for vessel B to have the lowest pH since it generated by far the most acid, but the pH data (Figure v) show that it remained slightly less acidic than the unbuffered vessels. We attribute this to the negative feedback response of CO_2 release to the headspace since vessel B had initially a much higher concentration of DIC.

The carbon isotopic data for TIC (Figure vii) support the observed timing of acetogenic versus methanogenic reaction. All three systems followed a similar trend of initial ^{13}C-enrichment followed closely by strong depletions. The enrichment of vessel A was early and very brief, prior to methane production accelerating and achieving a peak.

Rapid turnover of IC from depleted organic sources may have been induced by a syntrophic relationship between CO_2- and H_2-producing organic fermenters and CO_2- and H_2-consuming acetogens. Methane production becomes significant later in the incubation (around day 30), but by this time, $\delta^{13}C$ of DIC has already decreased to very depleted values. Without quantitative or isotopic data for DOC, it is not feasible to speculate on whether methane production had any effect on maintaining $\delta^{13}C$ of DIC at steady state values above that of $\delta^{13}C_{DOC}$. So early isotopic enrichment of TIC is driven by acetogenesis.

The early $\delta^{13}C_{DIC}$ enrichment trend is more clearly defined for vessels B and C, in which methane production was either delayed (vessel B) or completely inhibited (vessel C). The high initial concentration of DIC in vessel B, that experiences a sharp decline concurrent with the early ^{13}C enrichment, is apparently consumed by acetogenesis, consistent with the observations for vessel A. The decrease in methanol concentration suggests that acetogenesis follows Reaction (7), above. Methanogenesis in vessel B begins only slowly after this initial period of acetate production, perhaps in response to the decrease in DIC and acetogenic competition for methanol substrate. Clearly, from the data in Table III, the amount of methane produced could not be responsible for the decrease of n_{TIC}, and it follows that methanogenesis could not be responsible for the ^{13}C enrichment of residual DIC.

Since acetate production was consistently higher in the presence of methanol as compared to other substrates tested (experiment 1), it is theorized that *heterotrophic acetogenesis* utilizing both methanol and CO_2 is occurring according to Reaction (7) where the (H_2 consumed):(acetate produced) ratio is 1:1. The carbon mass balance of vessel B bears this out initially with similar amounts of carbon from DIC and methanol being consumed; the balance of "excess" acetate is likely the result of acetate release by organic fermentative organisms and acetogenic activity from CO_2 also released by fermenters.

<u>Delayed methanogenesis following acetogenesis</u>

The methane production results (Figure iii) complement the notion of competitive substrate (H_2) usage. In vessel A, acetogenic activity was limited by low levels of IC, supporting rapid CH_4 production after day 10. In vessel B, access to IC initially favoured a longer period of acetogenic activity and so precluded any significant methanogenic production until about day 40. By this time, IC became a limiting reagent (Figure vi), acetate production slowed down, and the CH_4 production rate was rapidly increased. Since the availability of methanol in the systems was not limited, methanogenesis via the fermentative reaction pathway, Reaction (4), would not have been inhibited in either vessel A or B at any time. The lack of methanogenic production during peak acetogenic activity and the accelerated methanogenic production after acetogenesis slowed are evidence that methanogenic production was dependent on the hydrogenotrophic reaction pathway using methanol in place of CO_2 (Reaction (3)).

High methanogenic productivity and low initial DIC levels likely had a positive feedback on organic decomposition in vessel A as CO_2 released by fermentation was quickly cycled so that a ^{13}C-enriched residual fraction was observed only very briefly. Aceticlastic methanogenesis (*i.e.* the fermentation pathway) was not observed with respect to changing levels of acetate in solution as the loss of acetate and methanol in vessels A and B occurred during a period of minor to no CH_4 production (after 50 days in vessel A, and after 180 days in vessel B; Figure iii).

$\delta^{13}C$ of methane and isotopic fractionation of IC

The experimental incubation systems have shown that IC is both a reactant and a product of diverse biogenic processes. The isotopic enrichment of TIC in the earliest stages of incubation (Figure vii) was due to biogenic activity reacting isotopically light substrate fractions. Calculations using the fractionation factors summarized in Clark and Fritz (1997) for aqueous and gaseous inorganic carbon species at equilibrium show that a pH shift from 7.0 to 5.6 would produce a net fractionation of aqueous DIC by less than

1‰ due to $CO_{2(g)}$ release from solution. Hence a measured $\delta^{13}C_{DIC}$ above -1.6‰ is the result of preferential biogenic uptake of $^{12}CO_2$.

Homoacetogenic consumption of CO_2 can create carbon isotopic fractionation similar to methanogenic CO_2-reduction (Murase and Sugimoto, 2001). Nonetheless, CH_4 should have low $\delta^{13}C$ values whether it was produced directly from CO_2 or indirectly from acetate generated from CO_2 by homoacetogens. Acetate cleavage is carried out by only two methanogenic genera, *Methanosarcina* and *Methanothrix* (Blair and Carter Jr, 1992). The results from Experiment 1 show that acetate did not stimulate methane production, though this is not necessarily an indication that no organisms capable of aceticlastic methanogenesis were present. Acetate cleavage is an "induced" characteristic (Baresi, 1984) and cultures growing on other substrates are less able to metabolize acetate compared to cultures that have previously adapted to acetate (Krzycki *et al.*, 1982). Notwithstanding, our results are consistent with other findings for natural cultures derived from cold climate terrains (Hines *et al.*, 2001). So acetogenic production in our incubation systems did not likely sustain any aceticlastic methanogenic activity.

According to Sugimoto and Wada (1993), the carbon isotopic composition of methane produced from acetate in rice field soil is very close to that of the acetate methyl group such that little fractionation results from fermentation of acetate to CH_4 and CO_2 (Reaction (3)). If these findings can be used in conjunction with the results of Murase and Sugimoto (2001) and Gelwicks *et al.* (1989), then it is feasible that the isotopic $\delta^{13}C$ fractionations associated with methanogenic CO_2-reduction (Reaction (1)) and homoacetogenesis (Reaction (6)) are very similar. The same cannot be assumed for heterotrophic acetogenesis (Reaction (7)). Unfortunately, isotopic analyses for methane were not performed until more than 1.5 years after incubation was initiated. The results obtained are as follows: vessel A, -80.2‰; vessel B, -81.1‰; and vessel C, -80.2‰. In addition, a result of -84.5‰ was obtained for the small system containing methanol from the first experiment. This would suggest that CO_2-reduction ($\delta^{13}C_{CH4}$ usually between -110 and -60‰ VPDB) rather than aceticlastic methanogenesis ($\delta^{13}C_{CH4}$ usually between -65 and -50‰ VPDB; Whiticar *et al.*, 1986). However, as the $\delta^{13}C$ of the DIC does not

increase, as predicted by CO_2 reduction, these results may indicate a common process in all of the vessels, namely methanogenesis from methanol.

Conclusions

The results of the incubation experiments have provided good indications of processes that may have played significant roles in endostromatolite production. However, while methanogenic activity is clearly present in these systems, the characteristic $\delta^{13}C$ enrichment of the carbonate phase preserved in the endostromatolite columns is apparently unrelated. Both methanogenic and acetogenic bacteria are capable of fractionating inorganic carbon with the result of enriching residual TIC in ^{13}C and of indirectly inducing carbonate precipitation by lowering P_{CO_2} . Our experimental evidence documents this characteristic enrichment in $\delta^{13}C_{DIC}$, although it clearly shows that it takes place during the early acetogenic phase, and that it precedes the methanogenic phase. This suggests that despite the association of such $\delta^{13}C$ enrichments with methanogenesis, it is more correctly due to CO_2 consumption during an initial stage of acetate production.

Methanol appears to be a preferred substrate of both groups of organisms, though our results indicate that methanogenic productivity is dependent on hydrogen produced symbiotically from organic fermentative bacteria. Accelerated acetogenic activity inhibited methane production, and inhibited acetogenic activity was followed by accelerated methanogenic production, particularly in vessel B. Without hydrogen, methanogenic production could only have proceeded via a fermentative pathway, and this was not observed in the reaction vessels.

The quantitative and isotopic data collected from closed-system incubation experiments using natural bacterial communities from periglacial soil demonstrate a symbiotic relationship between H_2-producing organic decomposers and H_2-consuming acetogens and methanogens that compete for H_2. It appears that when CO_2 is not initially restricted in the presence of methanol, *heterotrophic* acetogenic bacteria become the

dominant consumers of H_2, outcompeting methanogens, and producing a strong ^{13}Cenrichment in the residual DIC, according to:

$$CO_2 + CH_3OH + H_2 \rightarrow CH_3CO_2H + H_2O$$

Under conditions of lowered P_{CO_2}, the competitive edge of the acetogenic community appears to be lost, and the methanogenic bacteria engage an increasing role in consuming H_2 and CO_2 from precursor reactions. The strong depletion in the $\delta^{13}C$ of methane produced in the experiments, and the trends in substrate consumption, is consistent with CH_4 production by CO_2 reduction rather than by acetate fermentation.

When both groups of H_2 consumers are inhibited, the symbiotic dependence with hydrogen-producing fermentative microorganisms is broken and the activity of organic decomposers is reduced. The result is a slower turnover of DIC and a much more gradual ^{13}C depletion trend.

The ^{13}C enrichments observed in the growth columns of endostromatolite may have resulted from processes similar to those that caused the early ^{13}C-enrichments of DIC in the incubation systems. Thus, in this setting, and perhaps other methanogenic environments characterized by enriched $\delta^{13}C_{DIC}$ values, it is acetogenic reactions that appear to be responsible. This makes subsequent methanogenesis a secondary reaction that may be unrelated to observed ^{13}C enrichments. More definitive evidence is required to prove the role of acetogenic reactions in the growth of endostromatolites. ^{13}C-depleted acetate is the product of homoactogenesis, but the isotopic composition of acetate derived from heterotrophic acetogenesis needs to be determined before a better assessment of the role of acetate in endostromatolite environments can proceed.

Acknowledgements

This research project was funded by NSERC Research Grant 42590 to I.D.Clark and by a research bursary (PGS-B) provided to M. Marschner. Most analyses were performed at the G. G. Hatch Stable Isotope Laboratories, Ottawa, Carleton Geosciences Centre, University of Ottawa, and we are most grateful to G. St. Jean, P. Middlestead, W. Abdi, and P. Wickham for their help, expertise and many suggestions. Much appreciation is also given to Dr. D. Fortin for the use of her facilities and to Dr. A. Clarke and his staff at the College of Biological Sciences, University of Guelph, for analyses performed.

References

Balabane M, Galimov E, Hermann M, Letolle R (1987) Hydrogen and carbon isotope fractionation during experimental production of bacterial methane. *Organic Geochemistry* **11**: 115-119.

Baresi L (1984) Methanogenic cleavage of acetate by lysates of *Methanosarcina barkeri*. *Journal of Bacteriology*. **160**: 365-370.

Blair N E, Carter Jr, W J (1992) The carbon isotope biogeochemistry of acetate from a methanogenic marine sediment. *Geochimica et Cosmochimica Acta*. **56**: 1247-1258.

Boehme S E, Blair N E, Chanton J P, Martens C S (1996) A mass balance of ^{13}C and ^{12}C in an organic-rich methane-producing marine sediment. *Geochimica et Cosmochimica Acta*. **60**: 3835-3848.

Brock T D, Madigan M T, Martinko J M, Parker J (1994) *Biology of Microorganisms*. Prentice Hall, 909p.

Burke Jr R A, Martens C S, Sackett W M (1988) Seasonal variations of D/H and $^{13}C/^{12}C$ ratios of microbial methane in surface sediments. *Nature*. **332**: 829-831.

Chanton J P, Bauer J E, Glaser P A, Siegel D I, Kelley C A, Tyler C S, Romanowicz E H, Lazrus A (1995) Radiocarbon evidence for the substrates supporting methane formation within northern Minnesota peatlands. *Geochimica et Cosmochimica Acta*. **59**: 3663-3668.

Chauret Y (2000) Étude sur le développement des calcrètes de fissures du Yukon Septentrional, du Pléistocène à aujourd'hui. (Master's Thesis, Department of Geography, University of Ottawa, 85p)

Clark I, Fritz P (1997) *Environmental Isotopes in Hydrogeology*. Lewis Publishers, Boca Raton, 328p.

Clark I D, Lauriol B, Harwood L, Marschner M (2001) Groundwater contributions to discharge in a permafrost setting, Big Fish River, N.W.T., Canada. *Arctic, Antarctic and Alpine Research*. **33**: 62-69.

Clark I D, Lauriol B, Marschner M, Sabourin N, Chauret Y, Desrochers A (2004) Endostromatolites from permafrost karst, Yukon, Canada: paleoclimatic proxies for the Holocene hypsithermal. *Canadian Journal of Earth Sciences*. **41**: 387-399.

Conrad R, Mayer H P, Würst M (1989) Temporal change of gas metabolism by hydrogen-syntrophic methanogenic bacterial associations in anoxic paddy soil. *FEMS Microbiology Ecology*. **62**: 265-274.

Conrad R (1999) Contribution of hydrogen to methane production and control of hydrogen concentrations in methanogenic soils and sediments. *FEMS Microbiology Ecology*. **28**: 193-202.

Drever J I (1997) *The Geochemistry of Natural Waters; Surface and Groundwater Environments*. Prentice Hall, New Jersey, 436p

Ehrlich H L (1996) *Geomicrobiology*. Marcel Dekker Inc., New York, 719p

Fuchs G, Thauer R, Ziegler H, Stichler W (1979) Carbon isotope fractionation by *Methanobacterium thermoautotrophicum*. *Archives of Microbiology*. **120**: 135-139.

Games L M, Hayes J M, Gunsalus R P (1978) Methane-producing bacteria: natural fractionations of the stable carbon isotopes. *Geochimica et Cosmochimica Acta*. **42**: 1295-1297.

Gelwicks J T, Risatti J R, Hayes J M (1989) Carbon isotope effects associated with autotrophic acetogenesis. *Organic Geochemistry*. **14**: 441-446.

Gelwicks J T, Risatti J R, Hayes J M (1994) Carbon isotope effects associated with aceticlastic methanogenesis. *Applied and Environmental Microbiology*. **60**: 467-472.

de Graff W, Wellsbury P, Porkes R J, Cappenburg T E (1996) Comparison of acetate turnover in methanogenic and sulfate-reducing sediments by radiolabeling and stable isotope labeling and by use of specific inhibitors: Evidence for isotopic exchange. *Applied and Environmental Microbiology*. **62**: 772-777.

Hines M E, Duddleston K N, Kiene R P (2001) Carbon flow to acetate and C_1 compounds in northern wetlands. *Geophysical Research Letters*. **28**: 4251-4254.

Hornibrook E R C, Longstaffe F J, Fyfe W S (1997) Spatial distribution of microbial methane production pathways in temperate zone wetland soils: Stable carbon and hydrogen isotope evidence. *Geochimica et Cosmochimica Acta*. **61**: 745-753.

Jedrysek M O (1995) Carbon isotope evidence for diurnal variations in methanogenesis in freshwater lake sediments. *Geochimica et Cosmochimica Acta*. **59**: 557-561.

Jones J G, Simon B M, Gardener S (1982) Factors affecting methanogenesis and associated anaerobic processes in the sediments of a stratified eutrophic lake. *Journal of General Microbiology*. **128**: 1-11.

Krzycki J A, Kenealy W R, DeNiro M J, Zeikus J G (1987) Stable carbon isotope fractionation by *Methanosarcina barkeri* during methanogenesis from acetate, methanol, or carbon dioxide-hydrogen. *Applied and Environmental Microbiology*. **53**: 2597-2599.

Krzycki J A, Wolkin R H, Zeikus J G (1982). Comparison of unitrophic and mixotrophic substrate metabolism by an acetate-adapted strain of *Methanosarcina barkeri*. *Journal of Bacteriology*. **149**: 247-254.

Lansdown J M, Quay P D, King S L (1992). CH_4-production via CO_2 reduction in a temperate bog: A source of ^{13}C-depleted CH_4. *Geochimica et Cosmochimica Acta*. **56**: 3493-3503.

Lauriol B, Clark I (1999). Endostromatolites in the arctic: a paleohydrologic indicator. *Applied Geochemistry*. **14**: 775-785.

Martens C S, Kelley C A, Chanton J P, Showers W J (1992) Carbon and hydrogen isotopic characterization of methane from wetlands and lakes of the Yukon-Kuskokwim delta, Western Alaska. *Journal of Geophysical Research* **97**: 16,689-16,701.

Murase J, Sugimoto A (2001) Spatial distribution of methane in Lake Biwa sediments and its carbon isotopic composition. *Geochemical Journal*. **35**: 257-263.

Schoell M (1980) The hydrogen and carbon isotopic composition of methane from natural gases of various origins. *Geochimica et Cosmochimica Acta*. **44**: 649-661.

Silverman M P, Oyama V I (1968) Automatic apparatus for sampling and preparing gases for mass spectral analysis in studies of carbon isotope fractionation during methane metabolism. *Analytical Chemistry*. **40**: 1833-1837.

Skoog D A, West D M, Holler F J (1994) *Analytical Chemistry : An Introduction*. Saunders College Publishing, Philadelphia ,612p

Sugimoto A, Wada E (1993) Carbon isotopic composition of bacterial methane in a soil incubation experiment: Contributions of acetate and CO_2/H_2. *Geochimica et Cosmochimica Acta*. **57**: 4015-4027.

West A E, Schmidt S K (2002) Endogenous methanogenesis stimulates oxidation of atmospheric CH_4 in alpine tundra soil. *Microbial Ecology*. **43**: 408-415.

Whiticar M J, Faber E, Schoell M (1986) Biogenic methane fromation in marine and freshwater environments: CO_2 reduction vs acetate fermentation- Isotope evidence *Geochimica et Cosmochimica Acta*. **50**: 693-709

Table I: Growth Media Recipes Used in the Experimental Incubation Systems

Media Reagent Names	**Compound Formulas**	**Reagent Concentration** (g/L)		$\delta^{13}C$ (‰ VPDB)
		Exp. #1	**Exp. #2**	
ammonium acetate	$CH_3CO_2NH_4$	0	1.33	-38.1
l-cysteine hydrochloride	$C_3H_7NO_2S{\bullet}HCl{\bullet}H_2O$	0.50	0	-14.5
magnesium chloride	$MgCl_2{\bullet}6H_2O$	0	1.00	-
2-mercaptoethanesulfonic acid	$C_2H_5O_3S_2Na$	0	0.33	N/A
potassium dihydrogen phosphate	KH_2PO_4	0	0.53	-
di-potassium hydrogen phosphate	K_2HPO_4	0	0.53	-
sodium chloride	NaCl	0	0.80	-
sodium sulphide	$Na_2S{\bullet}9H_2O$	0.30	0	-
tryptic soy broth	N/A	0.50	1.47	N/A
yeast extract	N/A	0.50	0.53	N/A
ferrous chloride	$FeCl_2{\bullet}4H_2O$	0	0.0030	-
cupric chloride	$CuCl_2{\bullet}2H_2O$	0	0.0002	-
cobalt nitrate	$Co(NO_3)_2{\bullet}6H_2O$	0	0.0025	-
nickel sulphate	$NiSO_4{\bullet}7H_2O$	0	0.0003	-
trimethylamine hydrochloride	$(CH_3)_3N{\bullet}HCl$	**18.00**	0	-38.2
methanol	CH_3OH	**20.10**	6.01	-39.6
sodium bicarbonate	$NaHCO_3$	4.00	**4.00**	-4.8
sodium formate	HCO_2Na	**30.00**	0	-23.1
sodium acetate	CH_3CO_2Na	**25.10**	0	-41.0
2-bromoethanesulfonic acid	$C_2H_4BrO_3SNa$	**10.00**	**2.00**	N/A

(values shown in bold are for specific vessels only, not all systems prepared for the given experiment; see text for setup of specific incubation systems)

Table II: Methane Production Results (mL) for the First Set of Incubation Systems

# days	Substrate				
	acetate	formate	methanol	trimethylamine	BES (control)
8	0.01	N/A	0.03	0.09	0
67	0.19	0	1.83	1.52	0
109	0.13	0	1.78	1.52	0
127	0.14	0.04	2.98	1.11	0.02
148	0.15	0.03	3.27	1.86	0.02
161	0.16	0.04	3.38	2.03	0.02
183	0.15	0.03	3.22	2.44	0.02
260	0.10	0.02	4.61	19.31	0.04
344	0.06	0.02	5.25	126.07	0.07
462	0.03	0.01	4.32	115.36	0.05
512	0.02	0.01	4.35	67.73	0.02
601	0.04	0.01	6.90	42.35	N/A
719	0	0	10.68	8.24	0

Table III: Carbon Budgets for the Large Incubation Systems

Vessel A

reagent	Day 0	Day 105 *		May 350 *	
	mg C	mg C	change	mg C	change
TIC	10	**55**	**45**	**70**	**60**
methane	0	277	277	186	186
methanol	2249	1755	-494	2188	-61
acetate	402	665	263	395	-7
coenzyme M	*(48)*	N/A		N/A	
total	**2661**	**2752**	**91**	**2839**	**178**

Vessel B

reagent	May 31 1999	Day 105 *		Day 350 *	
	mg C	mg C	change	mg C	change
TIC	572	**88**	**-484**	138	**-433**
methane	0	30	**30**	211	**211**
methanol	2249	1603	**-646**	1283	**-966**
acetate	402	2339	**1937**	1067	**665**
coenzyme M	*(48)*	N/A		N/A	
total	**3223**	**4059**	**836**	2700	**-523**

Vessel C

reagent	May 31 1999	Day 105 *		Day 350 *	
	mg C	mg C	change	mg C	change
TIC	10	**37**	**27**	42	**32**
methane	0	0.1	**0.1**	0.2	**0.2**
methanol	2249	2123	**-126**	2113	**-136**
acetate	402	649	**247**	366	**-36**
coenzyme M	*(48)*	N/A		N/A	
BES	*(223)*	N/A		N/A	
total	**2661**	**2772**	**111**	2479	**-182**

* It was not possible to accomplish all of the analyses on the same date. These values are average elapsed times for the analyses since the start of incubation.

Figure i : A thin section photograph of endostromatolite columns showing light and dark bands corresponding to layers of low and high organic matter content, respectively. The rock sample was cut orthogonally to the growth surface. The field of view is 2 cm vertically.

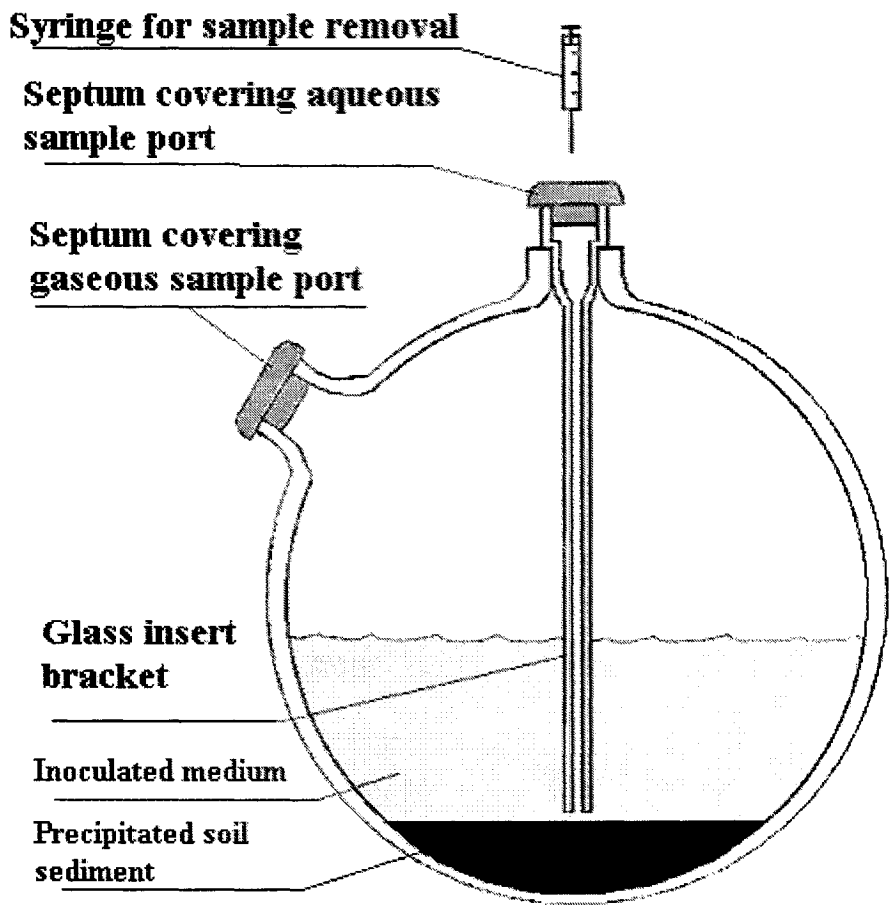

Figure ii: A schematic diagram of one of the reaction vessels used to contain the incubation systems for the second experiment. Originally, the port to access the liquid phase was to be used for direct measurements of pH, but high vessel pressures from excessive methane production forced water up the glass tubing so that the septum sealing the port could not be removed.

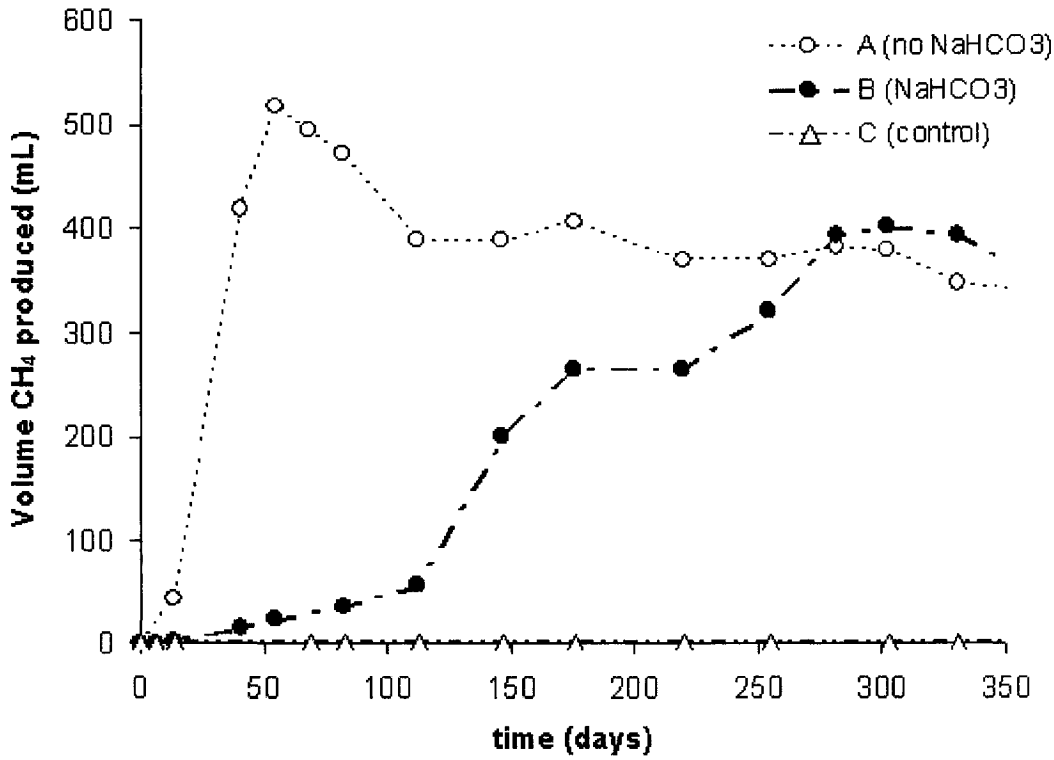

Figure iii: Methane production results for the large vessels of the second experiment. The values take into account methane that was lost due to sample removal; budgets for CH_4 and CO_2 were kept. There is an evident decrease in methane in vessel A over time after an early peak. This is likely due to overpressurization inducing a leak that exceeded production. Since the vessels were kept in an anaerobic chamber, no losses of methane were anticipated to be due to oxidation reactions from electron-accepting compounds leaking into the vessels.

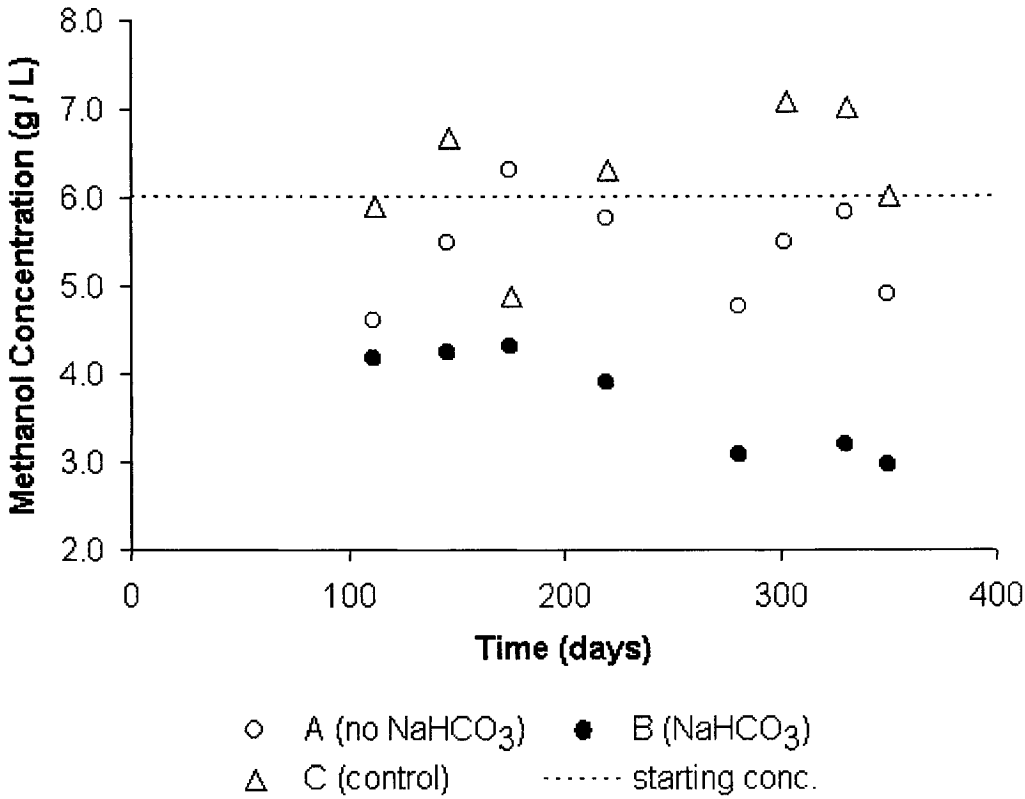

Figure iv: Methanol concentration data for the large incubation systems. Data for the first 100 days is not available due to the lack of a method for detecting methanol. The high variability in the data may be an indication that calibration of the quantitative data was not significant. Clearly, however, vessel B always had the lowest concentration, and vessel C had the highest concentration measured on all but one occasion.

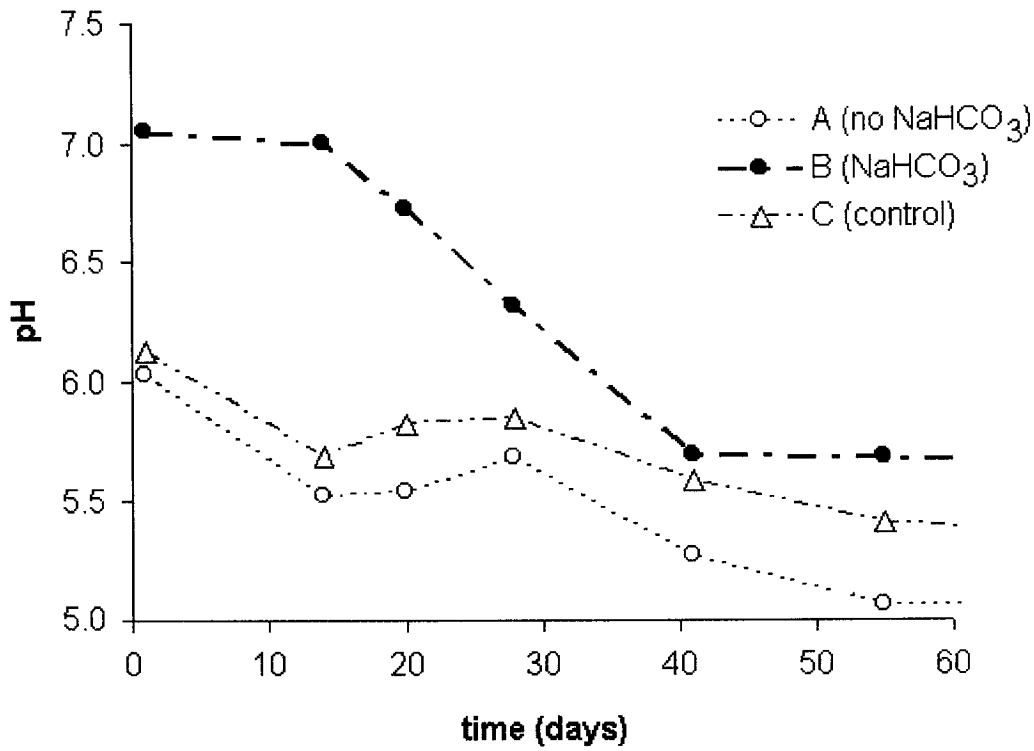

Figure v: pH data up to sixty days for the large incubation systems. Trends after this period of incubation are very stable.

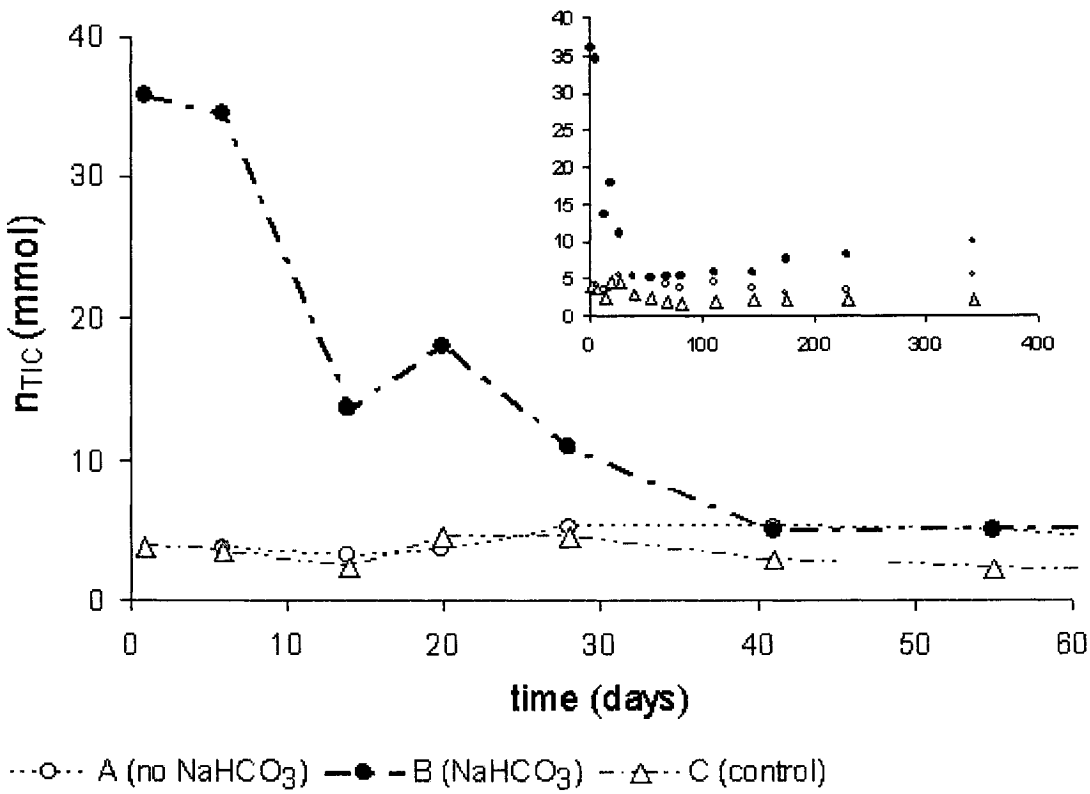

Figure vi: Total inorganic carbon (n_{TIC}) data for the large incubation systems over the first sixty days. Inset shows data for entire data collection period.

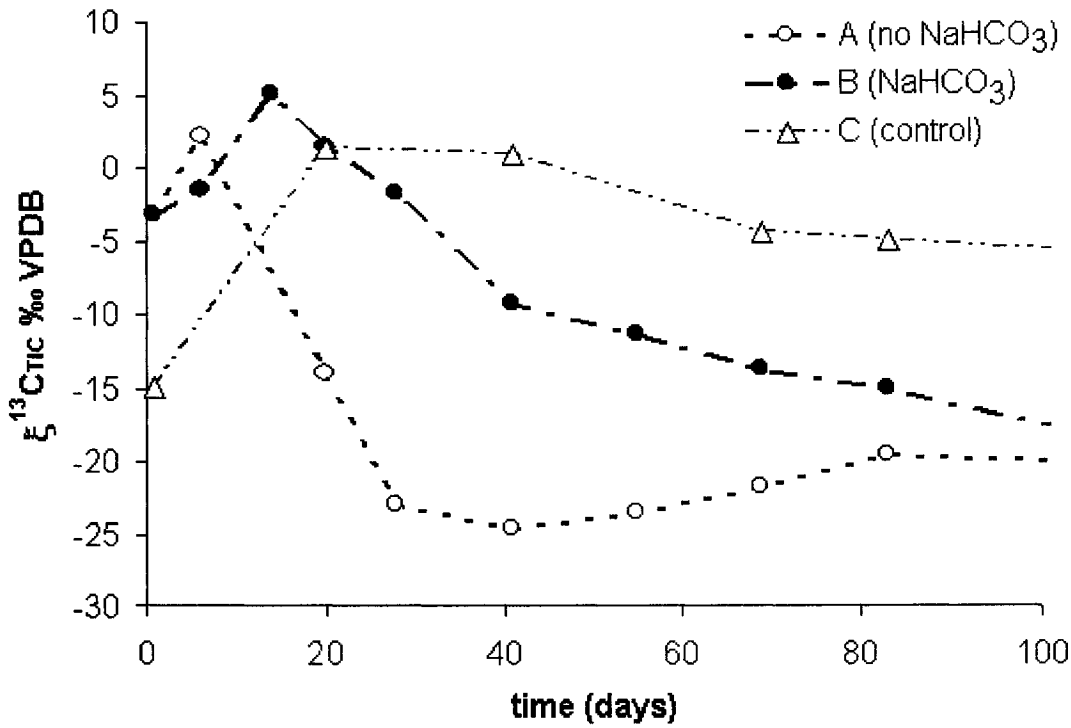

Figure vii: ^{13}C isotopic data for total inorganic carbon (TIC) during the first 100 days of incubation. Results for DIC (dissolved inorganic carbon) were used to calculate $\delta^{13}C_{TIC}$ using equilibrium constants at 25°C.